TECHNISCHE UNIVERSITÄT MÜNCHEN

Department Chemie

Lehrstuhl für Biotechnologie

Modulation of the Hsp90 cycle by the Glucocorticoid receptor

Oliver Robin Lorenz

Vollständiger Abdruck der von der Fakultät für Chemie der Technischen Universität München zur Erlangung des akademischen Grades eines Doktors der Naturwissenschaften genehmigten Dissertation.

Vorsitzender: Univ.- Prof. Dr. A. Itzen

Prüfer der Dissertation:

1. Univ.- Prof. Dr. J. Buchner

2. Univ.- Prof. Dr. M. Sattler

3. Univ.- Prof. Dr. S. Weinkauf

Die Dissertation wurde am 27.02.2014 bei der Technischen Universität München eingereicht und durch die Fakultät für Chemie am 14.04.2014 angenommen.

Für Daniela und Charlotte

Inventory

1 Introduction

1.1 Protein folding

Proteins are one of the major macromolecules in living organisms and essential for many cellular processes. They are linear chains of amino acids (polypeptides) which are specified by the nucleotide sequence of their genes. To fulfil their biological functions, they have to adopt a defined three-dimensional structure in a process called protein folding, even though some exceptions exist (Fink, 2005). Pioneer work by Anfinsen showed that protein folding *in vitro* is spontaneous and that the formation of the proteins' native fold is dictated by the amino acid sequence (Anfinsen et al., 1961). In 1968, Levinthal noted that proteins cannot find their native, three-dimensional structure by a random search, as unbiased sampling of all possible polypeptide conformations would take billions of years (Levinthal, 1968). Later on, several folding pathways were postulated to explain the folding problem (Fersht, 1999). Examples are the framework-model (Kim and Baldwin, 1990), the nucleation-model (Wetlaufer, 1973), the diffusion-collision model (Karplus and Weaver, 1994), the hydrophobic-collapse model (Kuwajima, 1989) or the jigsaw-puzzle model (Harrison and Durbin, 1985).

A popular theoretic formulation to approach the Levinthal paradoxon is the folding funnel, which explains protein folding from an energy landscape perspective (Clark, 2004). It describes the way of an ensemble of unfolded protein molecules to their native form at the global energy minimum via several intermediates (Figure 1).

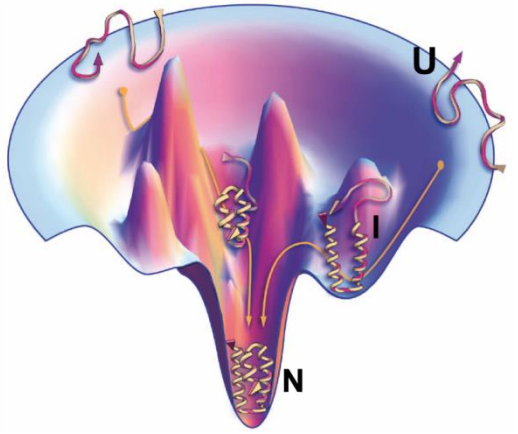

Figure 1 Protein folding energy landscape. (U) Many high energy and unfolded conformations, (I) Folding intermediates located at local energy minima, (N) Low energy, folded structures at the global energy minimum; adapted from Dill and MacCallum, (2012).

Folding intermediates, present at local energy minima, can accelerate the folding process (Wagner and Kiefhaber, 1999). However, they are only partially folded and expose hydrophobic surfaces to some extent. Thus, during folding their collision may lead to self-association, polymerization or aggregation - processes, which are not considered in the classical folding funnel (Clark, 2004).

1.2 Molecular chaperones

Under physiological conditions, protein folding is far more complex. The folding funnel as described in 1.1 explains the *in vitro* folding behavior of single, isolated polypeptide chains at infinite solutions (Clark, 2004). However, *in vivo*, the striking difference to test-tube conditions is the crowded environment of the cell. In a typical mammalian cell, the protein concentration reaches about 300 milligram per milliliter (Ellis, 2007). Molecular crowding effects markedly influence productive folding of freshly synthesized proteins which may result in protein misfolding or aggregation. Besides folding catalysts such as peptidylprolyl isomerases (PPIases) or protein disulfide isomerases (PDIs), the cell evolved molecular chaperones - a sophisticated protein machinery - that counteract the above-mentioned nonproductive side reactions which are also implicated in many human diseases (Balch et al., 2008). As folding helpers, molecular chaperones assist proteins to fold to their native states by increasing their folding efficiency (Buchner and Walter, 2008). Moreover, besides their protective function during protein synthesis, they also play a role in protein degradation and are thus important elements for protein homeostasis (McClellan et al., 2005). Molecular chaperones are ubiquitous and highly conserved in all kingdoms of life (Richter et al., 2010). Many of them are up-regulated under heat-stress and thus belong to the class of heat-shock proteins (Hsps). Heat-shock proteins can be divided into five families according to their molecular weight: the Hsp100 family, the Hsp90 family, the Hsp70 family, the Hsp60/chaperonin family and small heat shock proteins (sHsps). Cells of higher eukaryotes comprise an interconnected network of distinct chaperone classes (Figure 2). Most of the molecular chaperones require ATP to fulfil their functions as foldases. Exceptions are sHsps, which display only passive holdase function. Small heat schock proteins form large oligomeric assemblies and seem to be optimized for interacting mainly with unfolded (unfolding) proteins to prevent their aggregation (Haslbeck et al., 2005). Substrate refolding may occur in conjunction with ATP-dependent chaperones such as the Hsp70 system (Lee et al., 1997).

Hsp70 recognizes unfolded proteins or partially folded intermediates. Its functional cycle is modulated by a variety of co-factors including nucleotide exchange factors (NEFs) and J-proteins (Hsp40s), which drive ATP turnover and regulate the recognition of its substrates (Kampinga and Craig, 2010). Members of the Hsp60 family, such as the CTT machinery, form double-ring like structures with an internal cavity similar to *E. coli* GroE (Horwich and Fenton, 2009; Xu et al., 1997). Folding intermediates, which could not be folded to their native states upon interaction with Hsp70 are encapsulated and allowed to fold in an environment shielded from the cytosol (Frydman, 2001). Hsp90 is not as promiscuous as Hsp70 in its substrate spectrum and binds a defined set of substrates (clients) that possess native-like structures (Jakob et al., 1995; Taipale et al., 2012). The Hsp90 system collaborates with the Hsp70 machinery. In many cases, Hsp70 transfers its substrates to Hsp90. The most prominent example is the complex maturation pathway of steroid hormone receptors (SHRs) (Pratt and Toft, 1997). Similar to Hsp70, Hsp90 acts in concert with a variety of co-chaperones to fold its clients along the way to their active states (1.3.3).

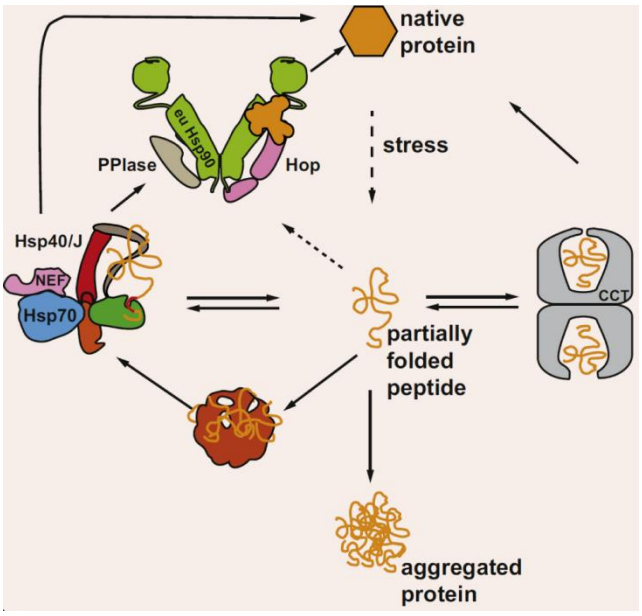

Figure 2 Chaperone network in higher eukaryotes. Hsp60/CCT (grey), Hsp70 (blue), Hsp90 (green) and sHsps (brown) determine the fate (arrows) of unfolded and partially structured proteins *in vivo*. Notably, higher eukaryotes do not comprise Hsp100 proteins. Adopted from Richter et al., (2010).

1.3 The Hsp90 chaperone machinery

1.3.1 Evolution of the Hsp90 family

Hsp90 is highly abundant in the eukaryotic cell, where it constitutes 1-2 % of the total protein level (Borkovich et al., 1989). Besides its function in stress tolerance, it is required for the maturation and activation of many proteins (so called clients), which play essential roles in many cellular processes including cell cycle control, cell survival and many signaling pathways (Jackson, 2013). Hsp90 is highly conserved and found in all kingdoms of life except archea (Figure 3) (Taipale et al., 2010).

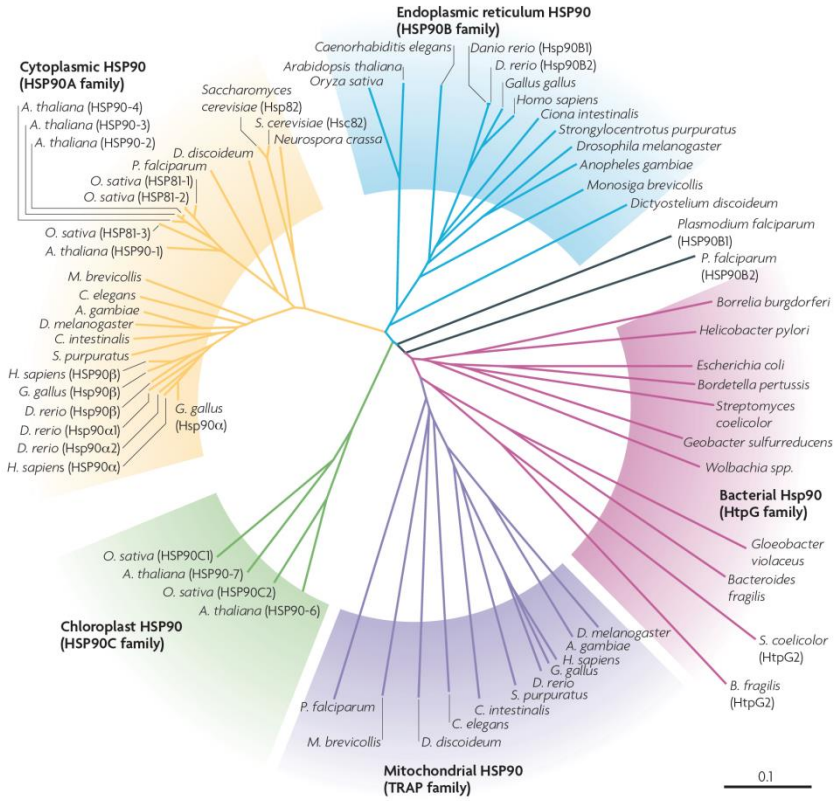

Figure 3 Evolution of the Hsp90 family. Hsp90 is highly conserved. Shown is the genetic distance of Hsp90 homologs from different organisms. Adopted from Taipale et al., (2010).

Prokaryotes comprise usually one cytosolic form (HtpG). Yeast and mammals possess two cytosolic isoforms of which one is constitutively expressed (Hsc82 and Hsp90ß, respectively) while the other one is induced by various stress conditions (Hsp90α and Hsp82, respectively) (Csermely et al., 1998). Interestingly, higher eukaryotes comprise also isoforms in other cellular compartments such as the tumor necrosis factor receptor-associated protein (TRAP1) in mitochondria, the 94 kDa glucose-regulated protein (Grp94) in the endoplasmatic reticulum (ER) and Hsp90C in chloroplasts (Chen et al., 2006).

In addition, Hsp90 is also found in the extracellular environment (Tsutsumi and Neckers, 2007) and may translocate into the nucleus in response to client binding or upon other stimuli (Akner et al., 1992; Galigniana et al., 2001).

1.3.2 Structure and conformational dynamics of Hsp90

Recent crystallographic studies uncovered the structures of Hsp90 from bacteria, yeast and mammals (Ali et al., 2006; Dollins et al., 2007; Lavery et al., 2014; Shiau et al., 2006). Members of the Hsp90 family share a common multi-domain architecture (Figure 4). Each subunit of the Hsp90 dimer consists of an N-terminal ATPase domain (Hsp90-N), a middle domain (Hsp90-M) and C-terminal dimerization domain (Hsp90-C).

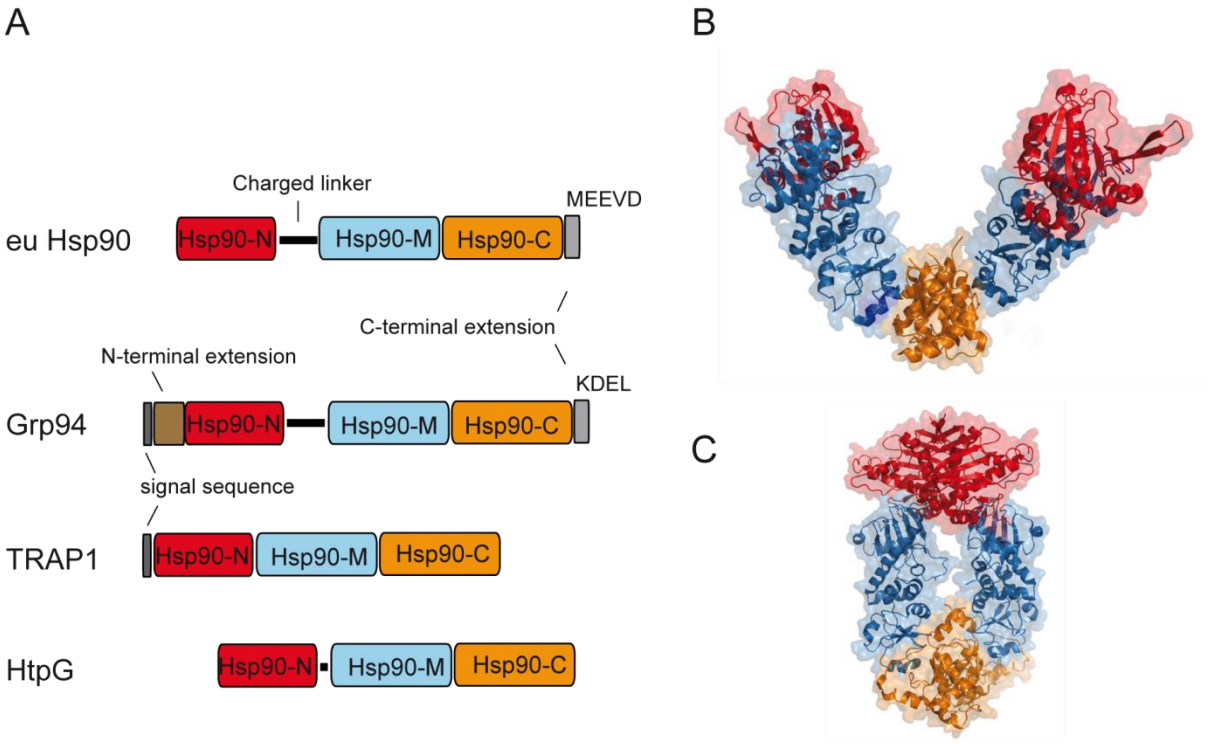

Figure 4 Hsp90 architecture. A) Schematic domain organization of the Hsp90 family. All three Hsp90 domains are conserved (Hsp90-N, Hsp90-M and Hsp90-C). The N-terminal domain of Grp94 possesses an N-terminal extension which follows the ER-import sequence. Eukaryotic Hsp90s (including ER members) show a massive extension of the linker region, which connects the N-terminal domain with the middle domain of Hsp90. Prokaryotic (mitochondrial) Hsp90s lack the typical MEEVD motif. Adopted from Richter et al., (2008a). B) Crystal structure of HtpG from *E. coli* (PDB 2IOQ) in the open conformation and of yeast Hsp90 in its nucleotide-bound, closed conformation (C) (PDB 2CG9) with domain color code as in (A).

The N-terminal domain shows a typical 'Bergerat fold' (Bergerat et al., 1997) and contains the nucleotide-binding pocket, in which ATP is bound in an unusual, kinked conformation (Prodromou et al., 1997). The orientation of ATP in Hsp90-N is shared with some other ATPases. Collectively they belong to the GHKL (gyrase, Hsp90, histidine kinase and MutL2) superfamily (Dutta and Inouye, 2000). Hsp90-N is connected to the middle domain of Hsp90 via a charged linker region of variable length. Besides providing structural flexibility, it also modulates the function of Hsp90 (Hainzl et al., 2009; Tsutsumi et al., 2012). Hsp90-M is characterized by two αβα-motifs which are linked by a series of short α-helices (Meyer et al., 2003). It also contains a catalytic loop with a conserved arginine residue which is critical for ATPase activity (Ali et al., 2006). Both Hsp90-C domains within the Hsp90 dimer pack together through two α-helices which form a four-helix bundle at the dimerization interface (Harris et al., 2004; Minami et al., 1994). Eukaryotic, cytosolic Hsp90s also possess a C-terminal extension which contains the MEEVD motif that allows binding of co-chaperones containing a tetratricopeptide repeat (TPR) domain (Young et al., 1998).

The above-mentioned Hsp90 crystal structures together with SAXS and EM models (Krukenberg et al., 2008; Southworth and Agard, 2008) provided a comprehensive picture of the conformational rearrangements within Hsp90 during its functional cycle. The ATPase cycle of Hsp90 is highly conserved (Richter et al., 2008b), although hydrolysis rates differ among species. For example, the ATPase activities of HtpG, yeast Hsp90, TRAP1 and Grp94 are quite similar (0.4-0.5 min^{-1}) (Felts et al., 2000; McLaughlin et al., 2002; Owen et al., 2002; Panaretou et al., 1998), whereas human Hsp90 shows an about 10 fold slower ATPase rate (McLaughlin et al., 2002). In the last years, the ATPase cycle was extensively studied and allowed the determination of its rate limiting steps (Hessling et al., 2009; Mickler et al., 2009; Richter et al., 2006; Weikl et al., 2000). During its functional cycle, Hsp90 progresses from an N-terminal open state (compare Figure 4B) to a closed state (compare Figure 4C) via several intermediates (Figure 5). Apo-Hsp90 is present in an open, v-shaped conformation. Upon ATP binding, the ATP-lid (a short segment of the N-terminal domain) is repositioned and flaps over the nucleotide binding pocket resulting in the first intermediate of the cycle (I1). In the next step, the N-terminal domains dimerize via an N-terminal swapping strand (I2) and further conformational changes lead to the closed and twisted state of the Hsp90 dimer, in which Hsp90-N contacts the Hsp90-M domain. ATP-hydrolysis facilitates the dissociation of the Hsp90-N domains and its products (ADP and P_i) are released. Finally, Hsp90 returns to its apo-state and the conformational cycle is completed.

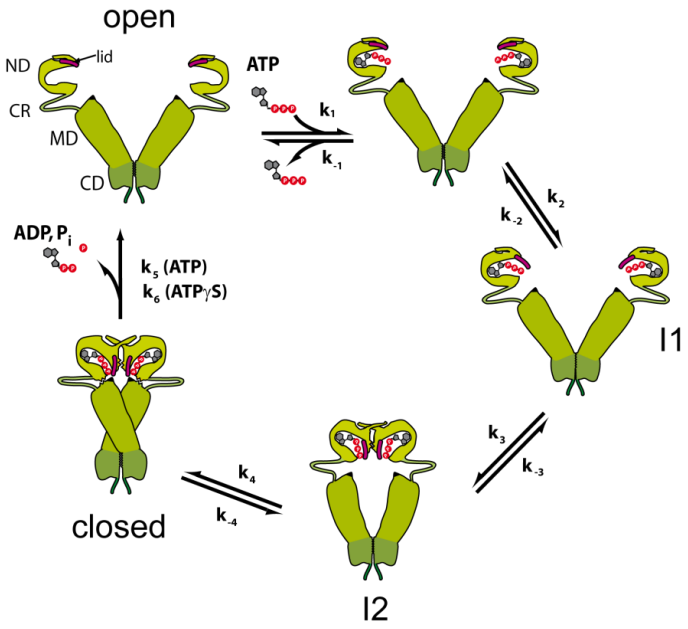

Figure 5 Schematic representation of the Hsp90 cycle. ATP binding leads to conformational changes in the N-terminal domain. These rearrangements include the ATP lid, which closes over the nucleotide binding pocket (I1). In a subsequent step, dimerization of the N-terminal domains occurs via an N-terminal swapping strand forming the next intermediate (I2). Finally, the association of the Hsp90-N and Hsp90-M domains leads to the fully closed state of the Hsp90 dimer. The Hsp90 cycle is further modulated by Hsp90 co-chaperones (1.3.3) and post-translational modifications. Adopted from Hessling et al., (2009).

For some eukaryotic members of the Hsp90 family these conformational changes seem to be iso-energenic. ATP binding does not necessarily lock Hsp90 into a specific conformation. Rather, nucleotides shift the continuous equilibrium of open and closed conformations towards more compact states (Mickler et al., 2009; Southworth and Agard, 2008). Besides ATP hydrolysis, which provides directionality (and which is not rate limiting), also members of the family of co-chaperones render the cycle deterministic. Of note, the conformational cycle of Hsp90 can be efficiently blocked by potent, high-affinity inhibitors such as radicicol, as they compete with ATP for binding to the Hsp90-N domain (Schulte et al., 1998). Since Hsp90 is implicated in stabilizing oncogenic proteins such as several kinases, these inhibitors might serve as anti-cancer therapeutics (Alarcon et al., 2012).

1.3.3 Hsp90 co-chaperones

In eukaryotic cells, a cohort of about 20 co-chaperones modulates Hsp90 function (Röhl et al., 2013; Wandinger et al., 2008). Besides post-translational modifications (including phosphorylation, acetylation, nitrosylation, glycosylation and methylation; reviewed in Mollapour and Neckers, (2012)) they provide an additional layer of Hsp90 regulation. Some of them are known to affect the ATPase rate of Hsp90, while others play import roles in client recruitment, localization or exhibit chaperone functions on their own (Röhl et al., 2013).

Most of them possess TPR domains, which interact with the MEEVD motif at the C-terminal end of Hsp90 (Figure 4A). Structurally, TPR domains are defined by tandem repeats of a 34-amino acid consensus motif that forms a cleft of seven antiparallel α-helices which can associate with TPR acceptor modules (Scheufler et al., 2000) (Figure 6).

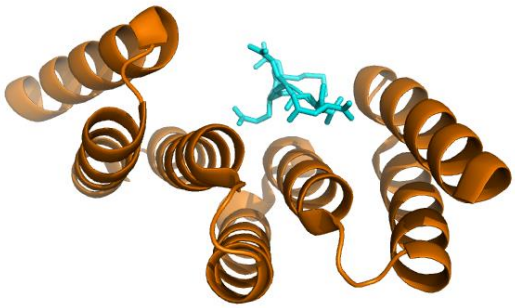

Figure 6 Structure of the TPR domain. Shown is the TPR2A domain of Hop (orange) in complex with the HSP90 peptide MEEVD (cyan) (PDB 1ELR).

The co-chaperones of cytosolic Hsp90 include Hop, Cdc37, SGT-1, p23, high molecular weight PPIases (FKBP51 and FKBP52, Cyp40), PP5, Aha1 and CHIP. These examples are described in the following to illustrate the intricate interplay of Hsp90 with its co-chaperones:

Hop (Sti1 in yeast) is a non-competitive inhibitor of the Hsp90-ATPase. It binds to the C-terminal tail of Hsp90 (and partly to Hsp90-N and Hsp90-M) and stabilizes its open conformation (Richter et al., 2003). Structurally, it comprises three TPR domains (TPR1, TPR2A and TPR2B) which facilitate simultaneous binding to both Hsp70 and Hsp90. In this respect, TPR2A and TPR2B seem to be specific for Hsp90, whereas TPR1 binds mainly to Hsp70 (Brinker et al., 2002; Scheufler et al., 2000; Schmid et al., 2012). Thus, Hop may act as a connecting platform and enables client delivery from the Hsp70 system to the Hsp90 machinery, a telling feature, which is crucial for the maturation of SHRs (Chen and Smith, 1998).

Similar to Hop, also Cdc37 (cell division cycle 37 homolog) is involved in client recruitment and inhibits the ATPase activity of Hsp90 (Gaiser et al., 2010; Vaughan et al., 2006). It has been shown that Cdc37 is important for chaperoning kinases (Taipale et al., 2012). Cdc37 binds to Hsp90-N via its C-terminal domain and links kinases through interaction with its N-terminal domain to the Hsp90 machine for folding (Roe et al., 2004). In addition, Cdc37 displays Hsp90-independent functions, as it supports yeast growth and functions as a chaperone on its own (Kimura et al., 1997; MacLean and Picard, 2003).

SGT-1 is a p23-related co-chaperone (see below), which has been extensively studied in plants (Kadota et al., 2010). It seems to transfer a diverse class of client proteins to the Hsp90 system. Interestingly, even though SGT-1 shows a TPR domain, it binds Hsp90 with its CS domain at the N-terminal domain (Kadota et al., 2008). The ATP lid is not affected upon interaction and could explain why the ATPase of Hsp90 is not influenced.

The small acidic co-chaperone p23 (Sba1 in yeast) plays an essential role in the maturation process of various Hsp90 clients and enters the chaperone cycle at rather late stages. It was first identified in complex with Hsp90 and SHRs in the early 1990s (Smith et al., 1990) and seems to stabilize the Hsp90-SHR complex *in vivo* (Morishima et al., 2003). In addition, it has been shown to be important for the maintenance of telomers (DeZwaan and Freeman, 2010) and for the transcriptional activity of various nuclear receptors (Freeman et al., 2000; Freeman and Yamamoto, 2002). The crystal structure of the Hsp90-p23 complex (Ali et al., 2006) shows that p23 binds at the interface of the N-terminal domains in the closed Hsp90 dimer. As a consequence, ATP-hydrolysis is slowed down. The exact mechanism of its mode of action is not clear, but it seems likely that ADP and P_i release from Hsp90 is prevented in complex with p23 (Ali et al., 2006). It has been also suggested, that client activation occurs in the Hsp90-p23 hetero-complex (Johnson and Toft, 1995). Further, p23 comprises additional chaperone activity which is governed by its unstructured C-terminal tail (Freeman et al., 1996; Weikl et al., 1999).

Another group of co-chaperones are high molecular weight PPIases, which have been found in complex with SHRs (Echeverria and Picard, 2010; Smith and Toft, 2008). These include FKBP51, FKBP52 and Cyp40 (Cpr6 and Cpr7 in yeast) (Johnson and Toft, 1994; Mayr et al., 2000; Pirkl and Buchner, 2001). Most of these PPIases display Hsp90-independent chaperone function (Pirkl and Buchner, 2001). Structurally, they comprise a TPR domain which facilitates binding to the C-terminal MEEVD motif of Hsp90 and a FKBP-like or cyclophilin-like domain with peptidylprolyl-isomerase activity. How the PPIase co-chaperones act on SHR complexes is not well understood. The PPIase activity seems dispensable for the maturation of most of the SHRs (Smith and Toft, 2008). Interestingly, SHRs seem to have a certain preference for these PPIases. For example, the estrogen receptor (ER) interacts mostly with Cyp40, whereas FKBP52 is recovered in preference for FKBP51 at relatively high levels from glucocorticoid receptor (GR), progesterone receptor (PR) and mineralocorticoid receptor (MR) complexes (Barent et al., 1998; Ratajczak et al., 1990). It has been also shown that FKBP52 elevates hormone binding affinity of GR, whereas FKBP51 has an inhibitory effect on GR hormone responsiveness (Reynolds et al., 1999; Riggs et al., 2003). In this respect, it

was also suggested that these co-chaperones directly interact with Hsp90-bound SHRs (Cluning et al., 2013; Ratajczak et al., 2009). Besides that, FKBP52 and Cyp40 have been also reported to influence SHR trafficking into the nucleus (Vandevyver et al., 2012).

The protein phosphatase 5, PP5 (PPT1 in yeast), is found in SHR complexes as well (Silverstein et al., 1997). Moreover, it plays an important role in the processing of kinases in concert with Cdc37 (Vaughan et al., 2008). PP5 is known to bind to the C-terminal end of Hsp90 via its TPR domain. As a result, PP5 gains activity and dephosphorylates Hsp90 which affects the function of Hsp90 as molecular chaperone and the maturation of its clients (Soroka et al., 2012). Similar to high molecular weight PPIases and Cdc37, it competes with Hop for binding to Hsp90 (Cliff et al., 2006; Silverstein et al., 1998).

Aha1, an activator of the Hsp90 ATPase activity, has the most pronounced effect on the Hsp90-ATPase (Panaretou et al., 2002). Structural studies revealed that both Hsp90-M and Hsp90-N domains are involved in Aha1 binding and that one Aha1 molecule per Hsp90 dimer is sufficient for stimulation of the ATPase activity (Meyer et al., 2004; Retzlaff et al., 2010). Aha1 accelerates the ATPase by promoting the conformational rearrangements leading to the N-terminal closed state of Hsp90 (Figure 5, see I2 intermediate) (Hessling et al., 2009). Aha1 has also been shown to contribute to kinase- and GR activation *in vivo* (Harst et al., 2005) and is also implicated in the correct folding and trafficking of the cystic fibrosis transmembrane conductance regulator (CFTR) (Wang et al., 2006).

CHIP (carboxyl-terminus of Hsc70 protein) is found in higher eukaryotes. It may interact with Hsp70 or Hsp90 via its TPR domain (Ballinger et al., 1999). CHIP also comprises a U-box domain that has ubiquitin ligase activity. Together with the Hsp70 and Hsp90 machinery, it regulates client protein ubiquitination and proteosomal degradation (McDonough and Patterson, 2003).

1.3.4 Hsp90 client recognition

Hsp90 works together with a large set of co-chaperones to assist the structure formation of hundreds of cellular proteins (Picard, 2002). Today, more than 300 proteins are known whose maturation depends on Hsp90 (http://www.picard.ch/downloads/Hsp90interactors.pdf). Besides kinases and E3 ligases, members of the SHR family represent the most stringent Hsp90 client proteins (Taipale et al., 2012). What makes an Hsp90 client a client is still under debate. They share no common sequence- or structural similarity. Instead, it seems that their high structural instability and their need for conformational changes drive their interaction with Hsp90 (Röhl et al., 2013; Taipale et al., 2010). Thus, together with the transient nature of Hsp90-client complexes, the detailed analysis of the Hsp90-client interplay is challenging. To this end, mainly indirect approaches, such as immunoprecipitation experiments or mutational studies in yeast were applied to narrow down the client binding site on Hsp90 (Röhl et al., 2013). It seems that all three Hsp90 domains are involved in client binding. However, predominantly the Hsp90-M domain has been reported in most of the cases to facilitate client binding (Röhl et al., 2013).

For three Hsp90 clients, namely p53, CDK4 and a staphylococcus nuclease fragment (Δ131Δ), structural information about the Hsp90-client complex is available (see Figure 7).

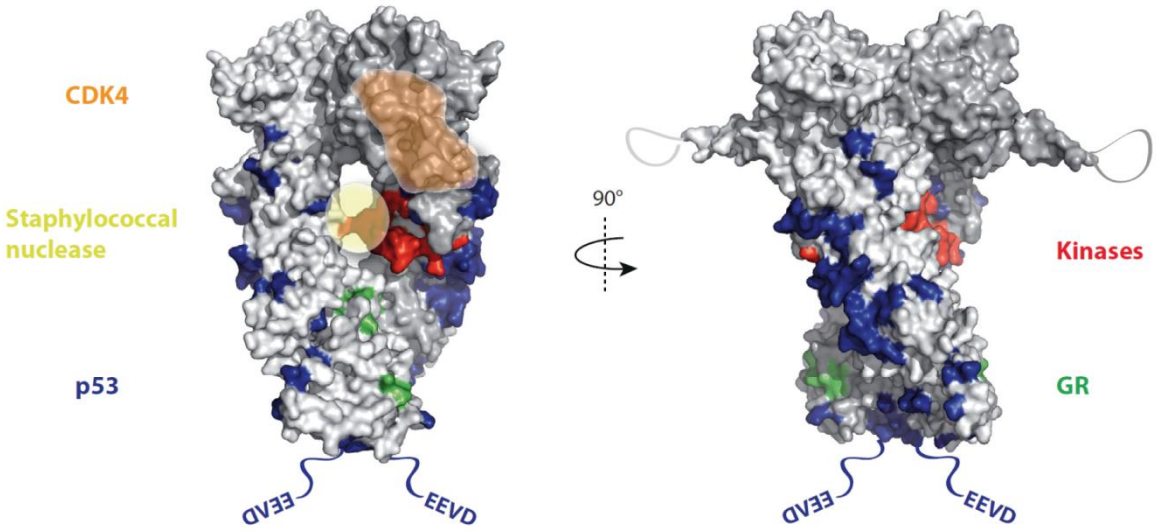

Figure 7 Hsp90 client binding sites. Shown are the binding sites for CDK4 or other kinases (orange and red, respectively), Staphylococcal nuclease (yellow), p53 (blue) and GR (green) on the closed Hsp90 dimer (derived from structural and biochemical studies). For GR, the Hsp90-MC interface was suggested as predominant binding site (Fang et al., 2006). Adopted from Röhl et al., (2013).

The binding site for the intrinsically disordered model client Δ131Δ is located mainly at the internal cleft formed by the Hsp90-M domains in the closed Hsp90 dimer with contributions from Hsp90-N (Street et al., 2011). The binding mode of CDK4 differs from Δ131Δ, even though Hsp90-M and Hsp90-N promote client binding as well. EM studies suggest that, in contrast to Δ131Δ, mainly hydrophobic and charged residues at the outside of the closed Hsp90 dimer contribute to binding of CDK4 (Vaughan et al., 2006). Specifically, a hydrophobic patch around Trp300 seems to modulate client binding. The DNA binding domain of the transcription factor p53 (p53-DBD) makes mainly contacts with the Hsp90-M and the Hsp90-C domain, which involves a highly negatively charged interaction surface (Hagn et al., 2011; Park et al., 2011). Consistent with earlier reports (Jakob et al., 1995; Nathan et al., 1997), the above-mentioned Hsp90 clients seem to bind in a folded or partially folded state. However, for p53-DBD there were also reports that binding of unstructured conformations is preferred (Park et al., 2011; Rüdiger et al., 2002).

A common feature of Hsp90 clients seems their stimulatory effect on the Hsp90-ATPase (McLaughlin et al., 2002; Motojima-Miyazaki et al., 2010; Street et al., 2011) demonstrating their impact on the conformational equilibrium of Hsp90 in addition to the influence of Hsp90 co-chaperones or post-translational modifications on the Hsp90 cycle (see 1.3.3). However, only few examples were studied so far and it has to be investigated whether this holds true for every client. From this perspective, it seems likely that each particular Hsp90 client adjusts the conformational cycle of Hsp90 for its specific needs with contributing co-chaperones and post-translational modifications.

1.4 The glucocorticoid receptor

The glucocorticoid receptor (GR) is a ubiquitously expressed, ligand-activated transcription factor. Its ligands, the glucocorticoids (GC), are the major stress hormones released by the hypothalamic-pituitary-adrenal (HPA) axis. They regulate a variety of cellular processes including reproduction, development and metabolism (Heitzer et al., 2007). GCs (natural or synthetic) display also immuno-suppressive - and anti-tumor proliferation profiles and are thus widely applied in therapy (Fuhrmann et al., 1998; Rhen and Cidlowski, 2005).
GR belongs to the steroid hormone receptors (SHRs), a sub-family of nuclear receptors (NRs) that comprises also the progesterone receptor (PR), the estrogen receptor (ER), the androgen receptor (AR) and the mineralocorticoid receptor (MR) as well as the ERR (estrogen-receptor-related receptor) orphan receptors (Escriva et al., 2004). In its inactive state, GR resides predominantly in the cytoplasm in a multimeric chaperone complex (compare 1.4.2). Ligand binding activates the receptor and leads to translocation of the GR into the nucleus where it acts as a transcription factor (Pratt and Toft, 1997).

1.4.1 Architecture of the glucocorticoid receptor

In 1985, the first cDNA of human GR was isolated by Evans and colleagues (Hollenberg et al., 1985). Two closely related receptor isoforms exist, termed GRα and GRβ. Both splice variants are identical up to amino acid 727, but then they differ in their sequence, with GRα encoding for additional 50 and GRβ comprising additional 15 non-homologous amino acids at its C-terminus (Nicolaides et al., 2010). GRα is the predominant physiological form and is referred as the classical GR that binds GCs and activates or represses its target genes. GRβ on the other hand, does not bind GCs and its physiological role is largely unknown (Kino and Chrousos, 2004). GRα, from now on referred as GR, possesses a modular structure with 5 regions (Figure 8A): An N-terminal A/B region (N-terminal domain, GR-NTD), and a C, D and E region which correspond to the DNA-binding domain (GR-DBD), the hinge region (GR-hinge) and the ligand binding domain (GR-LBD) (Kino et al., 2002).
The N-terminal domain (1-420) comprises a ligand-independent activation function (AF-1) that facilitates transcriptional activity by recruiting co-regulators, chromatin modulators and basal transcription factors. The GR-NTD contains also several amino acids which are susceptible to post-translational modifications such as phosphorylation and sumoylation which affect transcriptional activity (Nicolaides et al., 2010). To date, no three-dimensional

structure of the GR-NTD or its AF-1 is available. Structurally, the individual AF-1 domain exists in an intrinsically disordered state *in vitro*. However, recent evidence suggests that the AF-1 domain becomes folded upon interaction with the transcriptional machinery *in vivo* (Kumar and Thompson, 2012).

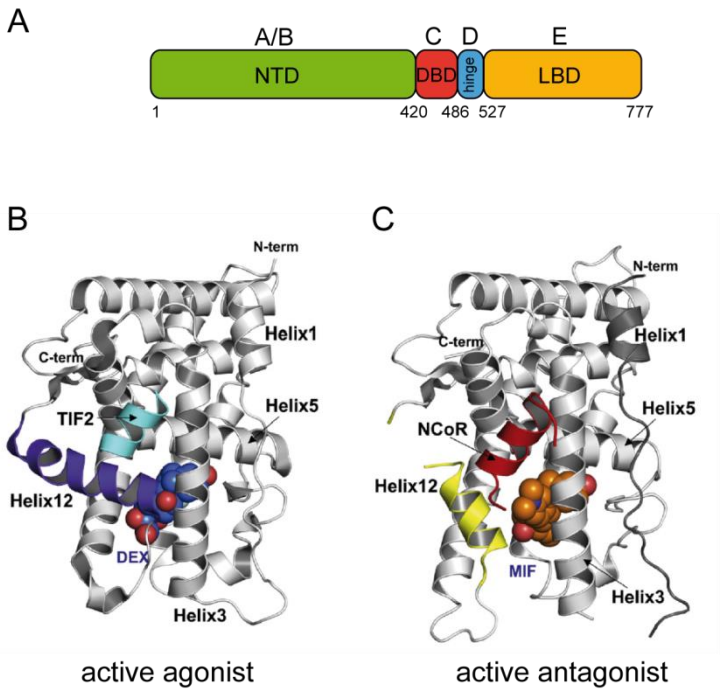

Figure 8 Architecture of the glucocorticoid receptor. A) Schematic domain representation. Domain regions A-E include the N-terminal domain (GR-NTD), the DNA binding domain (GR-DBD), and a hinge region (GR-hinge) as well as a ligand binding domain (GR-LBD). Domain borders as indicated. B) Structure of GR-LBD-F602S in its agonist conformation with bound co-activator peptide Tif2 as indicated. C) Structure of GR-LBD-F602S, C638D, W712S in its antagonist conformation with bound co-repressor peptide NcoR as indicated. The position of helix 12 occupies different locations upon agonist (dexamethasone, DEX) or antagonist (mifepristone, MIF) binding and thus creates compatible interaction sites for co-regulators. Note, also intermediate GR-LBD conformations were reported such as partial agonist or passive antagonist states. Adopted from Schoch et al., (2010).

The GR-DBD (421-485) mediates receptor binding to specific DNA sequences named glucocorticoid-response elements (GREs) within promoter regions of GR target genes. These GRE elements contain two inverted, hexameric repeat AGAACA sequences, separated by three nucleotides which provide high-affinity receptor binding (John et al., 2011). The globular structure of the GR-DBD is highly conserved among other NR members and contains two Cys_4-Zn clusters and two α-helices of which one helix is involved in site-specific DNA binding (Luisi et al., 1991). Moreover, the GR-DBD contains a defined set of amino acids that facilitate receptor dimerization upon association with DNA which is believed to be a general prerequisite for GR activity. However, dimerization seems to occur mainly on activating GREs, as repressive elements (nGREs) were shown to promote binding of GR in an orientation in which the GR dimerization interface of each GR monomer is directed away from the other one (Hudson et al., 2013).

The GR-LBD (527-777) is the second highly conserved region among members of the NR family. The GR-LBD facilitates binding of GCs and contains also the AF-2 transactivation sub-domain. The AF-2 domain is important for transcriptional activity. It interacts with numerous co-activators (such as Tif2) or co-repressors (such as NcoR) which are part of the transcriptional machinery (see 1.4.4 and Figure 8B, C) (Kumar et al., 2004). For a long time, the high intrinsic instability of the individual GR-LBD has hindered its structural elucidation. In 2002, Bledsoe and coworkers achieved a breakthrough by mutating phenylalanine to serine in helix 5 (F602S) which significantly improved the solubility and stability of the GR-LBD that in turn allowed the determination of its three-dimensional structure in its hormone-bound state (Bledsoe et al., 2002) (Figure 8B). The GR-LBD consists of 12 α-helices and four small β-strands which form a globular, three layer helical fold that comprises the central hormone binding pocket. The C-terminal helix at the very end of the GR-LBD (helix 12 or AF-2 helix) is believed to close the cavity upon hormone binding resulting in an interaction surface for co-regulators. Receptor-bound agonist (such as dexamethasone, DEX) and antagonist (such as mifepristone, MIF), respectively, alter the conformation of helix 12 (Figure 8B, C) which modulates the affinity for co-regulators and thus may switch the receptor response from a gene activator- towards a gene repressor function (Schoch et al., 2010) (compare 1.4.4).

1.4.2 Maturation of the glucocorticoid receptor

The glucocorticoid receptor is among other SHRs the most stringent Hsp90 client. GR function *in vivo* strictly depends on the physical interaction with Hsp90 (Picard et al., 1990) which is governed by the GR-LBD (Figure 8A) (Howard et al., 1990).

Its complex maturation pathway involves the Hsp90 and Hsp70 chaperone machinery and has been established by reconstitution experiments with apo-receptor-Hsp90 complexes that were initially immuno-adsorbed from eukaryotic cells (Pratt and Toft, 1997). Early studies showed that GR loses its hormone binding ability upon Hsp90 removal by high salt solutions. High-affinity ligand binding can be restored by the addition of concentrated eukaryotic cell lysates (e.g. rabbit reticulocyte lysate). Later on, the five active components and their sequential mode of action for efficient GR hetero-complex assembly and restoration of the steroid-binding ability were established. The so-called minimal system includes Hsp90, Hsp70, Hsp40, Hop and p23 (Morishima et al., 2000; Pratt and Dittmar, 1998).

A current model (Grad and Picard, 2007) proposes that, in the first step, Hsp40 acts on *de novo* synthesized GR as it was demonstrated for the progesterone receptor (Hernandez et al., 2002) (Figure 9).

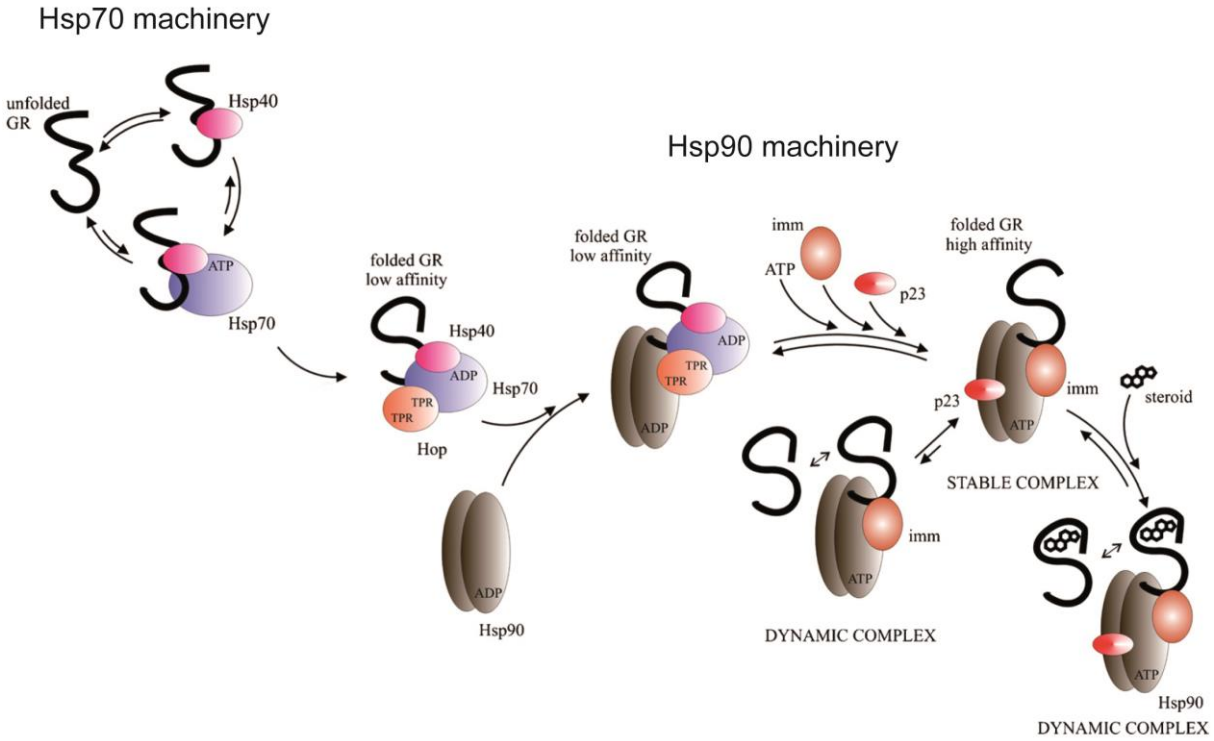

Figure 9 Maturation of the glucocorticoid receptor. In the first step, Hsp40 recruits GR to Hsp70. In an ATP-dependent reaction, the receptor is pre-folded and the steroid binding cleft is primed. The GR-Hsp70-ADP complex is then transferred to Hsp90 through Hop which links the Hsp70 machinery to Hsp90. Binding of ATP together with the entry of PPIases weakens the affinity for Hsp70 and Hop which results in their release. The ligand binding cleft of the GR-LBD is now opened and allows high-affinity hormone binding. p23 binding stabilizes the complex. Ligand binding may, according to Pratt (Pratt et al., 2008), shift the equilibrium from stable hetero-complexes to dynamic GR-Hsp90 complexes that either dissociate or translocate into the nucleus. Adopted and modified from Grad and Picard, (2007).

In the next step, Hsp40 loads GR on Hsp70, which binds the client in an ATP-dependent reaction. During assembly with the Hsp70 machinery, the ligand binding cleft is preformed (‘primed’) (Pratt et al., 2008). Different Hsp70 co-chaperones such as Bag-1, Hip or CHIP may act on the GR-Hsp70-ADP complex and modulate GR activation or even promote its degradation (Hohfeld et al., 1995; Kullmann et al., 1998; Luders et al., 2000; McDonough and Patterson, 2003). The transfer of the client to Hsp90 is achieved through Hop (see 1.3.3), which connects the Hsp70 system with the Hsp90 machinery (Chen and Smith, 1998). ATP binding to Hsp90 and subsequent release of Hsp70 and Hsp40 leads to an opening of the steroid binding cleft and allow high-affinity ligand binding (Grenert et al., 1997; Pratt et al., 2008). Finally, together with the exchange of Hop by PPIases like FKBPs, Cyp40 or PP5 which seem to promote Hsp90 cycle progression and trafficking of the receptor, the hetero-

complex is stabilized by p23 (Dittmar et al., 1997; Li et al., 2011; Prodromou et al., 1999; Ratajczak et al., 2003; Vandevyver et al., 2012) (see also 1.3.3). Whether Hsp90 dissociates from hormone-bound GR prior to its translocation into the nucleus is currently under debate. Although a hormone-dependent Hsp90 release mechanism would explain why immuno-adsorbed holo-receptors contain no associated Hsp90 (Pratt and Toft, 1997), the proposed mechanism has to be very likely revised based on the current literature evidence (see 1.4.3 and 1.4.4). To explain the above-mentioned observations, Pratt and co-workers suggested a model in which hormone binding triggers the closing of the binding cleft that converts the receptor complex from stable to dynamic cycling with Hsp90 (Pratt et al., 2008) (Figure 9).

1.4.3 Trafficking of the glucocorticoid receptor

It has been believed for a very long time, that hormone binding triggers receptor dissociation from hetero-complexes, and that this process - referred as 'receptor transformation' - is the first mandatory step for its nuclear import (Pratt and Toft, 1997). It was suggested, that nuclear localization signals (NLSs) at the GR-LBD and at the GR-hinge region (see Figure 8A) are unmasked upon Hsp90 release and that this allows the interaction with nuclear import receptors (importins) which in turn govern GR transport into the nucleus (Freedman and Yamamoto, 2004; Picard and Yamamoto, 1987). However, it could be shown that addition of geldanamycin (GA) decreased the rate of nuclear translocation by a factor of 10 ($t_{1/2}$ = 0.5 min^{-1} in the absence of GA and $t_{1/2}$ = 40-60 min^{-1} in the presence of GA, respectively) (Galigniana et al., 2010). This suggested a second, more efficient translocation pathway besides the simple diffusion mechanism. It was also shown that dynein motor complexes co-immunoprecipitate with Hsp90, FKBP52 and GR, which implicated these motor proteins in trafficking of GR together with Hsp90 and FKBP52 into the nucleus (Galigniana et al., 2001). These studies among others (Echeverria et al., 2009; Galigniana et al., 2004; Galigniana et al., 2002; Tao et al., 2006) established a model for retrograde movement of the receptor on microtubule tracks (Vandevyver et al., 2012) (Figure 10).

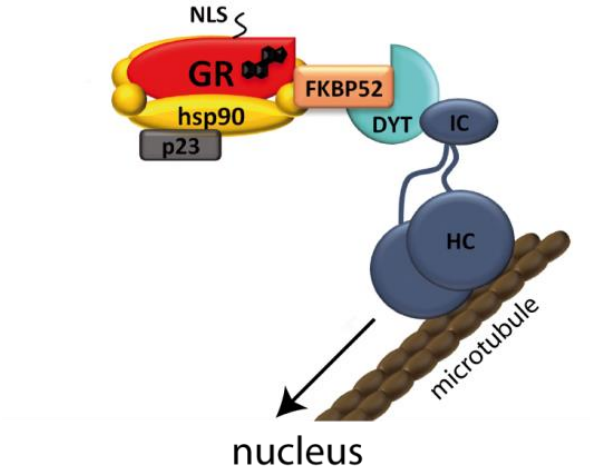

Figure 10 Efficient transport of the GR along microtubule tracks. The final GR hetero-complex is linked to dynein which guides movement into the nucleus along microtubules. (DYT) dynamitin, (IC) interchain of dynein, (HC) heavy chain of dynein, (NLS) nuclear localization signal. Adopted from Vandevyver et al., (2012).

1.4.4 Transcriptional regulation of the glucocorticoid receptor

In the nucleus, the holo-glucocorticoid receptor facilitates the activation and repression of many target genes. These processes are highly complex and involve a wide array of components (Acevedo and Kraus, 2004; Moehren et al., 2004). For gene activation, GR binds GRE elements within the chromatin structure through its GR-DBD (Figure 11A). To stimulate target gene expression, this initial complex recruits co-activators to the GR that possess chromatin remodeling- , histone-, or factor modifying activities, which nucleate the interaction with the basal RNA polymerase II transcription machinery (Lemon and Tjian, 2000). Examples of these scaffolding steroid receptor co-activators (SRCs) are SRC-1, SRC-2 (Tif2) or SRC-3 (RAC3). They show a common LXXLL-motif which allows direct interaction with the ligand binding domain of agonist-bound GR (Figure 8B) (Bledsoe et al., 2002; Heery et al., 1997). In addition, they seem to possess another region that mediates binding to the AF-1 in the GR-NTD (Khan et al., 2012).

Gene repression through GR is mediated by a variety of mechanisms (Figure 11B). These include the inhibition of other signaling pathways by GR (cross-talk) (McKay and Cidlowski, 1999), negative response elements (Surjit et al., 2011) or co-repressor binding (Burke and Baniahmad, 2000). Repression can be also facilitated through binding of anti-hormones (antagonists) to the GR-LBD. Mifepristone is a typical example with anti-glucocorticoid properties. It is also an effective PR, ER and AR antagonist and is applied in prostate- and breast cancer therapies (Fuhrmann et al., 1998). Further, as powerful anti-progesterone, it is also used in combination with prostaglandins for medical abortion (Spitz, 2010).

Co-repressors such as SMRT or NcoR possess a hydrophobic ΦXXΦΦ-motif (Φ is any hydrophobic amino acid) (Nagy et al., 1999) that contacts the GR-LBD in the presence of an antagonist (e.g. mifepristone) (Figure 8C) and most likely also in the absence of ligand, as it was shown for several other nuclear receptors like the thyroid hormone receptor (Horlein et al., 1995; Schoch et al., 2010). Considering studies with the androgen receptor (Hodgson et al., 2008), it seems likely that similar to co-activators also co-repressors can bind to the AF-1 in the GR-NTD to mediate gene repression.

Besides co-regulators, also molecular chaperones such as Hsp90 and p23 have been shown to modulate GR transcriptional activity (Freeman et al., 2000; Freeman and Yamamoto, 2002). In this respect, the Hsp90 machinery seems to recycle GR after termination of transcription, whereas Hsp70 promotes its degradation in concert with the proteasomal system and additional factors (compare 1.4.2) (Grad and Picard, 2007; Pratt et al., 2004).

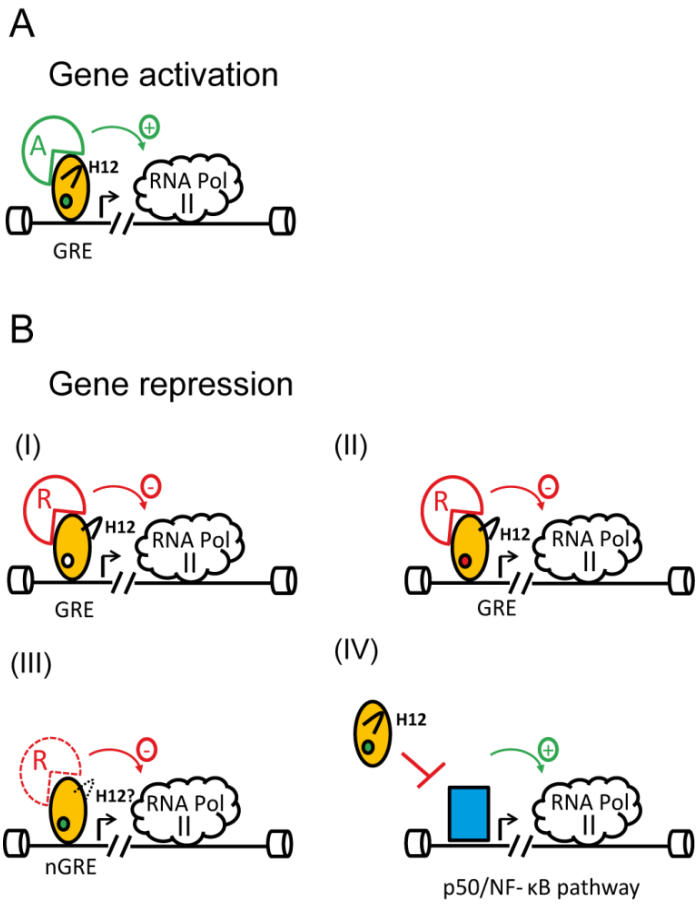

Figure 11 Regulation of the transcriptional activity of the glucocorticoid receptor by co-regulators that act at the GR-LBD. A) Gene activation. Agonist binding induces a conformation of helix 12 of the GR-LBD that allows the co-activator to bind which in turn recruits the RNA polymerase II transcription machinery. See also Figure 8B. B) Gene repression. (I) GR with an open ligand binding pocket is transcriptional inactive in complex with a co-repressor. (II) Antagonist-bound receptor is inactivated through a co-repressor that blocks the assembly of the transcription machinery. The antagonist induces repositioning of helix 12 (H12) of GR-LBD that allows co-repressor binding. Compare also Figure 8C. The conformation of helix 12 might be similar to that seen in the apo-GR-LBD (I). (III) Gene repression upon binding to negative GREs (nGRE). GR is bound in a head-to-tail fashion by nGREs, which might modulate conformational changes within the GR-LBD enabling co-repressor binding even with a bound agonist (compare 1.4.1). (IV) Agonist-bound GR blocks the NF-κB signal pathway via cross talk. (orange) GR-LBD, (green circle) agonist, (red circle) antagonist, (open circle) ligand-free binding cleft, (A) co-activator, (R) co-repressor and (RNA Pol II) RNA polymerase II transcription machinery.

2 Objective

The glucocorticoid receptor (GR) is one of the major Hsp90 clients. In order to become functional as hormone-dependent transcription factor, it has to assemble with the Hsp70- and Hsp90 chaperone machinery. Much effort has been spent to elucidate its complex relationship with both chaperone systems. The picture that emerged from these studies showed how its maturation pathway and retrograde transport as well as its transcriptional activity are regulated by molecular chaperones. However, the molecular details of the intricate interplay between GR and Hsp90 remained elusive and were thus focus of the present thesis.

The first aim of this work was to establish a robust expression and purification system for GR and its respective domain fragments. Besides recombinant expression analysis using *E. coli* or insect cells, refolding experiments should be carried out to explore possibilities for functional GR production. Once recombinant and functional protein was available, reconstitution experiments with purified components should be performed to dissect the essential parameters for the formation of functional GR-Hsp90 complexes. As Hsp90 is a highly dynamic protein that undergoes dramatic conformational rearrangements during its ATPase cycle, the client loading conformation and the influence of Hsp90 co-chaperones should be investigated. Also, the impact of Hsp90 on GR should be analyzed to answer the question, how the chaperone mediates the changes in GR conformation that govern its transformation from its low-affinity- to its high-affinity binding state. Finally, the GR binding-site on Hsp90 should be addressed by structural methods to provide new insights in how Hsp90 recognizes and activates its client.

3 Material and Methods

3.1 Material

3.1.1 Microorganisms and cell lines

The following strains and cell lines were used (Table 1).

Table 1 Strains and cell lines

Organism	Genotype	Source
E. coli Mach1	F^- Φ80(Δ*lac*Z)ΔM15 Δ*lac*X74 *hsd*R(r_K^- m_K^+) Δ*rec*A1398 *end*A1 *ton*A	Invitrogen (Karlsruhe, Germany)
E. coli DH10B	F^- *mcr*A Δ(*mrr-hsd*RMS-*mcr*BC) Φ80*lac*ZΔM15 Δ*lac*X74 *rec*A1 *end*A1 *ara*D139 Δ(*ara,leu*)7697 *gal*U *gal*K λ^- *rps*L *nup*G	Invitrogen (Karlsruhe, Germany)
E. coli BL21-CodonPlus(DE3)-RIL	F^- *omp*T *hsd*S($r_B^-m_B^-$) *dcm*$^+$ Tet^r *gal* λ(DE3) *end*A Hte [*arg*U *ile*Y *leu*W Cam^r]	Stratagene (La Jolla, USA)
E. coli HB101	F^- *thi*-1 *hsd*S20(r_B^- m_B^-) *sup*E44 *rec*A13 *ara*-14 *leu*B6 *pro*A2 *lac*Y1 *gal*K2 *rps*L20(Str^r) *xyl*-5 *mtl*-1	Promega (Madison, USA)
E. coli DH10Bac	F^- *mcr*A Δ(mrr-*hsd*RMS-*mcr*BC) Φ80*lac*ZΔM15 Δ*lac*X74 *rec*A1 *end*A1 *ara*D139 Δ(*ara, leu*) 7697 *gal*U *gal*K λ^- *rps*L *nup*G/ pMON14272 / pMON7124	Invitrogen (Karlsruhe, Germany)
S. cerivisae BY4741	MATa *his3Δ0 leu2Δ0 met15Δ0 ura3Δ0*	Euroscarf (Frankfurt, Germany)
Spodoptera frugiperda Sf9	clonal isolate of IPLBSF21 - AE (Sf21)	Invitrogen (Karlsruhe, Germany)

3.1.2 Chemicals

Common laboratory chemicals were purchased from Roth (Karlsruhe, Germany) or Merck (Darmstadt, Germany) and were of p.a. grade. Buffers and media were prepared with deionized H_2O.

Media	
LB-medium powder	Serva (Heidelberg, Germany)
Agar Agar	Serva (Heidelberg, Germany)
Bacto Tryptone	Difco (Detroit, USA)
Bacto Yeast extract	Difco (Detroit, USA)
Bacto Peptone	Difco (Detroit, USA)
Yeast Nitrogene Base	Difco (Detroit, USA)
YPD- medium powder	Roth (Karlsruhe, Germany)
Antibiotics	
Ampicillin	Roth (Karlsruhe, Germany)
Kanamycin	Roth (Karlsruhe, Germany)
Chloramphenicol	Roth (Karlsruhe, Germany)
Tetracycline	Roth (Karlsruhe, Germany)
Gentamicin	Roth (Karlsruhe, Germany)
Nucleotides	
Adenosin-5`-[γ-thio]-triphosphate (ATPγS) tetralithium salt	Roche Diagnostic GmbH (Mannheim, Germany)
Adenosin-5`-triphosphate (ATP)	Roche Diagnostic GmbH (Mannheim, Germany)
Adenosine-5´-diphosphate (ADP), Disodium salt	Roche Diagnostic GmbH, Mannheim, Germany
5'–Adenylyl-ß,γ-imido-diphosphate (AMP-PNP)	Roche Diagnostic GmbH (Mannheim, Germany)
Deoxyadenosine triphosphate (dATP)	Roth (Karlsruhe, Germany)
Deoxycytidine triphosphate (dCTP)	Roth (Karlsruhe, Germany)
Deoxyguanosine triphosphate (dGTP)	Roth (Karlsruhe, Germany)
Deoxythymidine triphosphate (dTTP)	Roth (Karlsruhe, Germany)
Fluorophores	
ATTO488-maleimid	ATTO-TEC (Siegen, Germany)
ATTO550-maleimid	ATTO-TEC (Siegen, Germany)
HaloTag TMR Ligand	Promega (Madison, USA)

Miscellaneous reagents	
11-Deoxycorticosterone (DOC)	Sigma (St. Louis, USA)
Dexamethasone (DEX)	Sigma (St. Louis, USA)
Dexamethasone Fluorescein (F-DEX)	Sigma (St. Louis, USA)
Dimethylsulfoxide (DMSO)	Sigma (St. Louis, USA)
3-[(3-Cholamidopropyl)dimethylammonio]-1-propanesulfonate (CHAPS)	Roth (Karlsruhe, Germany)
Isopropyl-β-D-thiogalactopyranoside (IPTG)	Roth (Karlsruhe, Germany)
Acrylamide (38 %, 2 % Bisacrylamide)	Serva (Heidelberg, Germany)
Sodium dodecyl sulfate (SDS)	Roth (Karlsruhe, Germany)
Ammoniumperoxodisulfate (APS)	Roth (Karlsruhe, Germany)
Tetramethylethylenediamine (TEMED)	Roth (Karlsruhe, Germany)
Bromphenolblue S	Serva (Heidelberg, Germany)
Coomassie Brilliant Blue R-250	Serva (Heidelberg, Germany)
Milk powder (blotting grade)	Roth (Karlsruhe, Germany)
Polyoxyethylen (20) sorbitan monolaurate (Tween 20)	Merck (Darmstadt, Germany)
Ethidium bromide	Sigma (St. Louis, USA)
Serva DNA Stain G	Serva (Heidelberg, Germany)
Xylencyanol	Serva (Heidelberg, Germany)
Nicotinamideadenine dinucleotide (NADH)	Roche Diagnostic GmbH (Mannheim, Germany)
Phosphoenolpyruvate (PEP)	Roche Diagnostic GmbH (Mannheim, Germany)
Protease Inhibitor Mix HP, Protease Inhibitor Mix FY	Serva (Heidelberg, Germany)
Protease Inhibitor Cocktail	Sigma (St. Louis, USA)
O-nitrophenyl-β-d-galactopyranoside (ONPG)	Sigma (St. Louis, USA)
Salmon sperm DNA	Sigma (St. Louis, USA)
Cellfectin II reagent	Invitrogen (Karlsruhe, Germany)
Blue-Gal	Sigma (St. Louis, USA)
Antifoam A	Sigma-Aldrich (St. Louis, USA)
Arginine	Sigma (St. Louis, USA)
Glutamine	Sigma (St. Louis, USA)
Triton X-100	Merck (Darmstadt, Germany)
Zwittergent 3-12	Merck (Darmstadt, Germany)
1,4-Dithithreitol (DTT)	Roth (Karlsruhe, Germany)
Tris-(2-Carboxyethyl)phosphine, hydrochloride (TCEP)	Sigma (St. Louis, USA)
Polyethylene glycol (PEG-6000 / 4000)	Merck (Darmstadt, Germany)
Thiamin hydrochloride	Sigma (St. Louis, USA)
Biotin	Sigma (St. Louis, USA)
Ammonium-15N chloride ($^{15}NH_4Cl$)	Cambridge Isotope Laboratories, Inc. (Andover, USA)

3.1.3 Buffers and solutions

Molecular biology

TAE (50X)	2 M	Tris/acetate pH 8,0
	50 mM	EDTA
DNA loading buffer	50 % (v/v)	Glycerol
	10 mM	EDTA pH 8.0
	0.2 % (w/v)	Bromphenolblue
	0.2 % (w/v)	Xylencyanol
Agarose solution	0.8-2 % (w/v)	Agarose
	100 ml	TAE (1x)
	1-2 µl	Serva DNA Stain G or Ethidiumbromide
dNTPs	10 mM	dATP
	10 mM	dGTP
	10 mM	dCTP
	10 mM	dTTP
CC solution	13 ml	3 M NaAc (pH 5.5)
	100 ml	1 M $CaCl_2$
	25 ml	2.8 M $MnCl_2$
	862 ml	H_2O
CC solution + glycerol	69 ml	Glycerol (87 %)
	331 ml	CC solution
Bacmid solution 1	15 mM	Tris pH 8.0
	10 mM	EDTA
	100 µg/ml	RNase A
Bacmid solution 2	0.2 M	NaOH
	1 % (w/v)	SDS
2X Quick ligation buffer	132 mM	Tris, pH 7.6
	20 mM	$MgCl_2$
	2 mM	DTT
	2 mM	ATP
	15 %	PEG-6000

SDS-PAGE and Western blotting

SDS running buffer (10X)	250 mM	Tris, pH 6.8
	2 M	Glycine
	1 % (w/v)	SDS
Laemmli sample buffer (5X)	312.5 mM	Tris, pH 6.8
	10 % (w/v)	SDS
	50 % (v/v)	Glycerol
	2.5 % (v/v)	β-Mercaptoethanol
	0.05 % (w/v)	Bromphenolblue

Fairbanks A	2.5 g 250 ml 80 ml ad 1l	Coomassie Brilliant Blue R-250 Ethanol Acetic acid H_2O
Fairbanks D	250 ml 80 ml ad 1l	Ethanol Acetic acid H_2O
WB transfer buffer	36 g 7.6 g 500 ml 0.3 % (w/v) ad 2.5 l	Glycine Tris Methanol SDS H_2O pH 8.3
PBS (10X)	40 mM 160 mM 1.15 M	KH_2PO_4 Na_2HPO_4 NaCl pH 7.4
PBST	0.1 % (v/v)	Tween-20 PBS (1X)
Blocking buffer 1	5 % (w/v)	Milk powder PBST
Blocking buffer 2	3 % (w/v)	BSA PBST
Blocking buffer 3	2 µg/ml	Avidin PBST

3.1.4 Plasmids

The following plasmids were used or created (Table 2).

Table 2 Plasmids

No.	Name	Insert/Cloning site	Origin
1	pET28b		Merck Biosciences GmbH (Schwalbach, Germany)
2	pGEX-4T1		GE Healthcare (Freiburg, Germany)
3	pHTN HaloTag CMV-neo		Promega (Madison, USA)
4	pMAL-C2X		New England Biolabs (Beverly, USA)
5	pT-TRX		Yasukawa et al., (1995)
6	peGFP		Clontech Laboratories, Inc. (Mountain View, USA)
7	pFASTBAC		Invitrogen (Karlsruhe, Germany)
8	p413-GPD		Mumberg et al., (1995)
9	pETGST	GST, NdeI/BamHI	This work
10	pETMBP	His_6-MBP, BbsI(NcoI)/BamHI	This work
11	pETSUMOmod	His_6-Sumo, BbsI(NcoI)/BamHI	This work
12	pETHALO	Halo, NdeI/BamHI	This work
13	pET-Sumo protease (403-621)		Alexander Bepperling
14	pMal-C2-Tev protease (S219P)		Addgene (Cambridge, USA)
15	pET28-yHsp90		Klaus Richter
16	pET28-huHsp90ß		Klaus Richter
17	pET28-yAha1		Klaus Richter
18	pET23-yp23		Brian Freeman
19	pRSETA-Cyp40 (Cpr6)		Chrisostomos Prodromou
20	pET28-huGR	huGR, NcoI/XhoI	This work
21	pETSUMO-huGR-LBD		Andreas Schmid
22	pMAL-SUMO-huGR-LBD		Andreas Schmid
23	pETHALO-huGR-LBD (wt and mutants)	huGR-LBD, BamHI/XhoI	This work
24	pETGST-huGR-LBD	huGR-LBD BamHI/XhoI	This work
25	pETSUMO-huGR-LBD-Sumo	huGR-LBD-Sumo, BamHI/XhoI	This work
26	pETSUMO-huGR-LBD-Trx	huGR-LBD-Trx, BamHI/XhoI	This work

27	pETSUMO-huGR-LBD-eGFP	huGR-LBD-eGFP, BamHI/XhoI	This work
28	pETMBP-huGR-LBD-SUMO	huGR-LBD-Sumo, BamHI/XhoI	This work
29	pETMBP-huGR-LBD-Trx	huGR-LBD-Trx, BamHI/XhoI	This work
30	pETMBP-huGR-LBD-eGFP	huGR-LBD-eGFP, BamHI/XhoI	This work
31	pFASTBAC-GST-huGR-LBD	His_6-GST-huGR-LBD,BbsI (BamHI)/XhoI	This work
32	p413GPD-huGR (wt and mutants)	huGR, BamHI/XhoI	This work
33	pUCΔSS-26X		Louvion et al., (1996)

3.1.5 DNA oligonucleotides

The following oligonucleotides were used for cloning (Table 3).

Table 3 DNA oligonucleotides

	Primer	Sequence (5‘-3‘)
1	GST-NdeI-FWD	GATCGTCATATGTCCCCTATACTAGGTTATTG
2	GST-BamHI-REV	ACGATCGGATCC ATCCGATTTTGGAGGATG
3	MBP-His-BbsI-FWD2	GATCGTGAAGACGCCATGGGCAGCCATCACCATCAC CATCACAGCAGCGGCATGAAAATC
4	MBP-His-FWD1	ATCACCATCACAGCAGCGGCATGAAAATCGAAGAAG GTAAAC
5	MBP-BamHI-REV	GATCTGGGATCCGAATTCTGAAATCC
6	Sumo-His-BbsI-FWD2	GATCGTGAAGACGCCATGGGCAGCCATCACCATCAC CATCACTCTTCTGGCATGTC
7	Sumo-His-FWD1	ATCACCATCACTCTTCTGGCATGTCGGACTCAGAAGT C
8	Sumo-BamHI-REV	GATCTGGGATCCACCAATCTGTTCTCTG
9	NHalo-NdeI-FWD	GATCGTCATATGGCAGAAATCGGTACTGGCTTTCC
10	NHalo-BamHI-REV	GATCTGGGATCCGCCGGAAATCTCCAGCGTCGACA
11	EGFP-Thr-FWD	AGCGGCCTGGTGCCGCGCGGCAGCATGGTGAGCAAG GGCGAGGAGC
12	EGFP-StrepII-REV1	GAACTGCGGGTGGCTCCAGCCGCTCTTGTACAGCTCG TCCATGCCGAGAGTG
13	Sumo-Thr-FWD	AGCGGCCTGGTGCCGCGCGGCAGCATGTCGGACTCA GAAGTCAATC
14	Sumo-StrepII-REV1	GAACTGCGGGTGGCTCCAGCCGCTTCCACCAATCTGT TCTCTG
15	Trx-Thr-FWD1	AGCGGCCTGGTGCCGCGCGGCAGCATGAGCGATAAA ATTATTCACCTGAC

16	Trx-StrepII-REV1	GAACTGCGGGTGGCTCCAGCCGCTGGCCAGGTTAGCGTCGAGGAAC
17	MBP-Thr-FWD1	AGCGGCCTGGTGCCGCGCGGCAGCATGAAAATCGAAGAAGGTAAAC
18	MBP-StrepII-REV1	GAACTGCGGGTGGCTCCAGCCGCTAGTCTGCGCGTCTTTCAGG
19	Fus-StrepII-XhoI-REV2	GATCTGCTCGAGTCATTTTTCGAACTGCGGGTGGCTCCAGC
20	GR-LBD-BamHI-FWD	GATCGTGGATCCCAACTCACCCCTACCCTGGTGTCAC
21	GR-LBD-Thr-REV	GCTGCCGCGCGGCACCAGGCCGCTCTTTTGATGAAACAGAAGTTTTTTGATATTTC
22	GR-LBD-TEV-BamHI-FWD	GATCGTGGATCCGAAAACCTGTATTTTCAGTCTCAACTACCCCTACCCTGGTGTCAC
23	GST-BbsI-FWD	GATCGTGAAGACAGGATCCATGGGCAGCAGCCATCATCATCATCATCACAG
24	GRFL-XhoI-REV	GATCTGCTCGAGTCACTTTTGATGAAACAGAAGTTTTTGAATTTCC
25	GRFL-NcoI-FWD	GATCGTCCATGGGCTCCGACTCCAAAGAATCATTAAC
26	GRFL-BamHI-FWD	GATCGTGGATCCAACAAAATGGACTCCAAAGAATCATTAACTCCTGGTAGAG
27	GR-F602S-FWD	GTACTCCTGGATGTCCCTTATGGCATTTGCTCTGGGG
28	GR-F602S-REV	AAATGCCATAAGGGACATCCAGGAGTACTGCAGTAGGG
29	GR-A605V-FWD	ATGTTTCTTATGGTGTTTGCTCTGGGGTGGAGATC
30	GR-A605V-REV	CCCCAGAGCAAACACCATAAGAAACATCCAGGAG
31	GR-F602S-A605V-FWD	CCTGGATGTCCCTTATGGTGTTTGCTCTGGGGTGGAGATC
32	GR-F602S-A605V-REV	GAGCAAACACCATAAGGGACATCCAGGAGTACTGCAGTAG
33	GR-M752T-FWD	CCCCGAGACCTTAGCTGAAATCATCACC
34	GR-M752T-REV	CAGCTAAGGTCTCGGGGAATTCAATACTC
35	GR-V702A-FWD	GCCATTGCGAAGAGGGAAGGAAACTCCAGC
36	GR-V702A-REV	CCCTCTTCGCAATGGCTTTTCCTAGCTCTTTG
37	GR-E705G-FWD	GTCAAGAGGGGCGGAAACTCCAGCCAGAACTGGC
38	GR-E705G-REV	GCTGGAGTTTCCGCCCCTCTTGACAATGGCTTTTCC
39	GR-V702A-E705G-FWD	GCCATTGCGAAGAGGGGCGGAAACTCCAGCCAGAACTGGC
40	GR-V702A-E705G-REV	GTTTCCGCCCCTCTTCGCAATGGCTTTTCCTAGCTCTTTGATGTAGGTCATTC

3.1.6 Media and antibiotics

Media for *E. coli* growth

LB		20 g/l LB-powder For plates: 15 g/l Agar Agar
2YT		17 g/l Bacto Tryptone 10 g/l Bacto Yeast extract 5 g/l NaCl
ZYM-5052 auto induction media	ZY	10 g/l Bacto Tryptone 5 g/l Bacto Yeast extract
	M	25 mM Na_2HPO_4 25 mM KH_2PO_4 50 mM NH_4Cl 5 mM Na_2SO4
	5052	0.5 % Glycerol 0.05 % D(+)-Glucose 0.02 % Lactose monohydrate
	1000X Trace elements*	0.2X
*1000X Trace elements	50 mM $FeCl_3$, 20 mM $CaCl_2$, 10 mM $MnCl_2$ 10 mM $ZnSO_4$, 2 mM $CoCl_2$, 2 mM $CuCl_2$, 2 mM $NiCl_2$, 2 mM Na_2MoO_4, 2 mM Na_2SeO_3, 2 mM H_3BO_3 in 60 mM HCl	
Minimal media (M9)		7.52 g/l Na_2HPO_4 x 2 H_20 3 g/l KH_2PO_4 0.5 g/l NaCl 1 ml 1 M $MgSO_4$ 0.3 ml 1 M $CaCl_2$ 10 ml 0.2 g/ml D(+)-Glucose 1 g $^{15}NH_4Cl$ 1 ml 1 mg/ml Biotin 1 ml 1 mg/ml Thiamine hydrochloride 10 ml 100X Trace metals* ad 1 l H_2O
*100X Trace metals	5 g EDTA, 0.83 g $FeCl_3$ x 6 H_2O, 84 mg $ZnCl_2$, 13 mg $CuCl_2$ x 2 H_2O, 10 mg $CoCl_2$ x 6 H_2O, 10 mg H_3BO_3, 1.35 mg $MnCl_2$ x 4 H_2O ad 1l, pH 7.5	

Media for yeast growth

YPD	50 g/l YPD For plates: 20 g/l Agar Agar
Dropout media (CSM)	6.7 g Yeast nitrogen base 1 ml 1M NaOH 0.87 g selective aa-mix* 20 g D(+)-Glucose ad 1 l For plates: 20 g Agar Agar
*selective aa-mix	0.5 g/l Adenin, 2 g/l Arginin, 2 g/l Aspartat, 2 g/l Histidin, 10 g/l Leucin, 2 g/l Lysin, 2 g/l Methionin, 2 g/l Phenylalanin, 2 g/l Threonin, 2 g/l Tryptophan, 2 g/l Tyrosin, 2 g/l Uracil

Cultivation of Insect cells

Insect Xpress media	purchased from Lonza (Basel, Switzerland)

Antibiotics and working concentration

Ampicillin	100 µg/ml
Kanamycin	50-100 µg/ml
Chloramphenicol	35 µg/ml
Tetracycline	10 µg/ml
Gentamicin	7 µg/ml

3.1.7 Peptides, proteins and reagents

Thermosensitive Alkaline Phosphatase (TSAP)	Promega (Madison, USA)
Restriction enzymes	New England Biolabs (Beverly, USA)
T4-DNA Ligase	Promega (Madison, USA)
DNase I	Roche Diagnostic GmbH (Mannheim, Germany)
RNase A	Sigma (St. Louis, USA)
Bovine serum albumin, 98% electrophoresis (BSA)	Sigma (St. Louis, USA)
Avidin	Sigma (St. Louis, USA)
Lysozyme	Sigma (St. Louis, USA)
Pyruvate kinase suspension	Roche Diagnostic GmbH (Mannheim, Germany)
Lactate dehydrogenase suspension	Roche Diagnostic GmbH (Mannheim, Germany)
Phusion High-Fidelity DNA Polymerase	New England Biolabs (Beverly, USA)
GoTaq DNA Polymerase	Promega (Madison, USA)
Expand High Fidelity PCR System	Roche Diagnostic GmbH (Mannheim,

	Germany)
Tif2, NcoR- peptides (unmodified and fluorescently labeled)	Biomatik (Cambridge, Canada)
GRE-DNA (unmodified and fluorescently labeled)	Eurofins MWG Operon (Ebersberg, Germany)
yeast Sti1	Jing Li, Alina Röhl
Hsp90 domain constructs	Bettina Karolina Zierer, Lee Freiburger
Rabbit reticulocyte Lysate (RLL)	Promega (Madison, USA)
HaloLink Magnetic beads	Promega (Madison, USA)
α-Hsp90 total (4F3.E8)	StressMarq Biosciences Inc. (Victoria, Canada)
α-Hsc70 (1F2-H5)	StressMarq Biosciences Inc. (Victoria, Canada)
α-Hop	Marc Cox
α-Hdj1 (3B9.E6)	StressMarq Biosciences Inc. (Victoria, Canada)
α-p23	Marc Cox
α-GR (P20)	Santa Cruz Biotechnology, Inc. (Dallas, USA)
α-mouse-POD	Sigma (St. Louis, USA)
α-rabbit-POD	Sigma (St. Louis, USA)
StrepTactin-POD conjugate	IBA GmbH (Göttingen, Germany)
α-His-POD	Sigma (St. Louis, USA)

3.1.8 Standards and kits

Low-Range-molecular weight marker (LMW)	Biorad (Munich, Germany)
Calibration proteins for HPLC	GE Healthcare (Freiburg, Germany)
SERVAChrom Protein Standard III	Serva (Heidelberg, Germany)
1 kb DNA ladder	Peqlab (Erlangen, Germany)
Wizard SV Mini-Preps DNA Purification System	Promega (Madison, USA)
Wizard SV Gel and PCR Clean-Up System	Promega (Madison, USA)
ECLplus Western Blotting Detection System	GE Healthcare (Freiburg, Germany)
BCA Protein assay kit	Thermo Scientific (Waltham, USA)
BugBuster Protein Extraction Reagent	Merck (Darmstadt, Germany)

3.1.9 Chromatography material

HisTrap FF (5 ml)	GE Healthcare (Munich, Germany)
His SpinTrap columns	GE Healthcare (Munich, Germany)
HiTrap Heparin HP (5ml)	GE Healthcare (Munich, Germany)
GSTrap FF (5ml)	GE Healthcare (Munich, Germany)
Hydroxyapatite	BioRad (Munich, Germany)
Resource Q (6 ml)	GE Healthcare (Munich, Germany)
HiLoad 16/60 Superdex 75 pg	GE Healthcare (Munich, Germany)
HiLoad 16/60 Superdex 75 pg	GE Healthcare (Munich, Germany)
HiLoad 16/60 Superdex 200 pg	GE Healthcare (Munich, Germany)
HiLoad 16/60 Superdex 200 pg	GE Healthcare (Munich, Germany)
Superdex 200 10/300GL (HPLC)	GE Healthcare (Munich, Germany)
Q-Sepharose	GE Healthcare (Munich, Germany)

3.1.10 Devices and additional material

Spectrophotometers

Spectrophotometer Nanodrop ND-1000 UV/VIS	Peqlab (Erlangen, Germany)
Spectrophotometer Varian Cary 50/100 Bio UV/Vis	Varian (Palo Alto, USA)
Circular Dichroism Spectropolarimeter Jasco J715 including PTC 343 Peltier temperature device	Jasco (Groß-Umstadt, Germany)
Fluoromax 3 Fluorescence Spectrometer equipped with polarizers	Horiba Jobin Yvon GmbH (Bernsheim, Germany)
Analytical balances	
Sartorius 1409 MP	Sartorius (Göttingen, Germany)
Sartorius BL 310	Sartorius (Göttingen, Germany)
Sartorius universal	Sartorius (Göttingen, Germany)
Centrifuges	
Analytical Ultracentrifuge XL-I with absorbance and interference detection systems	BeckmanCoulter (Krefeld, Germany)
Analytical Ultracentrifuge XL-A equipped with absorption and fluorescence detection systems	BeckmanCoulter (Krefeld, Germany) and AVIV Biomedical (Lakewood, USA)
Avanti J-25 and J-26 XP with rotors JA-10 and JA-25.50	BeckmanCoulter (Krefeld, Germany)
BenchtopCentrifuge 5418	Eppendorf (Hamburg, Germany)
Eppendorf Centrifuge 5810	Eppendorf (Hamburg, Germany)
Heraeus Biofuge stratos	Thermo Scientific (Waltham, USA)

Chromatography devices	
Äkta FPLC	GE Healthcare (Munich, Germany)
Shimadzu HPLC system equipped with autosampler	Shimadzu (Munich, Germany)
Gel electrophoresis	
Hoefer Mighty Small dual gel caster	Hoefer (Holliston, USA)
Mighty Small II SE 250/SE 260 electrophoresis unit	Hoefer (Holliston, USA)
Power supply	
Electrophoresis Power Supply – EPS 3501 XL	GE Healthcare (Freiburg, Germany)
Electrophoresis Power Supply – EPS 601	GE Healthcare (Freiburg, Germany)
Electrophoresis Power Supply – EPS 1001	GE Healthcare (Freiburg, Germany)
Fermentation	
Biostat-C Fermenter	Sartorius (Göttingen, Germany)
Plate reader	
Tecan Sunrise	Tecan Group Ltd. (Maennedorf, Switzerland)
PHERAstar Plus with FP module (485/520 nm)	BMG Labtech (Ortenberg, Germany)
Additional equipment	
Fastblot B44	Biometra (Göttingen, Germany)
Cell Disruption System Basic Z	Constant Systems (Warwick, United Kingdom)
40 mL Tissue Grinder, Dounce	Wheaton (Millville, USA)
Bandelin Sonopuls HD2200	Branson (Danbury, USA)
Image Quant 3000, LAS 4000	GE Healthcare (Freiburg, Germany)
EppendorfThermomixer compact	Eppendorf (Hamburg, Germany)
EppendorfThermoStat plus	Eppendorf (Hamburg, Germany)
Freezer Ultra-low temperature C760, -80 °C	New Brunswick Scientific (Nürtingen, Germany)
Homogenizer Heidolph DIAX 900	Heidolph (Kelheim, Germany)
Ice maker 105439	Ziegra (Isernhagen, Germany)
Overhead shaker Heidolph Reax 2	Heidolph (Kelheim, Germany)
Incubator Certomat BS-1	Sartorius (Göttingen, Germany)
Incubator Mytron WB	Mytron (Heiligenstadt, Germany)
Incubator Binder KB 115	Binder GmbH (Tuttlingen, Germany)
Magnetic stirrer Heidolph MR 3001	Heidolph (Kelheim, Germany)
Platform shaker HeidolphPolymax 2040	Heidolph (Kelheim, Germany)
Shaking device Certomat SII, GFL 3005	Sartorius (Göttingen, Germany)
pH-Meter 538 MultiCal	WTW (Weilheim, Germany)
Vortex Heidolph REAX top	Heidolph (Kelheim, Germany)
Mixer Mill MM 400	Retsch (Haan, Germany)

Ribolyser Hybaid Fast Prep FP 120	Thermo Scientific (Waltham, USA)
Thermo cycler MJ Mini Personal	Biorad (Munich, Germany)
Dialysis tubes Spectra/Por (6-8 kDa)	Spectrum (Houston, USA)
Cuvettes	Zefa (Munich, Germany)
PD10 column	GE Healthcare (Munich, Germany)
PVDF membranes	Roth (Karlsruhe, Germany)
Cell culture equipment (plates, flasks, sterile pipettes)	Sarstedt (Newton, USA)
Microscopes	Leica Mikrosysteme Vertrieb GmbH (Wetzlar, Germany) Carl Zeiss Microscopy GmbH (Jena, Germany)

3.1.11 Computer programs

Microsoft Office 2010	Microsoft (Redmond, USA)
Origin 8	OriginLab (Nothampton, USA)
Adobe CS2	Adobe Systems (San Jose, USA)
ProtParamTool	ExPasy (http://www.expasy.ch)
BioEdit 7	Ibis Biosciences (Carlsbad, USA)
Endnote X6	Thomson Reuters (New York City, USA)
Mmass 2.4	http://www.mmass.org

3.2 Molecular biological methods

3.2.1 Purification of DNA

3.2.1.1 Plasmid-DNA and bacmid-DNA isolation from *E. coli* cells

Plasmid-DNA was isolated from *E. coli* using the Wizard SV Mini-Preps DNA Purification System (Promega) according to the manufacturers' instructions. Plasmid-DNA was stored at -20 °C in sterile, deionized H_2O.

To isolate bacmid-DNA, 1.5 ml bacterial culture was pelleted at 16,000 x g for 1 min and resuspended in 300 µl Bacmid solution 1 (3.1.3). Next, 300 µl Bacmid solution 2 was added under gentle mixing. After 5 min of incubation at RT, 300 µl of 3 M potassium acetate (pH 5.5) was added to remove *E. coli* proteins and genomic DNA. In the next step, samples were spun down for 10 min at 16,000 x g and the supernatant was transferred to 800 µl isopropanol. Afterwards, samples were gently inverted and placed on ice. After centrifugation at 16,000 x g for 15 min at RT, the supernatant was removed and the pellet was washed for several times with 500 µl 70 % ethanol. The pellet was dried at RT and dissolved in 40 µl sterile, deionized H_2O. Bacmid-DNA was stored at 4 °C.

3.2.1.2 Agarose gel electrophoresis

For analytic and preparative separation of plasmid-DNA and DNA fragments, 0.8-1 % agarose gels containing Serva DNA Stain G or ethidium bromide were used (3.1.3). Samples were mixed with DNA loading buffer and were separated with a constant voltage of 120 V. After 30-45 min, DNA was visualized using the Image Quant 3000 system (GE Healthcare). The molecular weight standard was a 1 kb ladder (Peqlab).

3.2.1.3 Extraction of DNA from agarose gels and reaction mixtures

DNA bands were excised from agarose gels using a scalpel. Agarose gel elution was carried out using the Wizard SV Gel and PCR Clean-Up System (Promega). DNA from reaction mixtures (e.g. PCR-products, restriction digests) was purified using the same kit.

3.2.2 Determination of DNA concentration

DNA concentration was determined by absorbance (UV/VIS) spectroscopy (see also 3.7.1) at 260 nm using the Nanodrop ND-1000 UV/VIS spectrophotometer (Peqlab). The Lambert-Beer equation applies, with A = absorbance at 260 nm, ε = extinction coefficient at 260 nm [µl x ng^{-1} x cm^{-1}], c = DNA concentration [ng x μl^{-1}], d = layer thickness [cm]:

$$A = \varepsilon \times c \times d$$

Equation 1

The extinction coefficient of double stranded DNA at 260 nm is 0.02 µl ng^{-1} x cm^{-1}. Purity was estimated form the ratio of absorbance at 260 nm and 280 nm (A_{260}/A_{280}).

3.2.3 Polymerase chain reaction (PCR)

PCR was used to amplify DNA fragments. Conditions were adjusted for each polymerase, template DNA and primer pair. PCR products were analyzed by agarose gel electrophoresis (3.2.1.2).

3.2.3.1 Gene amplification

Gene amplification from plasmids or PCR products was carried out using the Expand High Fidelity PCR System (Roche Diagnostic GmbH). The following standard mixture was used:

Template DNA	1-25 ng
dNTPs (10 mM each)	2 µl
Forward primer (100 µM)	1 µl
Reverse primer (100 µM)	1 µl
Expand High Fidelity Buffer (10X, with $MgCl_2$)	10 µl
Expand High Fidelity Enzyme Mix (3.3 U/µl)	1.5 µl
H_2O	ad 100 µl

For gene amplification, samples were placed in a thermocycler (MJ Mini Personal, Biorad) pre-heated to 94 °C (pseudo hot start). After initial denaturation for 1 min at 94 °C, a sequence of 20-30 cycles was repeated (a-c):

a	Denaturation	94 °C	15 s
b	Annealing	X °C	30 s
c	Elongation	72 °C	1-2 min

Final elongation was performed for 5 min at 72 °C. Samples were cooled down to 4 °C after synthesis.

3.2.3.2 Colony-PCR

After transformation of competent *E. coli* cells with ligation products, positive clones can be identified by colony-PCR using insert specific primers. Single colonies were picked from selective agar plates, resuspended in the following reaction mixture and gene amplification was performed as described in 3.2.3.1:

dNTPs (10 mM each)	1 µl
Forward primer (100 µM)	0.1 µl
Reverse primer (100 µM)	0.1 µl
5X Green GoTaq Buffer	4 µl
GoTaq DNA Polymerase (5 U/µl)	0.2 µl
H_2O	ad 20 µl

3.2.3.3 Mutagenesis

For site-directed mutagenesis, Phusion High-Fidelity DNA Polymerase (New England Biolabs) was used. To generate point- or multiple mutants, a primer pair containing the desired mutation(s) was added to the reaction.

Reaction mixture:

Template DNA	10 ng
dNTPs (10 mM each)	1 µl
Forward primer (10 µM)	2.5 µl
Reverse primer (10 µM)	2.5 µl
5X Phusion HF or GC Buffer	10 µl
Phusion DNA Polymerase (2 U/µl)	0.5 µl
DMSO	3 %
H_2O	ad 50 µl

Reaction protocol:

	Initial denaturation	98 °C	1 min
a	Denaturation	98 °C	10 s
b	Annealing	X °C	20 s
c	Elongation	72 °C	2-4 min
Repeat a-c 30x			
	Final elongation	72 °C	10 min
	Storage	4 °C	

3.2.3.4 Overlap extension PCR

To splice two DNA fragments (fragment A, fragment B), overlap extension PCR (OE-PCR) was performed. Fragment A and fragment B were separately PCR-amplified (3.2.3.1) with special primers generating complementary 5' overhangs. Then, both sequences were mixed in a 1:1 molar ratio and subjected to further PCR cycles resulting in hybridization of the two DNA molecules. Joined DNA fragments were amplified by the addition of external primers. OE-PCR was performed with 35 PCR cycles as described in 3.2.3.1 using the Expand High Fidelity PCR System (Roche Diagnostic GmbH) or GoTaq DNA Polymerase (Promega). To splice the fragments efficiently prior to amplification of the joined fragments, primers were added to the reaction after 10-15 cycles were reached.

Standard reaction mixture:

PCR fragment A, PCR fragment B	Molar ratio 1:1, total DNA = 20-30 ng
dNTPs (10 mM each)	2 µl
External forward primer (100 µM)	1 µl
External reverse primer (100 µM)	1 µl
Expand High Fidelity Buffer (10X, with $MgCl_2$) or 5X Green GoTaq buffer	10 µl and 20 µl, respectively
Expand High Fidelity Enzyme Mix (3.3 U/µl) or GoTaq DNA Polymerase (5 U/µl)	1.5 µl and 1µl, respectively
H_2O	ad 100 µl

3.2.4 Cloning

3.2.4.1 Restriction digest and dephosphorylation of DNA

Restriction enzyme digestion of DNA was performed according to the manufacturers' instructions. To dephosphorylate 5' ends of linearized vector DNA, samples were treated with TSAP (0.4 U/µl) (Promega) for 1 h at 37 °C.

3.2.4.2 Ligation of DNA fragments

Digested insert-DNA or linearized, dephosphorylated vector-DNA was mixed with T4-DNA-Ligase (Promega) in a molar ratio ranging from 1:1 to 3:1 and incubated for 15 min at 20 °C.

Reaction mixture:

2X Quick Ligation buffer (see 3.1.3)	10 µl
Insert-DNA	x µl
Vector-DNA	x µl
T4-DNA-Ligase (5 weiss U/µl)	1 µl
H_2O	ad 20 µl

3.2.4.3 Transformation

3.2.4.3.1 Preparation of competent *E. coli* cells

Competent cells were prepared as described (Sambrook et al., 1989). 200 ml LB media was inoculated with 2 ml of stationary *E. coli* overnight culture. Cells were grown to OD_{600} ~ 0.6 at 37 °C and then treated with 4 ml 1 M $MgCl_2$. After further growth for 10 min, cells were placed on ice for 1 h. Next, cells were pelleted at 3,500 x g for 10 min at 4 °C and resuspended in 40 ml CC solution. Again, cells were incubated on ice for 1 h, harvested by centrifugation and resuspended in 10 ml CC solution + glycerol. Finally, cells were aliquoted and stored at -80 °C.

3.2.4.3.2 Transformation of *E. coli*

For transformation of *E. coli*, 10-100 ng plasmid-DNA or ligation products were pipetted to 100 µl competent cells. The mixture was incubated on ice for 20 min and then heat-shocked for 45 s at 42 °C. After heat-shock, samples were incubated on ice for 10 min, transferred to 1 ml LB media and incubated for 30-45 min in a shaking incubator. Cells were pelleted at 10,000 x g for 2 min and plated on selective media. Plates were incubated overnight at 37 °C.

3.2.4.3.3 Transformation of *S. cerivisae*

Four hundred microliter of a stationary yeast culture was centrifuged at 10,000 x g for 1 min. Then, the supernatant was decanted and pelleted cells were resuspended in 50-100 µl remaining media. Next, 2 µl carrier-DNA (Sigma) and 1 µl plasmid-DNA was added to the mixture. The resuspension was then subjected to 300 µl plate mixture (see below) followed by the addition of 12 µl 1 M DTT. Samples were mixed and left overnight at RT. The next day, the cell resuspension was heat-shocked at 42 °C for 1 h and plated on selective media. Plates were incubated at 30 °C for two days.

Plate mixture:

1 M Tris, pH 7.5	1 ml
Sterile 45 % PEG-4000	90 ml
1 M LiOAc	10 ml
0.5 M EDTA	0.2 ml

3.2.5 DNA sequencing

Plasmid-DNA was verified by DNA sequencing. Samples (50-100 ng/µl) were analyzed at GATC Biotech AG (Konstanz, Germany).

3.3 Microbiological methods

3.3.1 Cultivation and storage of *E. coli*

E. coli was generally grown in shaking cultures at 37 °C using various media (3.1.6). Cell growth was followed by determination of the optical density at 600 nm (OD_{600}) using a spectrophotometer. To select plasmid-carrying cells, antibiotics were added to the medium at the appropriate concentration given in 3.1.6. Agar plates were incubated at 37 °C. For long-term storage of *E. coli* cells, glycerol stocks were prepared. Therefore, 750 µl of mid-log-phase *E. coli* cells were mixed with 250 µl 80 % glycerol and stored at -80 °C.

3.3.2 Cultivation and storage of *S. cerivisae*

S. cerivisae was cultivated at 30 °C in YPD or in CSM media (3.1.6). Cell growth was monitored photometrically at 600 nm. Selection of plasmid-carrying clones was carried out by omission of the appropriate nucleotides or amino acids in the media. Glycerol stocks for long-term storage were prepared as described in 3.3.1.

3.4 Cell culture techniques

3.4.1 Cultivation of insect cells

Sf9 cells were cultivated in Insect Xpress media (Lonza) at 27 °C in monolayer culture or in liquid culture with gentle agitation. Cells were routinely sub-cultured every third day to $5x10^5$ cells/ml using fresh media to maintain viability at 95 %.

3.4.2 Determination of cell count and viability

Cell count and viability was determined by a microscope using a Neubauer counting chamber. Therefore, the chamber was loaded with 10 µl insect cell suspension pre-mixed with 0.4 % trypan blue at a ratio of 1:11. Next, cells in the middle positioned Neubauer big square were counted. The cell count in cells per milliliter is given by the following equation:

$$\boldsymbol{Cell\ count}\ [\boldsymbol{cells/ml}] = \frac{\boldsymbol{number\ of\ cells}}{\boldsymbol{0.0001\ ml}} \times \boldsymbol{1.1}\ (\boldsymbol{dilution\ factor})$$

Equation 2

Cell viability was calculated using the following equation:

$$\boldsymbol{viablity}\ [\,\%] = \frac{\boldsymbol{white\ cells}}{\boldsymbol{white\ cells + blue\ cells}} \times \boldsymbol{100}$$

Equation 3

3.4.3 Generation of recombinant bacmid-DNA and transfection of insect cells

To generate recombinant bacmid-DNA for insect cell transfection, the Bac-to-Bac Baculovirus Expression System Guide (Invitrogen) was followed. The gene to be expressed was inserted into a pFASTBAC vector and introduced into competent *E. coli* DH10Bac cells (3.2.4.3.2) followed by the selection on agar plates containing 50 µg/ml kanamycin, 7 µg/ml gentamicin, 10 µg/ml tetracycline, 100 µg/ml Bluo-gal, and 40 µg/ml IPTG at 37 °C for 48 h. Next, 3-6 white colonies were picked and re-streaked on fresh agar plates and incubated at 37 °C overnight. Then, 2 ml LB media containing 50 µg/ml kanamycin, 7 µg/ml gentamicin, 10 µg/ml tetracycline was inoculated with single colonies with a white phenotype and

incubated overnight at 37 °C with shaking. Bacmid-DNA was isolated as described in 3.2.1.1. Recombinant bacmid-DNA was confirmed by PCR (3.2.3.1) utilizing M13-forward and –reverse primers.

Transfection of Sf9 cells was performed according to Invitrogen's instructions in 6-well plates. $8x10^5$ Sf9 cells/well (viability >95 %) were plated and allowed to attach for 15 min at RT. Cellfectin II reagent (Invitrogen) was diluted 1:13.5 and mixed with 1-3 µg of recombinant bacmid-DNA pre-diluted in 100 µl media. After 30 min of incubation at RT, the prepared complex was added onto the cells in a drop-wise fashion followed by incubation of the samples at 27 °C for 2-5 h. Finally, the transfection mixture was removed and replaced with fresh media. Transfected monolayer cultures were incubated at 27 °C for at least 72 h.

3.4.4 Virus harvest, amplification and storage

Once the transfected cells from 3.4.3 showed signs of viral infection, virus containing media was collected and centrifuged at 500 x g for 5 min to remove cells and large debris. For virus amplification, 10 ml of fresh Sf9 cells ($2x10^6$ cells/ml) were infected with 200 µl of the supernatant above (P1-virus). After incubation at 27 °C for several days with gentle agitation, the amplified virus was harvested (P2-virus). While up-scaling the culture volume to 100 ml, virus amplification was repeated twice to obtain a high-titer P4-virus stock suitable for medium scale protein expression. All baculoviral stocks were stored at 4 °C protected from light.

3.5 Protein expression in *E. coli* and insect cells

Most of the recombinant proteins were expressed from pET-vectors in *E. coli* BL21-CodonPlus(DE3)-RIL cells. *E. coli* protein expression from pQE-vectors was carried out in *E. coli* HB101 cells. For protein production in insect cells, recombinant bacmid-carrying Sf9 cells were generated.

3.5.1 Small-scale protein expression and analysis

Expression studies with expression plasmid-carrying *E. coli* cells were conducted in small-scale. 50-100 ml selective LB media was inoculated with stationary *E. coli* overnight culture and incubated at 37 °C with shaking until an OD_{600} of 0.6-0.7 was reached. Then, 1 mM IPTG was added to induce target protein expression and cultures were further incubated at varying temperatures (e.g. 20 °C, 37 °C). After several time points, the optical density was determined and 1 ml of the bacterial culture was sampled and pelleted at 10,000 x g for 2 min. In addition to conventional protein expression in LB media, selective ZYM-5052 auto induction media (Studier, 2005) was utilized as well. In this case, the main culture was shaked for 4 h at 37 °C to reach an OD_{600} of ~ 1.5 and then cultured at 20 °C overnight.

Cell pellets were resuspended in a defined volume of PBS (1X), supplemented with DNase I (Roche Diagnostic GmbH) and 1 mM PMSF to reach a theoretical OD_{600} of 10 if not otherwise stated. Then, cells were either disrupted with a bead mill (Mixer Mill MM 400, Retsch) or lysed using the BugBuster Protein Extraction Reagent from Merck.

To separate the soluble fraction from insoluble protein, cell extracts were centrifuged at 16,000 x g for 30 min at 4 °C. The insoluble fraction was further washed with 1 ml PBS (1X), and then resuspended in a defined volume of Urea buffer (see below). Forty microliters of both fractions were mixed with 10 µl Laemmli sample buffer (5X) and were analyzed by SDS-PAGE (3.6.3) or Western Blot (3.6.4).

Urea buffer:

100 mM	Tris, pH 8.0
8 M	Urea
1 mM	EDTA

For analysis of recombinant protein expression in insect cells, 20 ml Sf9 cells ($2x10^6$ cells/ml) were infected with baculovirus (3.4.4) and grown for several days at 27 °C. Each day 1 ml was sampled, pelleted for 2 min at 10,000 x g and resuspended in 80 µl Urea buffer and 20 µl Laemmli sample buffer (5x). Protein expression was analyzed by Western Blot analysis (3.6.4).

3.5.2 Medium and large-scale protein expression

For large-scale protein production in *E. coli*, 2-12 l selective LB media was inoculated 1:20 with stationary *E. coli* pre-culture. After an OD_{600} of 0.6-0.7 was reached, cells were induced with 1 mM IPTG and further cultivated for 4 h at 37 °C or overnight at 20 °C with shaking. Selective ZYM-5052 auto-induction media was inoculated 1:1000 with stationary *E. coli* pre-culture (supplemented with 1 % glucose) and cultivated for 4 h at 37 °C followed by overnight incubation at 18-20 °C with shaking.

In addition to *E. coli* shaking cultures, fed batch fermentation was performed to produce recombinant protein in high amounts. First, the fermenter (Biostat-C Fermenter, Sartorius) was filled with 5 liter media (60 g/l yeast extract, 0.6 g/l NH_4Cl) and sterilized for 30 min at 121 °C. Then, temperature was set to 37 °C and 1 liter phosphate buffer containing 13.2 % (w/v) K_2HPO_4, 1.6 % (w/v) $MgSO_4$ and 6 % D(+)-glucose (w/v) was added. In the next step, the media was supplemented with 50 µg/ml kanamycin, 1 ml Antifoam A and inoculated with 400 ml of a stationary *E. coli* overnight culture. After each hour, 1 ml was sampled and analyzed for glucose concentration and OD_{600}. Once all glucose was consumed, feeding solution (30 g/l, 125 g/l D(+)-glucose) was added drop-wise. At an OD_{600} of ~ 30, temperature was set to 20 °C followed by the addition of 1 mM IPTG and further cultivation overnight.

For medium scale insect cell expression, 500 ml Sf9 cells ($2x10^6$ cells/ml) were infected 1:100 with the P4-baculovirus stock obtained in 3.4.4 and incubated for 48 h with gentle agitation.

3.5.3 Cell harvest and cell disruption

E. coli cells were harvested at 10,000 x g for 15 min at 4 °C. For cell disruption, cells were resuspended in the respective lysis buffer supplemented with protease inhibitor and DNase I (Roche Diagnostic GmbH) and subjected to ultrasonication (3 x 45 s, 5 x 10 % duty cycle, 60 % output) or to a cell disruption system (1.8 kbar). Insect cells were disrupted by dounce homogenization. Whole cell lysates were cleared by a centrifugation step at 50,000 x g and 4 °C for 1 h.

3.6 Protein chemical methods

3.6.1 Protein purification

All chromatography steps after cell lysis were performed on ÄKTA FPLC Systems (GE Healthcare) at 4 °C. Typically, a combination of affinity chromatography, ion exchange chromatography and gel filtration was carried out to purify the protein of interest. Utilized columns or column material are listed in 3.1.9. Flow rates for each column were adjusted according to the manufacturer's recommendations. Purification efficiency was judged by SDS-PAGE (3.6.3) and MS analysis.

3.6.1.1 Purification of human GR *wt* and mutants

Human GR-LBD-F602S and GR-LBDm (527-777) were expressed in *E. coli* BL21-CodonPlus(DE3)-RIL cells as His_6-Halo-fusion proteins. 3-4 x 1 l ZYM-5052 auto induction media (Studier, 2005) was inoculated with 1 ml pre-culture and incubated at 37 °C. After 4 h, temperature was set to 18 °C for 60 min, followed by the addition of 500 µM dexamethasone (DEX) and further growth at 18 °C overnight.

Cells were harvested by centrifugation for 15 min at 10,000 x g and 4 °C and washed with ice-cold PBS (1X). The purification strategy was adopted from (Seitz et al., 2010). Cells were resuspended in Ni-A buffer (see below) supplemented with DNase I (Roche Diagnostic GmbH) and Protease Inhibitor HP (Serva). Cells were lysed (3.5.3) and centrifuged for 1 h at 50,000 x g and 4 °C. Cleared lysate was applied onto a Ni-column (HisTrap FF 5 ml, GE Healthcare), pre-equilibrated in Ni-B buffer. The column was then gradient-equilibrated in Ni-B buffer and His_6-Halo-GR-LBD variants were eluted with Ni-C buffer. GR-protein containing fractions were pooled, supplemented with his-tagged TEV protease and dialyzed against Dialysis buffer overnight. Then, digested protein was passed through a Ni-column to remove the N-terminal His_6-Halo-tag and TEV protease. The flow through was concentrated and loaded onto a gel filtration column (Superdex 200, GE Healthcare) equilibrated in Gel filtration buffer. The fractions containing GR-LBD mutants were pooled and shock-frozen in liquid nitrogen.

For the preparation of isotopically labeled GR, cells were grown in minimal media (3.1.6) and induced with 0.5 mM IPTG followed by overnight cultivation at 18 °C. The purification strategy was identical.

Apo-GR-LBDm was expressed in ZYM-5052 auto induction media and purified without stabilizing hormone. To prevent association with *E. coli* chaperones (DnaK and GroE), 2 mM ATP was added to Ni-A and Ni-B buffer. Further, buffers were supplemented with 0.5 % CHAPS.

Ni-A buffer	50 mM	Tris, pH 7.9
	2 M	Urea
	100 mM	NaCl
	5 mM	MgCl2
	10 mM	Imidazole
	2 mM	ß-Mercaptoethanol
	50 µM	Dexamethasone
Ni-B buffer	50 mM	Tris, pH 7.9
	500 mM	NaCl
	10 mM	Imidazole
	10 %	Glycerol
	2 mM	ß-Mercaptoethanol
	50 µM	Dexamethasone
Ni-C buffer	50 mM	Tris, pH 7.9
	500 mM	NaCl
	350 mM	Imidazole
	10 %	Glycerol
	2 mM	ß-Mercaptoethanol
	50 µM	Dexamethasone
Dialysis buffer	50 mM	Tris, pH 7.9
	100 mM	NaCl
	10 %	Glycerol
	2 mM	ß-Mercaptoethanol
	0.5 %	CHAPS
	50 µM	Dexamethasone
Gel filtration buffer	25 mM	Tris, pH 7.9
	100 mM	NaCl
	10 %	Glycerol
	2 mM	DTT
	50 µM	Dexamethasone

Human GR-DBD-LBDm (420-777) was expressed in *E. coli* BL21-CodonPlus(DE3)-RIL cells as His_6-Sumo fusion protein. The purification strategy was similar with the exception that the N-terminal Sumo-moiety was cleaved with Sumo protease and separated by a Heparin column.

Human GR-LBD *wt* was purified from Sf9 cells or refolded from *E. coli* inclusion bodies. In Sf9 cells, GR-LBD *wt* was expressed as N-terminal GST-fusion as described in 3.5.2. Cells were resuspended in GST buffer (10 mM Hepes, 1 mM EDTA, 20 mM Na_2MoO_4, pH 7.4 supplemented with 1 mM PMSF and protease inhibitor (Sigma)) and disrupted by dounce homogenization. The cleared lysate (3.5.3) was loaded onto a GSTrap FF column (5ml, GE Healthcare), pre-equilibrated in GST buffer. Then, the column was washed with 10 column volumes (CV) GST buffer and the protein was eluted in GST buffer supplemented with 10 mM GSH. Protein containing fractions were pooled and shock-frozen in liquid nitrogen. For refolding, bacterial pellets from fermentation of *E. coli* BL21-CodonPlus(DE3)-RIL cells carrying a plasmid encoding for His_6-Sumo-GR-LBD *wt* (3.5.2) were thoroughly resuspended in Ib buffer (see below) supplemented with DNase I (Roche Diagnostic GmbH) and Protease Inhibitor HP (Serva). Following cell disruption (3.5.3), 2.5 % Triton X-100 was added and the lysate was stirred for 1 h at 4 °C. Next, the solution was centrifuged at 50,000 x g for 30 min at 4 °C and washed three times with Ib buffer. Then, inclusion bodies were dissolved in Solubilization buffer, cleared by centrifugation at 50,000 x g for 20 min at 4 °C and loaded onto a Ni-column pre-equilibrated in Solubilization buffer. In the next step, Solubilization buffer was gradually replaced by Refolding buffer over 15 CV and the refolded protein was step-eluted using Ni-Elution buffer. To remove aggregates, GR-protein was further loaded onto a Superdex 200 pg column (GE Healthcare) equilibrated in RF-Gel filtration buffer. Protein containing fractions were pooled and shock-frozen in liquid nitrogen. The individual GR-LBD *wt* domain was obtained by a Sumo protease-digest afterwards. Non-cleaved protein and the N-terminal His_6-Sumo tag as well as the Sumo protease was separated by a Ni-column (5 ml, GE Healthcare).

Ib buffer	100 mM	Tris, pH 7.5
	150 mM	NaCl
Solubilization buffer	50 mM	Tris, pH 7.5
	5 M	GdnCl
	20 mM	Imidazole
	2 mM	ß-Mercaptoethanol
Refolding buffer	50 mM	Tris, pH 7.5
	150 mM	NaCl
	50 mM	Arginine
	50 mM	Glutamine
	2 mM	ß-Mercaptoethanol
	0.1 %	Zwittergent 3-12
Ni-Elution buffer	50 mM	Tris, pH 7.5
	150 mM	NaCl
	50 mM	Arginine
	50 mM	Glutamine
	2 mM	ß-Mercaptoethanol
	0.1 %	Zwittergent 3-12
	500 mM	Imidazole
RF-Gel filtration buffer	50 mM	Tris, pH 7.5
	150 mM	NaCl
	50 mM	Arginine
	50 mM	Glutamine
	5 mM	DTT
	0.1 %	Zwittergent 3-12

3.6.1.2 Purification of Hsp90, co-chaperones and others

Hsp90 and co-chaperones were expressed in *E. coli* (3.5.2) and purified using a three-column chromatography approach:

1. Immobilized-metal affinity chromatography or anion exchange chromatography
2. Anion exchange chromatography
3. Gel filtration

Hsp90 was further purified using a hydroxyl apatite column to reduce ATPase background. TEV protease and Sumo protease were purified after *E. coli* expression (3.5.2) via a combination of nickel affinity chromatography and gel filtration.

3.6.2 Protein labeling

Proteins were fluorescent labeled at lysine or cysteine residues by incubation of the protein solution with a 2-3 fold excess of a fluorescent dye for 1 h at RT or overnight on ice. Labeling reactions were quenched with excess Tris-buffer (lysine residues) or DTT (cysteine residues). To separate free label, samples were dialyzed overnight against freshly prepared buffer or applied onto PD10 columns (GE Healthcare). Labeling efficiency was determined photometrically according to the manufacturer's instructions.

3.6.3 Sodium dodecyl sulfate polyacrylamide gel electrophoresis (SDS-PAGE)

To analyze cell extracts or to judge protein purity, SDS-PAGE according to Laemmli, (1970) was performed. Samples were mixed with Laemmli sample buffer (5X) (3.1.3) and boiled for 95 °C at 5 min prior to gel loading. The acrylamide concentration of separation gels was adjusted for each protein to be analyzed (see below).

Separation gel (10-15 %)	
2.5-3.75 ml	40 % Acrylamide (40 % w/v, Acrylamide/Bisacrylamide 38:2)
2.5 ml	4X SDS buffer (0.8 % SDS, 1.5 M Tris/HCl, pH 8.8)
Ad 10 ml	H_2O
Stacking gel (5 %)	
0.625 ml	40 % Acrylamide (40 % w/v, Acrylamide/Bisacrylamide 38:2)
2.5 mL	2X SDS buffer (0.4 % SDS, 0.25 M Tris/HCl, pH 6.8)
Ad 5ml	H_2O
	Polymerization was induced by the addition of TEMED and APS

Typically, SDS-PAGE was performed at a constant current of 35 mA per gel for 45 min. After electrophoresis, gels were washed with deionized H_2O and stained with Coomassie according to Fairbanks et al., (1971). The molecular weight of the analyzed protein was compared to a LMW standard (Biorad).

3.6.4 Western blotting

For Western blot analysis, first SDS-PAGE (3.6.3) with the protein samples to be analyzed was carried out. A pre-stained protein mix (SERVAChrom Protein Standard III) was used as a molecular weight standard. Next, proteins were electro-blotted onto PVDF membranes in a semi-dry blotting apparatus (Biometra) at a constant current of 72 mA per SDS gel for 90 min. After transfer, membranes were incubated in Blocking buffer 1 (3.1.3) for 1 h with gentle agitation. Then, PVDF membranes were incubated for 1 h with a primary antibody diluted in PBST buffer (3.1.3) supplemented with 1 % milk powder. After 3 washing steps with PBST for 5 min, PVDF membranes were incubated with a Peroxidase (POD)-conjugated secondary antibody for 1 h, if not otherwise stated. Following three washing steps in PBST, proteins were detected using the ECLplus Western Blotting Detection System (GE Healthcare) according to the manufacturer's recommendations.
For Western blot analysis with a StrepTactin-POD conjugate, the membrane was blocked with Blocking buffer 2 and Blocking buffer 3 (3.1.3).

3.6.5 Analytical gel filtration

Analytical gel filtration was performed on a Shimadzu HPLC system (Shimadzu). Refolded GR (3.6.1.1) was analyzed at RT on a Superdex 200 10/300 GL column (GE Healthcare) equilibrated in HPLC buffer. The flow rate was set to 0.5 ml/min. Protein was detected at 280 nm or 350 nm (intrinsic fluorescence). The apparent molecular mass was estimated using a calibration curve generated with standard proteins (3.1.8).

HPLC buffer:

50 mM	Tris, pH 7.5
150 mM	NaCl
5 mM	DTT
0.1 % (w/v)	Zwittergent 3-12

3.6.6 Analytical ultracentrifugation (AUC)

Analytic ultracentrifugation sedimentation velocity experiments were performed by Maike Krause (Technische Universität München). Sedimentation velocity analysis of GR-LBDm was performed on an Optima-XL-I Beckman centrifuge (Beckman Coulter) with absorbance and interference optics.

AUC Buffer 1:

20 mM	Hepes, pH 7.4
200 mM	NaCl
1mM	TCEP
	For holo-GR-LBDm:10 µM Dexamethasone

For Hsp90-interaction studies, GR-LBDm and Hsp90 co-chaperones were random labeled with ATTO-488 (ATTO-TEC) at cysteine or lysine residues (3.6.2). His_6-Halo-GR-LBDm was fluorescent labeled at the Halo moiety with the HaloTag TMR ligand (Promega).
Measurements were conducted with a ProteomLab Beckman XL-A centrifuge (Beckman Coulter) equipped with an AVIV fluorescence detection system (Aviv Biomedical Inc.) using 400 nM fluorescently labeled protein (e.g. *GR-LBDm, *Sti1 or *Cpr6) and 3-9 µM of the unlabeled components of interest.

AUC Buffer 2:

20 mM	Hepes, pH 7.5
20 mM	KCl
5 mM	MgCl
5 mM	DTT
50 µM	Dexamethasone

Nucleotides (ADP, ATP, ATPγS and AMP-PNP) were added at a concentration of 2 mM. For GR-release experiments, 10 mM ADP was added. Titration experiments were carried out with 400 nM *GR-LBDm, 2 mM of the respective nucleotide and increasing amounts of Hsp90 (200 nM-14.4 µM).
All samples were filled in quartz-capped charcoal-filled epon double sector centerpieces with an optical pathlength of 12 mm (Beckman). Experiments were performed at 42,000 rpm and 20 °C in an eight-hole Ti-50 Beckman-Coulter rotor. Data were analyzed by Maike Krause (Technische Universität München) using dcdt+ v. 2.4.0 (Philo, 2006), SEDFIT v. 14.1

(Schuck, 2000) and OriginPro 8 (OriginLab). Solvent densitiy and viscosity were calculated with SEDNTERP (Laue, 1992).

Analytical ultracentrifugation sedimentation equilibrium experiments with refolded GR-LBD *wt* was performed by Alexander Bepperling (Technische Universität München). Analysis was performed on a ProteomLab XL-I centrifuge (Beckman) supplied with absorbance and interference optics. The sample was diluted with AUC Buffer 3 to final concentrations of 0.2 mg/ml, 0.15 mg/ml and 0.1 mg/ml. 105 µL of the samples and 10 µl FC43 were loaded into the sample channels, and 120 µl AUC Buffer 3 was loaded into the reference channels of assembled cells with sapphire windows and 12-mm path length graphite-filled epoxy six channel top-loading Epon centerpieces (Beckman). The 0.2 mg/ml sample was placed in the inner channel, the 0.15 mg/ml sample in the middle channel and the 0.1 mg/ml sample in the inner channel. Experiments were conducted at 25,000 rpm and 30,000 rpm as well as 35,000 rpm in a four-hole Beckman–Coulter AN60-Ti rotor until equilibrium was reached. Equilibrium was verified by subtracting scans 1 h apart from each other after the simulated time to reach equilibrium was over and until the root-mean-square deviation (rmsd) was constant. Simulations were performed using UltrascanII and the 'estimate equilibrium times' module. Scans were recorded with absorbance optics at 280 nm with a radial step size of 0.001 cm and 25 replicates were taken. Data analysis was carried out with UltrascanII (http://www.ultrascan.uthscsa.edu) using the global fit module and a single species model. A partial specific volume of 0.72 cm^3/g and a buffer density of 1.0523 g/cm^3 was used.

AUC Buffer 3:

1X	PBS
0.1% (w/v)	Zwittergent 3-12
2 mM	TCEP
	pH 7.7

3.7 Spectroscopy

3.7.1 Absorbance (UV/VIS) spectroscopy

Similar to nucleic acids (3.2.2), also peptides and proteins absorb UV light. Peptides bonds absorb in the range of 180 to 240 nm, whereas from 250-300 nm aromatic amino acids as well as disulfide bonds contribute to the signal (Cantor and Schimmel, 1980):

	λ(max) [nm]	ε(max) [$M^{-1}cm^{-1}$]
Tryptophan	280	5700
Tyrosine	274	1400
Phenylalanine	257	200
Disulfide bond	250	300

with λ(max) = absorbance maximum, ε(max) = molar extinction coefficient

To determine the protein concentration, the law of Lambert-Beer was applied (Equation 1) with $A =$ absorbance at 280 nm, ε = molar extinction coefficient at 280 nm [M^{-1} x cm^{-1}], $c =$ protein concentration [M], $d =$ layer thickness [cm].

Absorbance spectra were recorded from 230-400 nm in Quartz cuvettes on a Varian Cary 50/100 Bio UV-VIS spectrophotometer (Varian Inc.). All spectra were buffer-corrected. Molar extinction coefficients were calculated from the amino acid sequence using the protparam tool (http://web.expasy.org/protparam). Nucleic acid contamination was estimated from the ratio of absorbance at 280 nm and 260 nm (A_{280}/A_{260}).

3.7.2 Fluorescence spectroscopy

3.7.2.1 Fluorescence polarization (anisotropy)

When fluorescent molecules are excited with plane-polarized light, depolarization occurs as light is emitted in both vertical and horizontal planes (Lea and Simeonov, 2011). This process is sensitive to changes in molecular size and therefore useful to study molecular interactions. The degree of polarization (P) or anisotropy (r) is given by the ratio of horizontally and vertically polarized fluorescence intensity, where I_v is the vertical component- and I_h is the horizontal component of emitted light (Equation 4, Equation 5).

$$\boldsymbol{P = \frac{I_v - I_h}{I_v + I_h}}$$

Equation 4

$$\boldsymbol{r = \frac{I_v - I_h}{I_v + 2I_h}}$$

Equation 5

In this thesis, fluorescence polarization (anisotropy) was used to determine the hormone-, DNA- and co-regulator binding properties of GR proteins. Experiments were conducted either on a Fluoromax Fluorescence Spectrometer 3 supplied with polarizers (Horiba Jobin Yvon GmbH) or were performed on a PHERAstar Plus plate reader with FP optics (BMG Labtech). Excitation and emission wavelengths were set to 484/485 nm and 520 nm, respectively. Measurement buffers, experimental parameters and fit functions varied and are described in the respective figure legends.

3.7.2.2 Fluorescence resonance energy transfer (FRET)

FRET describes the energy transfer from an excited donor dye to an acceptor dye in a radiation-free process (Helms, 2008). In this thesis, FRET was utilized to measure GR-induced conformational changes in Hsp90. Yeast Hsp90 was labeled with donor dye (ATTO 488, ATTO-TEC) and acceptor dye (ATTO 550, ATTO-TEC) (3.6.2) at an engineered cysteine residue (C61) located in the N-terminal domain as described previously (Hessling et al., 2009).

FRET measurements were carried out on a Fluoromax Fluorescence Spectrometer 3 (Horiba Jobin Yvon GmbH) at 30 °C as described (Hessling et al., 2009). 200 nM donor- and 200 nM acceptor-labeled yeast Hsp90 were mixed in ATPase buffer (see below), incubated with increasing amounts of GR-LBDm and the closing reaction was followed after the addition of 2 mM ATPγS. The apparent half-time of the reaction was determined with an exponential decay function. For chase-experiments, 4 µM unmodified yeast Hsp90 or 50 mM ADP was added to disrupt the FRET complex.

ATPase buffer:

40 mM	Hepes, pH 7.5
150 mM	KCl
5 mM	$MgCl_2$
50 µM	Dexamethasone

3.7.3 Circular dichroism (CD) spectroscopy

Circular dichroism (CD) is based on the fact that optically active (chiral) molecules absorb left and right circularly polarized light to different extents (Kelly et al., 2005). In proteins, the most important chiral elements are peptide bonds, which absorb at 260-170 nm (far-UV) and aromatic amino acid residues, which contribute to the CD-signal at 350-250 nm (near-UV).

Far-UV measurements provide useful information about the secondary structure of proteins. The conformation of the polypeptide chain causes a characteristic signal. For example, α-helices show typical minima at 208 nm and 222 nm, whereas ß-sheets display a signal with a single minimum at 218 nm. The signals in the near-UV region are much weaker, but they give rise to certain aspects of tertiary structure as the chiroptical characteristics of the

aromatic amino acid residues rely on their asymmetric environment and thus on the protein's native fold.

Far-UV experiments were performed in 1 mm quartz cuvettes on a Jasco J715 CD-Spectrometer with a PTC343 Peltier unit with the following standard measurement parameter if not otherwise indicated:

Parameter	**Setting**
Wavelength range	260-200 nm
Scanning speed	20 nm/min
Accumulations	15
Protein concentration	0.1 mg/ml
Temperature	20 °C

All spectra were buffer-corrected and normalized to the mean residual weight ellipticity as given by the following equation with Θ_{MRW} = mean residue ellipticity, $\Theta =$ obtained ellipticity [mdeg], M = molecular weight [g x mol^{-1}], d = layer thickness [cm], c = protein concentration [mg x ml^{-1}], N_{aa} = number of amino acids:

$$\boldsymbol{\Theta}_{\boldsymbol{MRW}} = \frac{\boldsymbol{\Theta} \times \mathbf{100} \times \boldsymbol{M}}{\boldsymbol{d} \times \boldsymbol{c} \times \boldsymbol{N_{aa}}}$$

Equation 6

Thermal transitions were monitored at 220 nm from 10 to 85 °C with a heating rate of 20 °C/h. The apparent melting point (T_M) was calculated from a Boltzmann fit.

3.8 Structural methods

3.8.1 Small angle x-ray scattering (SAXS)

SAXS is a powerful technique to study the structure and interactions of proteins in solution. The elastic scattering of x-rays by a sample at very low angles (0.1-10 °) provides information on the overall shape, oligomeric state and size of the molecules. In addition, computational methods allow the determination of low-resolution three-dimensional structures from scattering data using *ab initio* or rigid body modeling approaches (Blanchet and Svergun, 2013; Madl, 2013).

In this thesis, SAXS was used to analyze the GR-Hsp90 interaction. SAXS experiments and analysis with GR, Hsp90 and co-chaperones were performed by Tobias Madl (Technische Universität München). The protein concentration ranged from 2-10 mg/ml. Three dilutions of each protein/protein complex were pipetted in 50 µl volumes on microtiter plates and measured on an in-house Anton Paar SAXSess mc2 SAXS instrument equipped with a Kratky camera, a sealed X-ray tube source and a two-dimensional PI•SCX:4300 Princeton Instruments CCD detector. The scattering patterns were recorded with a 180-min exposure time (1080 frames, each 10 seconds). All SAXS data were analyzed with ATSAS (version 2.5). The data were processed with the SAXSQuant software (version 3.9). The forward scattering, I(0), the radius of gyration, R_g, the maximum dimension, D_{max}, desmearing and the inter-atomic distance distribution functions, P(R), were computed with the program GNOM (Svergun, 1992). The structures of Hsp90 and its complexes were modeled using the program CORAL (Petoukhov et al., 2012). SAXS data and NMR constrains for the Hsp90-GR-LBDm binding interface (4.2.1.4, 4.2.1.5, Supplemental table 1, Supplemental table 2) (residues L18, E28, I29, L93, R279, E287, L331, D356, N386, V391, E431, K449, H467, T511, Q512 of Hsp90) as well as high-resolution crystal structures of the Hsp90-N (PDB 2CG9, residues 11-210), -M (PDB 2CG9, residues 270-527), -C domains (PDB 2CG9, residues 533-677), GR (PDB 1M2Z) and p23 (PDB 2CG9) were used as input. Long stretches of disordered regions such as the N-, and C-termini and the linkers connecting the Hsp90-N, -M, and -MC were randomized throughout the calculations. To calculate the P(R)s of mixtures of ‘closed’ and ‘open’ Hsp90 complexes, the experimental P(R) of ‘open’ Hsp90 complexes and the P(R) back-calculated for the ‘closed’ form of Hsp90 complexes (PDB 2CG9), using the program Crysol (Svergun et al., 1995) were normalized and combined at different ratios.

3.8.2 Nuclear magnetic resonance (NMR) spectroscopy

To map the GR-Hsp90 binding interface, NMR spectroscopy was carried out. All NMR experiments and data analysis were performed by Lee Freiburger (Technische Universität München). NMR spectra were recorded on a Bruker AV900 spectrometer (Bruker Topspin 2.1, Bruker, Billerica, USA) at 25 °C. For GR-Hsp90 binding experiments, GR was diluted in NMR buffer (see below) containing the isotopically enriched Hsp90 component of interest (e.g. Hsp90-N, -M and segmentally labeled Hsp90-NM). The protein solution was then concentrated and diluted multiple times with NMR buffer to remove trace glycerol in GR storage buffer. Binding analysis of isotopically enriched GR-LBDm (3.6.1.1) with Hsp90-M and -NM domain constructs were carried out in an alternative buffer (25 mM deuterated Tris, 200 mM NaCl, 2 mM $MgCl_2$, 500 µM DEX, 2 mM DTT, 0.2 % NaN_3, pH 7.0). NMR experiments were processed using NMRPipe (Delaglio et al., 1995) and the data were analyzed using CcpNMR analysis (Vranken et al., 2005).

NMR buffer:

20 mM	Sodium phosphate, pH 6.5
200 mM	NaCl
2 mM	$MgCl_2$
2 mM	DTT
500 µM	Dexamethasone
0.2 %	NaN_3

Chemical shift assignments were already available for both Hsp90-N domain (1-210) (Dehner et al., 2003; Salek et al., 2002) and Hsp90-M domain (277-527) (Hagn et al., 2011). Assignments for the segmentally ligated Hsp90-NM constructs were transferred from the individual domains as spectra are very similar, thus providing 64 % complete backbone assignment for the Hsp90-NM construct. These included the 67-residue charged linker region which was excluded from previous studies.

Chemical shift perturbations (CSP) were based on 2D ^{1}H, ^{15}N water-flip-back HSQC or TROSY correlation experiments and calculated as follows with $\Delta\delta_{N-H}$ = weighted CSP, $\Delta\delta_{^1H}$ = difference in chemical shift [ppm] of the amide proton in the absence and presence of GR, $\Delta\delta_{^{15}N}$ = difference in chemical shift [ppm] of the amide nitrogen in the absence and presence of GR:

$$\Delta\boldsymbol{\delta_{N-H}} = \sqrt{\left(\Delta\boldsymbol{\delta}_{^1\boldsymbol{H}} * \mathbf{10}\right)^{\mathbf{2}} + \left(\Delta\boldsymbol{\delta}_{^{15}\boldsymbol{N}}\right)^{\mathbf{2}}}$$

Equation 7

3.9 Functional assays

3.9.1 GR activity assay in *S. cerivisae*

A yeast reporter assay was utilized to assess Hsp90-dependent GR transactivation *in vivo*. For this, cDNA encoding for full-length human GR and mutants was cloned (3.2.4) into a p413-GPD vector (Mumberg et al., 1995) and introduced into yeast cells (3.2.4.3.3) together with the reporter plasmid pUCΔSS-26X (Louvion et al., 1996) that expresses ß-galactosidase under the control of specific GR response elements (GRE elements).

Individual clones were grown in selective yeast media to stationary phase at 30 °C. Then, cells were diluted to an OD_{600} of 0.3, exposed to 10 µM 11-deoxycorticosterone (DOC) or dexamethasone (DEX) and grown overnight at 30 °C. To block Hsp90 function, 20 µM radicicol (dissolved in DMSO) was added. The next day, 300 µl cells were harvested and resuspended in 300 µl Z-buffer (see below). Following cell disruption at 4 °C using a bead mill (Mixer Mill M400, Retsch) and a quick centrifugation step at 16,000 x g for 2 min, cleared lysates were transferred onto 96 well microtiter plates. To measure protein concentration, 200 µl BCA premix (Thermo Scientific) was added to 25 µl yeast lysate and absorbance was read at 562 nm (A_{562}) after incubation at 30 °C for 30 min using a plate reader (Tecan Sunrise, Tecan Group Ltd). To determine ß-galactosidase activity, 50 µl of ONPG (4 mg/ml, in Z buffer supplemented with 0.27 % ß-mercaptoethanol) was added to 50 µl lysate and the change in absorbance at 405 nm over time was recorded. Obtained ß-galactosidase activities were divided by A_{562} and normalized.

Z buffer:

60 mM Na_2HPO_4, pH 7.0
40 mM NaH_2PO_4
10 mM KCl
1 mM $MgSO_4$

3.9.2 Regenerative ATPase assay

ATPase assays were performed utilizing an ATP-regenerating system. ADP, which is formed during the reaction, is converted back to ATP by a coupled enzyme assay containing the enzymes pyruvate kinase (PK) and lactate dehydrogenase (LDH) as well as the substrates phosphoenol pyruvate (PEP) and NADH:

$ATP + H_2O$	$\longrightarrow$	$ADP + P_i$	(1)
$PEP + ADP$	$\longrightarrow$	$Pyruvate + ATP$	(2)
$Pyruvate + NADH/H^+$	$\longrightarrow$	$Lactate + NAD^+$	(3)
$PEP + NADH/H^+$	$\longrightarrow$	$Lactate + NAD^+ + P_i$	(4)

The ATPase activity can be determined by NADH consumption using absorbance spectroscopy employing the molar extinction coefficient of NADH of 6,200 [M^{-1} x cm^{-1}] at 340 nm. Hydrolysis rates were calculated as follows with k_{hyd} = hydrolysis rate [min^{-1}], m = slope [min^{-1}], d = layer thickness [cm], ε_{NADH} at 340 nm = extinction coefficient of NADH at 340 nm [M^{-1} x cm^{-1}], c_{ATPase}= concentration of the ATPase [M]:

$$\boldsymbol{k_{hyd} = \frac{m}{d \times -(\varepsilon_{NADH} at\ 340\ nm) \times c_{ATPase}}}$$

Equation 8

ATPase assays were performed on a Varian Cary 50 Bio UV-VIS spectrophotometer (Varian Inc.). 3 µM of the ATPase (Hsp90, Hsp90 domain constructs) was analyzed in 150 µl volumes using 100 µl of the premix below.

Premix:

8656 µl	ATPase buffer (see 3.7.2.2)
240 µl	100 mM Phosphoenolpyruvate
48 µl	50 mM NADH
12 µl	Pyruvate kinase suspension (Roche Diagnostic GmbH)
44 µl	Lactate dehydrogenase suspension (Roche Diagnostic GmbH)

Samples were pre-incubated for 10 min and read after addition of 2 mM ATP. Background-ATPase activity was determined by the addition of 50 µM of the Hsp90 inhibitor radicicol.

3.9.3 Immunoprecipitation (IP)

For IP experiments with GR, 20 µg of purified His_6-Halo-GR-LBDm and 20 µg His_6-Halo-tag, respectively, was incubated for 2 h at 30 °C with 45 µl rabbit reticulocyte lysate (RLL, Promega) and 5 mM ATP (final concentration). Then, 10 µl Halolink Magnetic beads (Promega), pre-washed in IP buffer (see below), were added to the mixture to allow covalent bead coupling. After 1 h incubation at RT using an overhead shaker, beads were washed twice with 1 ml ice-cold IP buffer, once with 200 µl IP buffer and were finally collected in 40 µl IP buffer. Elution from the beads was performed with TEV protease which cleaves the GR-LBDm from the Halo-moiety. Protease cleavage was performed at RT for 1 h using an overhead shaker. Then, supernatants were separated from the beads and were mixed with Laemmli sample buffer (5X), boiled for 5 min and subjected to SDS-PAGE- (3.6.3) and Western blot analysis (3.6.4).

IP buffer:

20 mM	Tris, pH 7.5
50 mM	KCl
5 mM	$MgCl_2$
0.01 %	NP-40
20 mM	Na_2MoO_4
2 mM	DTT

4 Results and Discussion

4.1 Expression, purification and characterization of GR

Parts of this work will be published soon (including figures, text and related methods):

'Modulation of the Hsp90 chaperone cycle by a stringent client protein'
Oliver Robin Lorenz, Lee Freiburger, Daniel Andreas Rutz, Maike Krause, Bettina Karolina Zierer, Sara Alvira, Jorge Cuéllar, José María Valpuesta, Tobias Madl, Michael Sattler & Johannes Buchner, Mol.Cell 2014, *Accepted*

4.1.1 Attempts to produce functional GR *wt* in *E. coli* and insect cells

The glucocorticoid receptor (GR) is one of the major Hsp90 clients. The established Hsp90-dependent GR maturation model as we know it today originates from immunoprecipitation experiments using receptor that was initially captured with antibodies from eukaryotic lysates (Pratt and Toft, 1997). Thus, many molecular and mechanistic aspects of the Hsp90-client relationship are not known. For detailed *in vitro* analysis, a source of functional GR protein is a key prerequisite. This chapter describes several attempts to produce recombinant GR in *E. coli* or insect cells. Since the C-terminal ligand binding domain of GR (GR-LBD) (1.4.1) is crucial for Hsp90 interaction (Howard et al., 1990), work was focused on this entity.

4.1.1.1 Soluble expression of GR-LBD *wt* in *E. coli*

The human GR-LBD is a very difficult – to – express protein. There is no established protocol for the soluble production of ligand-free GR in *E. coli* cells. Different approaches can be taken to facilitate heterologous expression of human proteins in bacteria including host strain selection or precise control of target gene expression. In addition, the fusion to highly soluble proteins such as the Maltose-binding-protein (MBP), Sumo or Glutathione-S-Transferase (GST) can significantly enhance soluble expression of the target protein (Sivashanmugam et al., 2009; Terpe, 2003).

In a first attempt, human GR-LBD (527-777) was expressed as an N-terminal Sumo-fusion and analyzed for solubility (3.5.1) (Figure 12). Although expression rates at 37 °C were fairly high, recombinant GR was entirely produced in inclusion bodies. In line with previous results, also reduction of the temperature to 20 °C during expression did not result in an increase of soluble protein (Schmid, 2009).

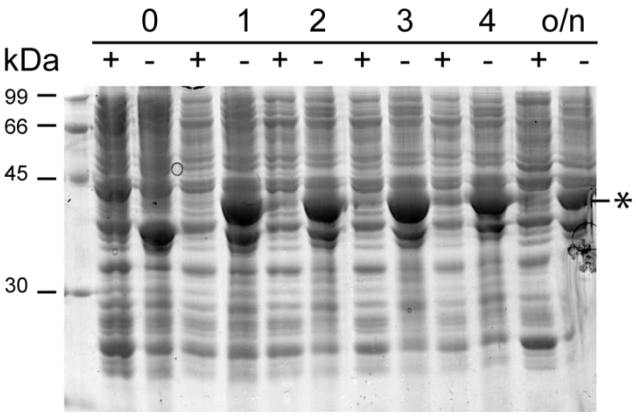

Figure 12 Expression analysis of His_6-Sumo-GR-LBD. Expression plasmid-carrying *E. coli* BL21-CodonPlus(DE3)-RIL cells were grown in LB media to an OD_{600} ~ 0.6 at 37 °C. Then, protein expression was induced with 1 mM IPTG and 1 ml samples were taken at the indicated time points. Overnight expression was performed at 20 °C after induction. Cells were spun down, resuspended and lysed as described in 3.5.1. Separated supernatant and insoluble fraction was loaded on an SDS-gel. (*) recombinant protein, (0) before induction, (1-4) hours after induction, (o/n) overnight expression, (+) soluble fraction, (-) insoluble fraction.

Thus, in a second approach, human GR-LBD was cloned (3.2.4) in-between two protein tags to suppress aggregation or degradation of freshly synthesized GR in *E. coli* (Figure 13A). An N-terminal His_6- and a C-terminal StrepII-affinity tag as well as a protease cleavage site (e.g. TEV protease site) at the N- and C- terminus of the GR-LBD were included, facilitating tag removal from the GR-LBD at both termini using e.g. a tandem purification approach later on.

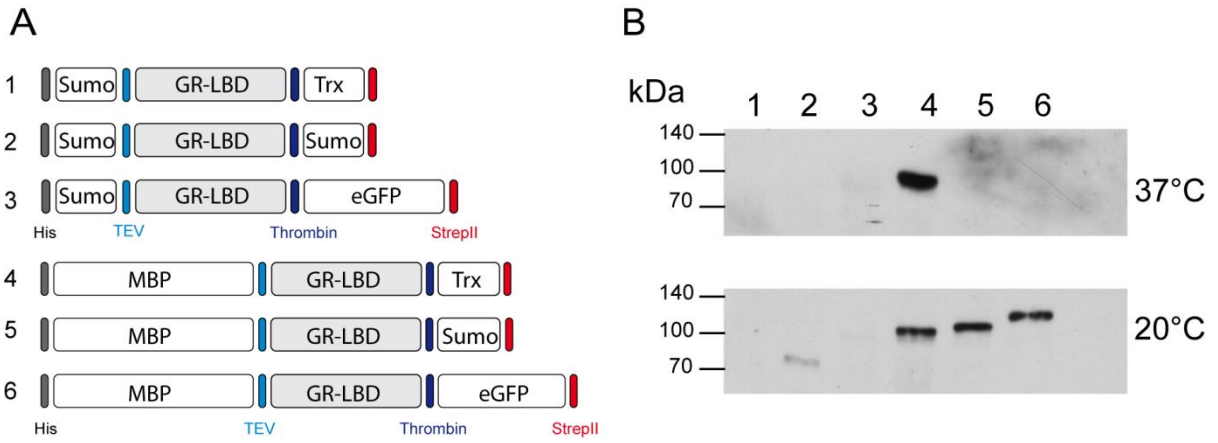

Figure 13 Construct design to facilitate soluble GR production in *E. coli* and expression analysis. A) GR-LBD was flanked by various solubility enhancing tags at its N- and C-terminus (constructs 1-6). TEV- and Thrombin protease sites were inserted to cleave GR-LBD from protein tags later on (TEV, Thrombin). A His_6- as well as a StrepII-affinity tag (His, StrepII) were added at the N- and C-terminus of the GR fusion to faciltitate purification using e.g. tandem affinity chromatography. B) Expression analysis of GR fusions at 37 °C and 20 °C. Expression plasmid-carrying *E. coli* BL21-CodonPlus(DE3)-RIL cells were grown in LB media to an OD_{600} ~ 0.6 at 37 °C and induced with 1 mM IPTG. After 1 h post-induction at 37 °C (upper panel) or after overnight expression at 20 °C (lower panel), 1 ml cells were sampled, resuspended and lysed as described in 3.5.1. The separated supernatant was loaded on an SDS-gel and further analyzed by Western blot analysis (3.6.4) using a StrepTactin-POD conjugate at a dilution of 1:100,000. 1) Sumo-GR-LBD-Trx, 2) Sumo-GR-LBD-Sumo, 3) Sumo-GR-LBD-eGFP, 4) MBP-GR-LBD-Trx, 5) MBP-GR-LBD-Sumo, 6) MBP-GR-LBD-eGFP.

Similar to the results with the Sumo-fusion (Figure 12), GR-proteins were expressed at very high rates (not shown). To judge the amount of soluble produced GR, protein extracts were further analyzed by Western blot (Figure 13B). It turned out, that especially GR-fusions with an N-terminal His_6-MBP-tag were partly produced in a soluble form (Figure 13B) and that expression at 20 °C promoted soluble expression. However, pilot purifications revealed that GR fusion proteins were expressed as soluble aggregates as assessed from gel filtration chromatography results (not shown).

4.1.1.2 Soluble expression of GR-LBD *wt* in insect cells

Soluble GR-LBD in its ligand free-form could not be obtained from *E. coli* cells. However, several articles reported on the successful expression and (partial) purification of functional full-length human GR in Sf9 cells, suggesting that GR synthesis in insect cells is guided by the endogenous Hsp90-Hsp70 chaperone machinery (Alnemri and Litwack, 1993; Srinivasan and Thompson, 1990). Thus, in a next approach, GR-LBD was expressed in insect cells. Bacmid-DNA encoding for human GR-LBD (527-777) fused to an N-terminal His_6-GST tag was generated and introduced into Sf9 cells to obtain recombinant baculovirus (3.4.3). Similar to the expression attempts in *E. coli*, the GST-tag was used to enhance soluble expression, since protein yields for the full-length receptor were reported to be in the microgram range (Hyodo et al., 2001; Srinivasan and Thompson, 1990). In addition, the protein-tag provides the possibility to purify the recombinant GR using Glutathione (GSH)-affinity chromatography under mild conditions, and further allows an on-column-strip of any associated insect cell chaperones by applying e.g. high-salt conditions prior to elution with GSH.

Using the generated baculovirus, small-scale insect cell expression analysis (3.5.1) was carried out to determine optimal infection parameters and time of cell harvest. 20 ml Sf9 cells ($2x10^6$ cells/ml) were incubated for 96 h post-infection and GR levels were analyzed each day by Western blot analysis (Figure 14).

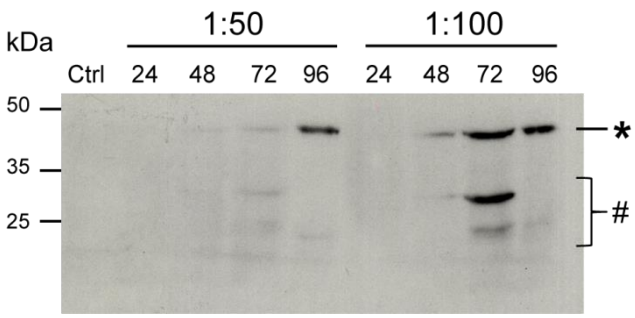

Figure 14 Expression analysis of His_6-GST-GR-LBD in insect cells. 20 ml Sf9 cells ($2x10^6$ cells/ml) were grown at 27 °C and infected with P4-baculovirus (1:50 and 1:100 dilution in culture media, respectively). While growing for 96 h post-infection at 27 °C (24-96), each day, 1 ml of insect cells was sampled and cell extracts were loaded on an SDS gel and analyzed by Western blotting (3.6.4) using an α-His-POD antibody at a dilution of 1:5,000. Cell extracts were compared to a sample of non-infected Sf9 cells (Ctrl). (*) recombinant protein, (#) truncation products.

The yield of total GR-protein (soluble and insoluble) was dependent on the applied baculovirus concentration and duration of protein expression. Whereas Sf9 cells that were treated with virus at a 1:50 dilution expressed only little protein until 96 h were reached, the infection of Sf9 cells with recombinant baculovirus at a 1:100 dilution resulted in stronger protein expression with maximum GR production after 72 h and some evidence of protein degradation (or incomplete translation of the GST-fusion).

For a protein purification attempt, expression of His_6-GST-GR-LBD was up-scaled to 500 ml culture volume ($2x10^6$ cells/ml). Sf9 Cells were infected with baculovirus at a final dilution of 1:100 and incubated for 48 h since cultivation for 72 h seems to negatively influence target protein stability (see Figure 14). After cell harvest and cell lysis (3.5.3), the supernatant was purified using GSH-affinity chromatography (3.6.1.1). Western blot analysis of the collected fractions (Figure 15A, lower panel), showed that the applied one-step column approach resulted in an enrichment of soluble GR, even though the fusion protein could not be completely captured by the GSH column or was in part lost during washing steps. As expected, Hsp90 co-purified with GR (Figure 15A upper panel, Figure 15B). Mass spectrometry (MS) analysis of prominent proteins in the eluate, besides GR, further suggested its engagement with Hsp70 (Figure 15B). However, even in insect cells, the majority of recombinant GR was produced in insoluble form (Figure 15A, lower panel). Only microgram amounts of soluble protein were obtained. In addition, soluble GR protein seems to be highly susceptible to proteolytic degradation (Figure 14, Figure 15B), although the co-purification of endogenous glutathione-binding proteins from insect cells seems possible as well (Bichet et al., 2000). Thus, the baculovirus system was not further considered to produce recombinant GR.

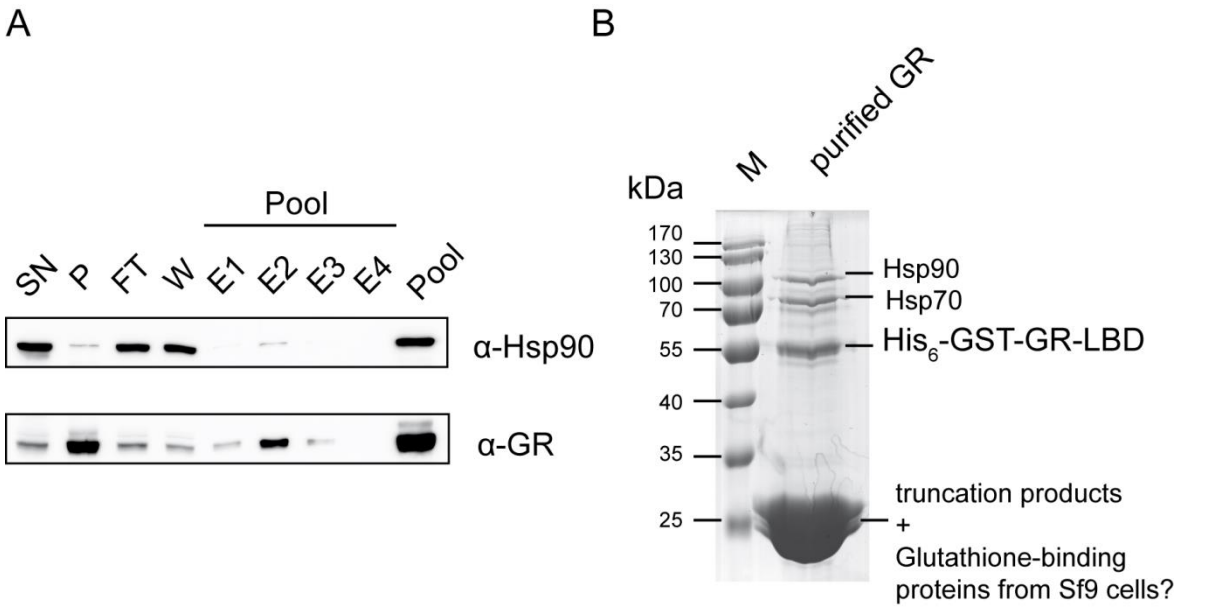

Figure 15 Purification of His_6-GST-GR-LBD. 500 ml Sf9 cells ($2x10^6$ cells/ml) were grown at 27 °C and infected with P4-baculovirus (1:100 dilution in culture media). After 48 h post-infection, cells were harvested, lysed and processed by GSH-affinity chromatography as described in 3.6.1.1. A) Western blot analysis of collected fractions using an α-GR and α-Hsp90 antibody at a concentration of 1:100 and 1:10,000, respectively. An α-rabbit- and α -mouse-POD conjugate, respectively, was used as a secondary antibody at a concentration of 1:30,000. (SN) supernatant after cell lysis, (P) insoluble protein, (FT) flow through, (W) wash, (E1-E4) elution fractions, (Pool) pooled and concentrated elution fractions E1-E4. B) SDS-PAGE analysis of the purified GR. (M) Marker.

4.1.1.3 Refolding of GR-LBD *wt* derived from *E. coli* inclusion bodies

The soluble expression of ligand-free GR-LBD in *E. coli* and insect cells was not successful. As high amounts of insoluble protein accumulate during expression in *E. coli* (4.1.1.1), a refolding strategy was applied to obtain functional GR. His_6-Sumo-GR-LBD was produced by fed-batch fermentation of *E. coli* and the resulting inclusion bodies were solubilized in buffer containing 5 M guanidinium chloride. Then, denatured protein was purified and refolded using an on-column approach as described in 3.6.1.1. Similar to a previous study (McLaughlin and Jackson, 2002), the detergent Zwittergent 3-12 was used to refold GR.

To determine folding and stability of the refolded protein, CD spectroscopy measurements (3.7.3) were carried out. The refolded receptor fusion showed α-helical and ß-sheet content in FAR-UV-CD measurements (Figure 16A), indicating that both N-terminal Sumo-tag and GR-LBD are well folded. In 6 M guanidium chloride, the protein was completely denatured. Interestingly, refolded GR exhibited an apparent extraordinary high thermal stability, as it did not unfold with increasing temperature (not shown).

To rule out any influence of the Sumo-tag, the tag was cleaved off using Sumo protease and GR-LBD was further analyzed by FAR-UV-CD spectroscopy. In line with previous measurements and consistent with published results (McLaughlin and Jackson, 2002), a significant amount of α-helical structure could still be observed at 90 °C (Figure 16B).

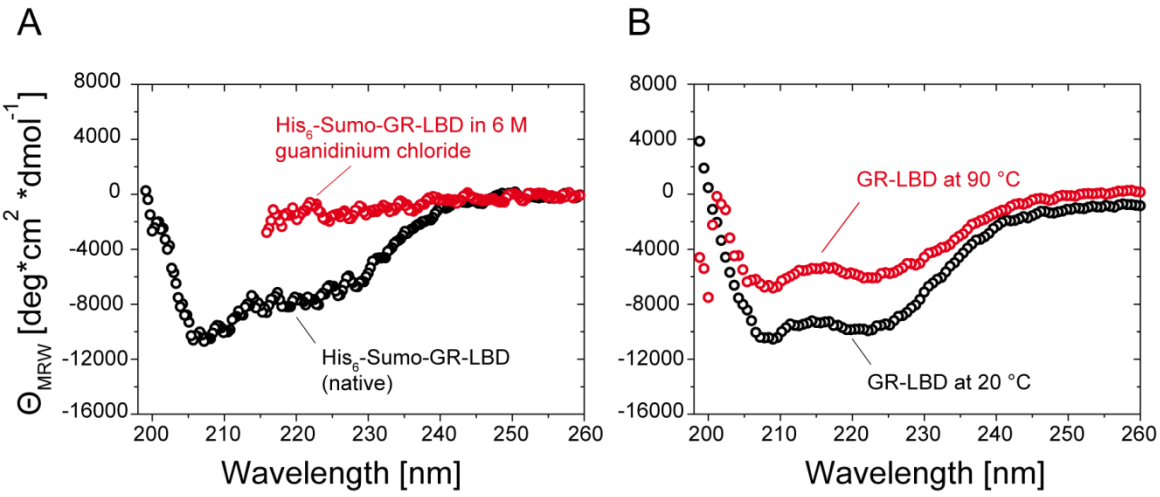

Figure 16 FAR-UV-CD spectra of refolded His$_6$-Sumo-GR-LBD and GR-LBD. A) 0.07 mg/ml His$_6$-Sumo-GR-LBD in PBS, 0.1 % (w/v) Zwittergent, pH 7.5 (black) and 0.06 mg/ml His$_6$-Sumo-GR-LBD in PBS, 6 M Guanidinium chloride, 0.1 % (w/v) Zwittergent, pH 7.5 (red) at 20 °C. B) 0.05 mg/ml GR-LBD alone in PBS, 0.1% (w/v) Zwittergent, pH 7.5 at 20 °C (black) and 90 °C (red). Spectra were recorded from 260 nm-215/200 nm with 5-10 accumulations. All spectra were buffer-corrected.

To assess the oligomeric state of the refolded receptor, analytical gel filtration (3.6.5) was performed (Figure 17A). GR eluted as a homogenous protein at 26.9 min, which corresponds to a molecular mass (MW) of 97 kDa indicating that the refolded receptor is predominantly a dimer (theoretical MW = 42.8 kDa). However, this result was not in agreement with analytical ultracentrifugation (AUC) sedimentation velocity experiments, in which His$_6$-Sumo-GR-LBD sedimented with a mass of 38.6 kDa (not shown). Thus, AUC sedimentation equilibrium analysis was carried out (Figure 17B). In contrast to previous measurements, this method gives rise to the molecular mass independently from the molecular shape of the protein. Experiments with three different GR concentrations were performed (0.2, 0.15 and 0.1 mg/ml, respectively). In turned out, that refolded receptor behaved monomeric in these measurements. From a global fit function using a single species model, a mass of ~ 30 kDa was calculated. Consistent with this, AUC sedimentation velocity experiments revealed, that refolded non-tagged GR-LBD was monomeric as well (calculated MW: 29.8 kDa, theoretical MW = 29.3 kDa), indicating that the N-terminal Sumo-tag does not influence oligomerization properties (not shown).

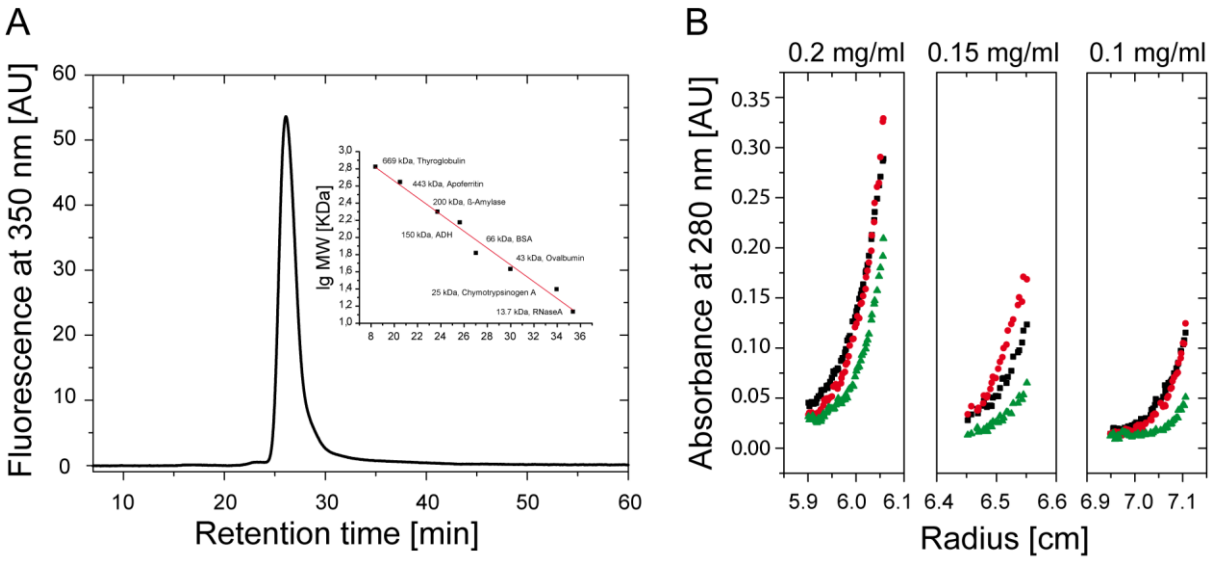

Figure 17 Analysis of the oligomeric state of refolded His_6-Sumo-GR-LBD. A) Analytical gel filtration analysis. A Superdex 200 10/300 GL column (GE Healthcare) was equilibrated with buffer containing 50 mM Tris, 150 mM NaCl, 5 mM DTT, 0.1 % (w/v) Zwittergent 3-12, pH 7.5. Prior to loading of 20 µl of 0.17 mg/ml His_6-Sumo-GR-LBD, 25 µl of various standard proteins with different size at a concentration of 4 mg/ml were applied to obtain a calibration curve (see inset). The flow rate was set to 0.5 ml/min and elution profiles were recorded at 350 nm (Excitation wavelength: 280 nm). Gain settings were adjusted for each analyzed protein. An apparent MW of 97 kDa was obtained for the refolded receptor. B) AUC sedimentation equilibrium experiments. Three concentrations of refolded His_6-Sumo-GR-LBD (0.2, 0.15 and 0.1 mg/ml, respectively) were tested at three different rotor speeds: 25,000 rpm (black), 30,000 rpm (red) and 35,000 rpm (green) in a four-hole Beckman–Coulter AN60-Ti rotor. PBS, 0.1 % (w/v) Zwittergent 3-12, 2 mM TCEP, pH 7.7 was used as measurement buffer. The obtained dataset was globally fitted using UltrascanII with a single species model. A mass of ~ 30 kDa was calculated. For further details see 3.6.6.

To determine the hormone binding properties of refolded GR, fluorescence anisotropy measurements with Dexamethasone Fluorescein (F-DEX) were performed (3.7.2.1). Even though McLaughlin and Jackson, (2002) provided some evidence for hormone binding activity of the GR-LBD refolded in Zwittergent 3-12 (dissociation constant, K_D = 46 µM), no specific ligand binding was observed here (not shown). Thus, although homogenous and apparently folded GR was obtained, refolding using the detergent Zwittergent 3-12 yielded no functional receptor protein. Zwittergent 3-12 induces most likely a non-native, artificial GR-LBD conformation in which the steroid binding site is collapsed such in a way that DEX is not able to enter (or remain bound in) the hydrophobic cleft.

4.1.2 Expression and purification of GR mutants produced in *E. coli*

4.1.2.1 Expression analysis and purification of GR-LBD mutants

So far, all purification attempts to obtain functional human GR-LBD in a ligand-free state from *E. coli* or insect cells had failed.

Thus, several reported human GR-LBD mutants, which can be expressed in *E. coli* cells in the presence of ligand, were examined as they might serve as GR *wt* surrogates to analyze the Hsp90-client interaction *in vitro*. Human GR-LBD (527-777) variants were generated by site directed mutagenesis and cloned into a novel, engineered pETHalo-vector (3.2.3.3, 3.2.4), allowing the expression of GR mutants fused to a cleavable N-terminal His_6-Halo-tag. Similar to MBP-, Sumo- or GST-fusions, the Halo-tag serves as a solubility enhancing tag. As the Halo-protein is designed to covalently bind synthetic ligands, *HaloTag-technology* (Promega; Ohana et al., 2009) can be used later on to specifically link fluorescent dyes or affinity handles to purified GR-LBD, without perturbing its structure and potential Hsp90 interaction surfaces, respectively. GR-LBD mutants were expressed in the presence of the stabilizing ligand dexamethasone (DEX) and analyzed for solubility as described in Figure 18.

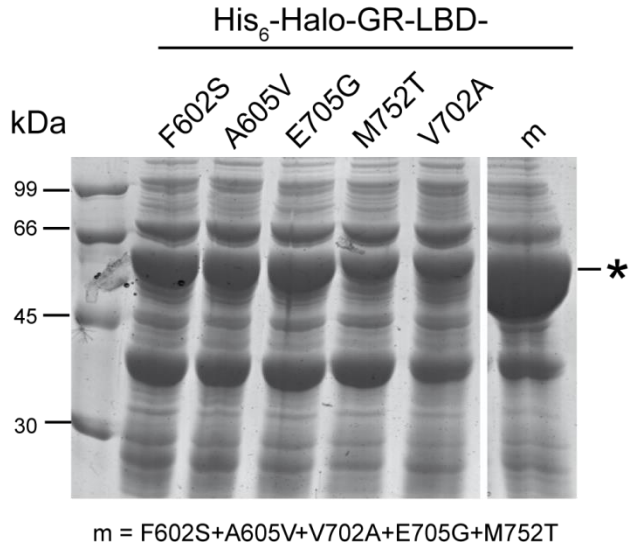

Figure 18 Expression analysis of His_6-Halo-GR-LBD mutants. Expression plasmid-carrying *E. coli* BL21-CodonPlus(DE3)-RIL cells were grown in 50 ml volumes for 4 h at 37 °C using ZYM-5052 auto induction media (Studier, 2005). Then, cultures were supplemented with 500 µM DEX, followed by overnight incubation at 20 °C. After cell harvest, bacterial pellets were resuspended in 50 mM Tris, 400 mM NaCl, 0.5 % CHAPS, 10 % Glycerol, 10 mM Imidazole, 50 µM DEX, 2 mM ß-Mercarptoethanol, pH 7.8 supplemented with Protease Inhibitor HP (Serva) and DNase I (Roche Diagnostic GmbH). Next, cells were disrupted with glass beads (Ribolyser, Thermo Scientific) and separated supernatants (500µl) were applied to His SpinTrap columns (GE Healthcare). Finally, proteins were eluted in the above-mentioned buffer supplemented with 500 mM Imidazole and analyzed by SDS-PAGE (3.6.3). Five single point mutants and a mutant, containing all 5 mutations were analyzed as indicated. (*) recombinant proteins.

In contrast to previous expression studies with GR *wt* (4.1.1.1), analyzed GR-LBD mutants were much more soluble compared to the *wt* protein. As expected, the highest yield of soluble produced protein was obtained for the mutant GR-LBD-F602S/A605V/V702A/E705G/M752T (GR-LBDm).

For analysis, GR-LBD mutants were manufactured in *E. coli* by applying an auto induction expression approach (Studier, 2005) and purified as outlined in Figure 19. High yields of recombinant protein was obtained for GR-LBDm, consistent with previous expression studies (see Figure 18). Approximately 1 mg of apo-GR-LBDm, and 10 mg of ligand-bound GR protein (holo-GR-LBDm) per liter high-density *E. coli* culture, respectively, were routinely achieved.

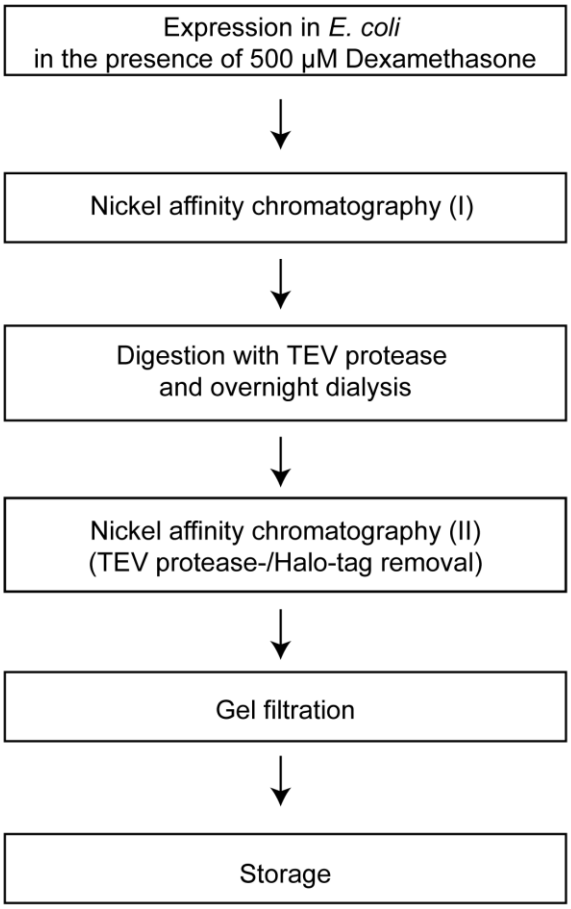

Figure 19 Expression and purification scheme of GR-LBD mutants. Expression was carried out at 18 °C in ZYM-5052 auto induction media (Studier, 2005) supplemented with 500 µM DEX. The purification strategy was adopted from Seitz et al., (2010) with minor modifications. Briefly, in the first step, His_6-Halo-GR-LBD mutants were purifed by nickel affinity chromatography. Then, the His_6-Halo-tag was cleaved off by TEV protease overnight, followed by a second nickel affinity chromatography step to separate his-tagged TEV protease, Halo-tag or uncleaved protein. Finally, GR-LBD mutants were polished by gel filtration and eluted fractions were pooled, concentrated and stored at -80 °C. Apo-GR-LBDm was expressed without hormone and purified according to same protocol with slight modifications. For purification of His_6-Halo-GR-LBDm, the TEV protease-cleavage step was omitted and GR protein was directly subjected to gel filtration chromatography. For further details see 3.6.1.1.

4.1.2.2 Characterization of GR-LBDm produced in *E. coli*

For basic characterization of the GR-LBD, work was focused on the mutant GR-LBDm (4.1.2.1). GR-LBDm was prepared either in the presence or in the absence of hormone (holo- and apo-GR-LBDm, respectively), resulting in GR preparations of ~ 98 % and ~ 85 % purity grade, respectively, as judged from SDS-PAGE and MS analysis.

GR proteins were characterized by FAR-UV-CD spectroscopy to determine their secondary structure content (Figure 20A). Holo-GR-LBDm showed high α-helical content, typical for steroid receptor LBDs (Wurtz et al., 1996) and in line with reported crystal structures of the hormone-bound GR-LBD (Bledsoe et al., 2002; Schoch et al., 2010; Seitz et al., 2010). Apo-GR-LBDm displayed decreased secondary structure compared to holo-GR-LBDm. Moreover, it was less stable with respect to thermal denaturation (Figure 20B). While holo-GR-LBDm shows a sharp cooperative transition with an apparent melting temperature of 59.6 °C, thermal induced denaturation of apo-GR-LBDm started already at 10 °C and continued over a wide temperature range.

Noteworthy, His_6-Halo-GR-LBDm (the non-TEV cleaved receptor preparation) displayed similar characteristics as it showed high α-helical content and cooperative folding behavior (T_M = 63.8 °C).

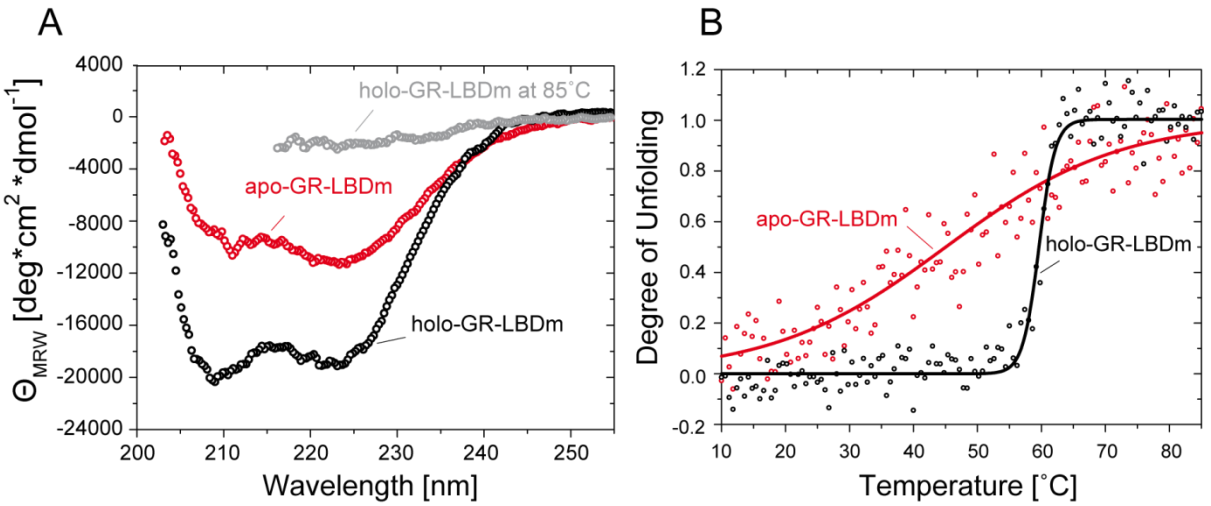

Figure 20 Secondary structure analysis and thermal stability of apo- and holo-GR-LBDm. A) 0.1 mg/ml apo-GR-LBDm (red) or holo-GR-LBDm (black) was analyzed by FAR-UV-CD spectroscopy. Spectra were recorded from 260 nm-203 nm at 10 °C (or for the holo-GR-LBDm (grey) from 260-215 nm at 85 °C). All CD-spectra were buffer-corrected. B) Thermal induced unfolding of apo-GR-LBDm (red) and holo-GR-LBDm (black) measured at 220 nm from 10-85 °C with a heating reate of 20 °C/h. An apparent melting temperature of 59.6 °C was determined for holo-GR-LBDm using a boltzman fit. CD experiments were performed in 25 mM NaH_2PO_4, 100 mM NaCl, 2 mM TCEP, 10 % Glycerin, pH 7.9. Holo-GR-LBDm was measured in the presence of 50 µM DEX. Experiments were performed in collaboration with Daniel Rutz (Technische Universität München).

The oligomeric state of apo- and holo-GR-LBDm was assessed by AUC sedimentation velocity experiments. Holo-GR-LBDm sedimented as homogenous, monomeric protein with an s-value of 2.3 S (Figure 21). In contrast, apo-GR-LBDm was aggregation-prone as judged from the AUC profile. Interestingly, aggregation could be suppressed to a significant extent when DEX was added to the apo-receptor during measurements (not shown), suggesting that present hormone stabilizes GR. This finding is also consistent with the CD spectroscopy experiments described above, which clearly demonstrated that cooperative folding and stability of the holo-receptor strikingly differ from the apo-form of GR-LBDm.

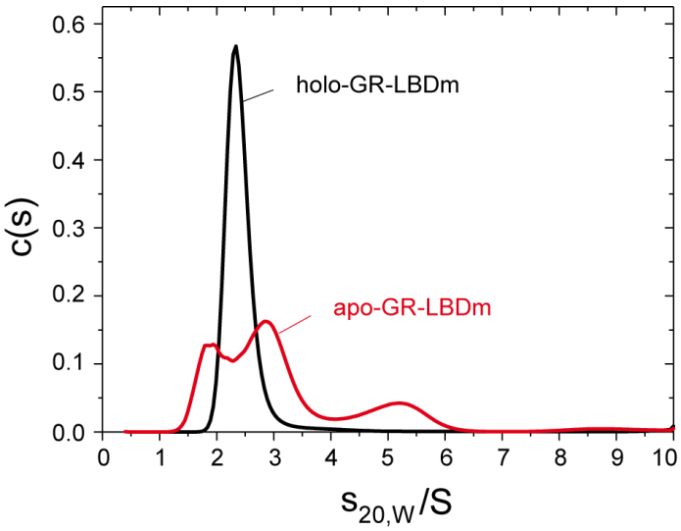

Figure 21 AUC sedimentation velocity experiments. Sedimentation profile of 5.7 µM holo-GR-LBDm (black) monitored at 280 nm and 2 µM apo-GR-LBDm (red) monitored at 230 nm, respectively. Measurements were performed at 20 °C in 20 mM Hepes, 200 mM NaCl, 1 mM TCEP, pH 7.4. Holo-GR-LBDm was analyzed in the presence of 10 µM DEX. Experiments were performed in collaboration with Daniel Rutz (Technische Universität München).

To determine the hormone binding activity of both GR preparations, apo-GR-LBDm and holo-GR-LBDm were analyzed by fluorescence anisotropy using F-DEX (3.7.2.1) (Figure 22). Apo-and holo-GR-LBDm bound F-DEX with nanomolar affinity, which is consistent with previous reports on other GR-LBD mutants such as GR-LBD-F602S (Bledsoe et al., 2002). Fitting of the titration data yielded apparent K_Ds of 97 nM and 77 nM, respectively. Also, competition experiments with excess unlabeled DEX after saturation of the apo-receptor with F-DEX demonstrated that the ligand can be readily exchanged (see inset Figure 22). Thus, hormone binding is dynamic and the ligand binding pocket of GR-LBDm is accessible to hormone in the absence of Hsp90. Of note, His_6-Halo-GR-LBDm bound F-DEX with a K_D in the low nanomolar range as well (K_D ~ 60 nM), showing that the Halo-tag does not influence hormone binding properties and suggests that also the unprocessed Halo-GR fusion is functional.

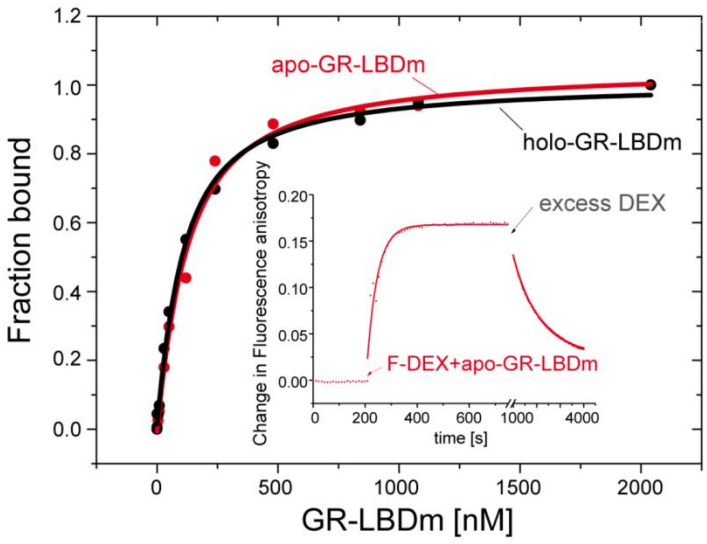

Figure 22 Hormone binding activity (ligand exchange) of apo- and holo-GR-LBDm. Increasing amounts of GR-protein was incubated with 50 nM F-DEX for 2 h to determine steady state ligand binding affinity. Holo-GR-LBDm was extensively dialyzed prior to measurements to remove unbound hormone carried over from purification. Affinity constants were calculated from a ligand-depletion fit. For apo-GR-LBDm and holo-GR-LBDm a K_D of 97 nM and 77 nM, respectively, was calculated. Inset: Ligand binding kinetics were recorded after the addition of 1 µM GR to 50 nM F-DEX. For dissociation kinetics, pre-formed F-DEX-GR-LBDm complexes were chased with 50 µM unlabeled DEX. Measurements were performed at 25 °C in 20 mM Hepes, 150 mM NaCl, 0.04 % CHAPS, 0.05 % BSA, 0.2 mM TCEP, pH 7.4 with excitation and emission wavelengths set to 484 and 520 nm, respectively.

In addition to previous hormone binding assays, receptor functionality was further assessed by co-regulator interaction studies (see also 1.4.4). To investigate the recruitment of co-regulators to GR-LBDm, agonist (DEX) or antagonist (mifepristone, MIF)-bound receptor protein was prepared, titrated to fluorescently labeled co-activator (*Tif2)- and co-repressor peptide (*NcoR), respectively, and the change in fluorescence polarization was recorded. For comparison, GR-LBD-F602S was assayed as well.

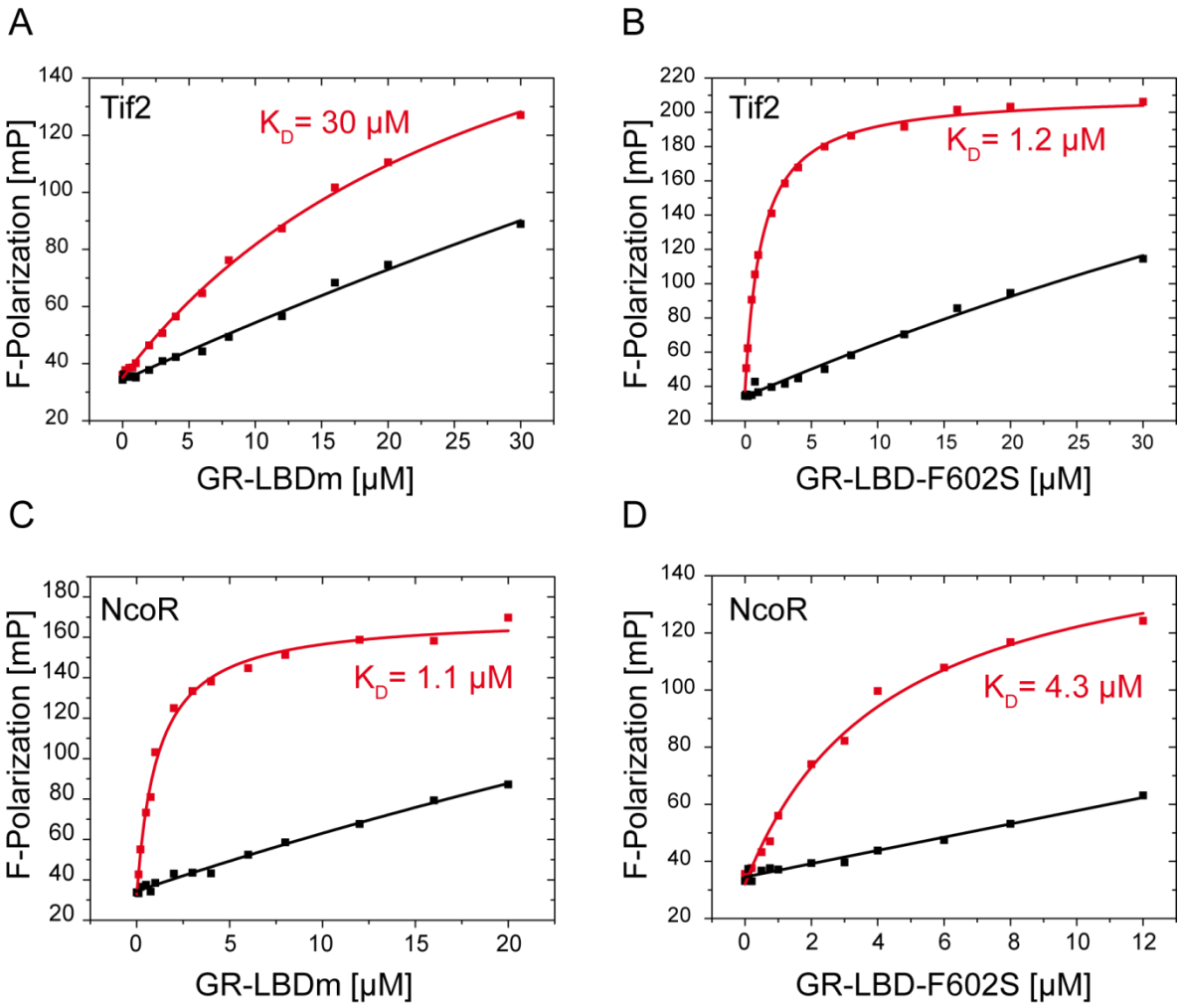

Figure 23 Binding of GR-LBDm and GR-LBD-F602S to co-regulator peptides. Increasing amounts of GR-LBDm and GR-LBD-F602S, respectively, were titrated to 50 nM fluorescently labeled peptide (red); *Tif2: FITC-(Ahx)- KENALLRYLLDKDD, *NcoR: FITC-(Ahx)-ASNLGLEDIIRKALMGSFD. Unspecific binding was determined by the addition of excess unlabeled peptide (black). Fluorescence polarization was measured at 25 °C in 20 mM Hepes, 150 mM NaCl, 0.04 % Chaps, 0.2 mM TCEP, 0.05-0.2 % BSA, pH 7.4. Excitation and emission wavelengths were set to 485 and 520 nm, respectively. For binding analysis to *NcoR, GR-LBDm and GR-LBD-F602S were extensively dialyzed to remove unbound DEX carried over from purification. After exposure to 200 µM MIF overnight at 4 °C, MIF-bound receptors (GR-LBDm-MIF and GR-LBD-F602S-MIF, respectively) were centrifuged and assayed. During measurements, hormone concentrations were set to 50 µM DEX and 200 µM MIF, respectively. A) Binding of GR-LBDm-DEX to *Tif2. B) Binding of GR-LBD-F602S-DEX to *Tif2. C) Binding of GR-LBDm-MIF to *NcoR. D) Binding of GR-LBD-F602S-MIF to *NcoR. A-D). K_D-values are indicated in figures and were obtained by a single-site binding fit.

Binding of both GR-LBDm and GR-LBD-F602S to co-regulator peptides was rapid and occurred in the time-scale of seconds. Steady-state peptide binding experiments revealed (Figure 23A, B) that DEX-bound GR-LBDm interacted only weakly with the co-activator peptide Tif2 (K_D = 30 µM), whereas, consistent with earlier reports (Bledsoe et al., 2002; Kroe et al., 2007; Seitz et al., 2010), much stronger binding was observed for GR-LBD-F602S (K_D = 1.2 µM). In the presence of MIF (Figure 23C, D), binding of GR-LBDm and GR-LBD-F602S to the co-repressor peptide NcoR was comparable (K_D = 1.1 µM and K_D = 4.3 µM, respectively). These experiments suggest that co-regulators can be recruited to GR-LBDm and show that GR-LBDm is a functional protein. The fact, that DEX-bound GR-LBDm has a ~ 30x fold lower affinity for the Tif2 peptide as agonist-bound GR-LBD-F602S could be explained by a slightly different conformation of helix 12 of GR-LBDm (see also 1.4.4). Together with the finding that GR-LBDm bound NcoR more tightly than GR-LBD-F602S, it is plausible that the combination of mutations present in GR-LBDm shift the equilibrium from an agonistic towards an antagonistic LBD conformation (see also 1.4.4). However, structural studies with GR-LBDm (e.g. crystallization) are required to fully understand the observations made here.

4.1.2.3 Expression, purification and characterization of GR-DBD-LBDm produced in *E. coli*

Human GR-LBDm was successfully purified from *E. coli* and displayed excellent biochemical properties in terms of folding, stability and hormone binding activity (4.1.2.2). Next, a longer GR construct was generated that comprises the *wt* human GR-DNA binding domain (GR-DBD) connected to the mutated GR-LBDm by a small hinge region. Similar to GR-LBDm, human GR-DBD-LBDm (420-777) was produced in *E. coli* in the presence of DEX using an auto induction expression approach (Studier, 2005) and purified as described in 3.6.1.1. Achieved protein yields ranged from 5-10 mg receptor protein per liter high-density *E. coli* culture and were thus comparable to protein yields obtained for GR-LBDm.
Folding, stability and hormone binding activity of ligand-bound GR-DBD-LBDm was compared to GR-LBDm by applying identical methods and assay conditions (4.1.2.3). It turned out, that GR-DBD-LBD displays highly similar characteristics (Table 4).

Table 4 Biochemical properties of GR-DBD-LBDm and GR-LBDm

Characteristics*	GR-DBD-LBDm	GR-LBDm
Secondary structure	high α-helical content	high α-helical content
Thermal stability (T_M)	56.0 °C	59.6 °C
Oligomeric state	monomeric	monomeric
Hormone binding (K_D)	130 nM	77 nM

* Applied methods and assay conditions were identical for both constructs. Folding and stability was assessed by CD spectroscopy measurements. The oligomeric state was addressed with AUC sedimentation velocity experiments. Fluorescence anisotropy was used to determine hormone binding activity. See figures in 4.1.2.2 for further experimental details.

DNA-binding activity was examined by an electrophoretic mobility gel shift assay (EMSA) and fluorescence polarization using fluorescently labeled GRE-DNA (GRE*-DNA). Qualitative analysis utilizing EMSA (Figure 24A) showed that GR-DBD-LBDm can bind a significant amount of GRE*-DNA. Moreover, the rather diffuse migration pattern suggests that dimerization occurs upon association with DNA, consistent with previous observations (Dahlman-Wright et al., 1991). Binding of GRE-DNA (and release) was fast and occurred within seconds. Steady state binding experiments (Figure 24B) demonstated that GR-DBD-LBDm binds GRE*-DNA with nanomolar affinity (IC_{50} = 410 nM) which is in agreement with published results for GR-DBD-LBD-F602S (Simmons et al., 2008).

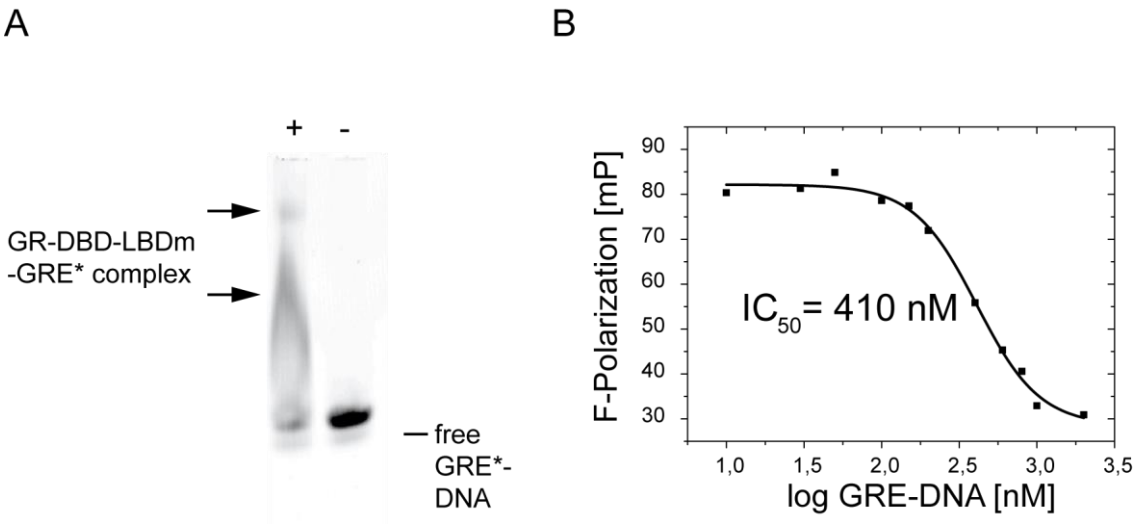

Figure 24 DNA binding properties of GR-DBD-LBDm. A) DNA binding analysis by EMSA. 6 nM double-stranded Cy5-labeled GRE-DNA (GRE*-DNA) was incubated with 0.1 µM GR-DBD-LBDm for 30 min at 4 °C; GRE-Sequence (5'-3'): gatccagaacaaaatgttctg. After sample loading on an native 4 % polyacrylamide gel, electrophoresis was carried out for 3 h at 4 °C with a constant current of 25 mA. After electrophoresis, GRE*-DNA was detected by a Typhoon 9600 Phosphoimager. Arrows indicate gel shifts. (+) GRE*-DNA was incubated with GR-DBD-LBDm, (-) GRE*-DNA alone. EMSA analysis was kindly performed by Julia Rohrberg (Technische Universität München). B) DNA binding analysis by fluorescence polarization. 400 nM GR-DBD-LBDm was pre-incubated with 10 nM FAM-labeled GRE DNA and chased with different amounts of unlabeled GRE-DNA. Measurements were performed at 25 °C in 25 mM Tris, 100 mM NaCl, 10 % Glycerol, 2 mM DTT, 50 µM DEX, pH 7.9 with excitation and emission wavelengths set to 485 and 520 nm, respectively. Data were fit using a dose-response equation. An IC_{50} of 410 nM was calculated.

Taken together, also a GR construct that comprises both the GR-DBD and the GR-LBD was successfully purified in a functional form.

4.1.3 Summary and conclusions

A source of pure and functional GR is required to elucidate the molecular determinants of the Hsp90-GR interplay. Despite several attempts, GR-LBD *wt* in its ligand-free state was not obtained from *E. coli* as homogenous protein. The formation of soluble and insoluble aggregates, presumably due to a collapse of the GR-LBD fold, likely reflects its demand on the Hsp90-chaperone system or the presence of hormone. Also, receptor refolding was not successful. Although denatured GR-LBD could be solubilized in the presence of Zwittergent 3-12, refolded GR showed no specific hormone binding affinity and was hence not further considered.

Insect cell expression did not yield satisfactory protein amounts. Possibly, expression conditions were sub-optimal and need further improvement. High amounts of insoluble protein accumulated also in insect cells, indicating that the endogenous insect chaperone system could not handle the amount of manufactured GR, which might be otherwise prone to aggregation or degradation. This is also consistent with the finding that in Sf9 cells only 0.35 % of the overexpressed GR assembles into Hsp90-receptor complexes, while the rest of the cytoplasmatic protein accumulates in the form of insoluble aggregates (Alnemri and Litwack, 1993). The following strategies can be applied to facilitate recombinant production of functional GR in insect cells: (1) Co-expression with human Hsp90 (Alnemri and Litwack, 1993), (2) Co-expression with a minimal human chaperone system containing Hsp90, Hsp70, Hop, Hsp40 and p23 (AB Vector LLC, San Diego, USA) and (3) Supplementation of the culture media with glucose to maintain intracellular ATP levels high. This seems to promote GR-Hsp90 complex formation, resulting in higher yields of functional GR (Srinivasan et al., 1997).

Mutated GR-LBD such as GR-LBDm, GR-LBD-F602S or longer constructs comprising the GR-DNA binding domain as well (GR-DBD-LBDm) were obtained in milligram quantities from *E. coli* in a functional form and may represent an ideal starting point to analyze the Hsp90-GR interaction in more detail using biochemical and biophysical methods beyond classical immunoprecipitation experiments. Besides stabilizing and solubility enhancing mutations, key parameters such as the usage of auto induction media (Studier, 2005) and the addition of the high-affinity ligand DEX during expression strongly contributed to the success of the strategy. Expression and purification of apo-GR-LBDm was less successful, as its purity grade was not as high compared to the holo-receptor (~ 85 % vs. ~ 98 %). In addition, the preparation was prone to aggregation and showed high intrinsic instability. Noteworthy,

apo-GR-LBDm could not be prepared by a dialysis approach, as mass analysis revealed that even extensive buffer exchange did not yield hormone-free receptor.

4.2 The GR-Hsp90 interplay

Parts of this work will be published soon (including figures, text and related methods):

'Modulation of the Hsp90 chaperone cycle by a stringent client protein'
Oliver Robin Lorenz, Lee Freiburger, Daniel Andreas Rutz, Maike Krause, Bettina Karolina Zierer, Sara Alvira, Jorge Cuéllar, José María Valpuesta, Tobias Madl, Michael Sattler & Johannes Buchner, Mol.Cell 2014, *Accepted*

4.2.1 Reconstitution of the GR-Hsp90 complex

4.2.1.1 Transcriptional activity and Hsp90 dependence of GR *in vivo*

It was shown in the previous chapter (4.1.2) that mutant GR domain constructs can be obtained as functional proteins from *E. coli* (e.g. GR-LBDm, GR-DBD-LBDm).

GR function *in vivo* strictly depends on the interaction of the GR-LBD with the Hsp90 chaperone machinery (Picard et al., 1990). Hence, the question arose whether transactivation of stabilized GR variants relies on Hsp90 to a similar extent. To address this issue, a yeast reporter assay was applied, in which Hsp90-dependent GR transactivation can be monitored by ß-galactosidase expression and activity (Nathan and Lindquist, 1995). Transcriptional activity of full-length GR-F602S/A605V/V702A/E705G/M752T (GRm) and GR point mutants, which contained only one of the stabilizing mutations, was analyzed and compared to GR *wt* (Figure 25).

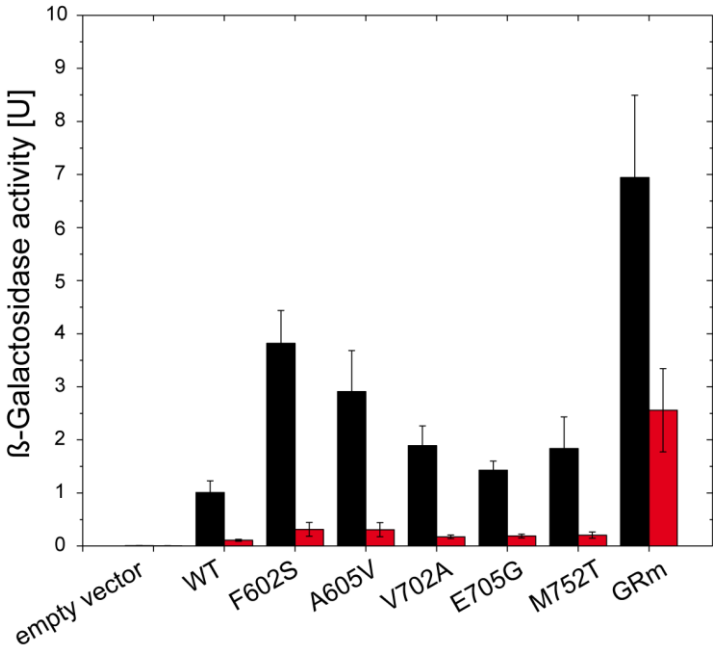

Figure 25 Hsp90-dependence of GR mutants assayed in yeast. Transcriptional activity was determined as described in 3.9.1. *S. cerivisae* BY4741 cells harboring the GR expression plasmid (or empty vector) and the reporter plasmid were grown at 30 °C, diluted to an OD_{600} ~ 0.3 and exposed to 10 µM DOC followed by overnight incubation. To measure Hsp90-dependent transactivation, 20 µM of the Hsp90 inhibitor radicicol (in DMSO) was added. Control cells were treated with DMSO. Then, yeast cells were lysed and assayed for ß-galactosidase activity. Shown are the averaged β-galactosidase activities and standard deviations of three independent experiments with each GR variant (GRm: GR-F602S/A605V/V702A/E705G/M752T). Black bars show ß-galactosidase activities of control cells, red bars show residual receptor activity after radicicol treatment.

Upon activation with the ligand 11-deoxycorticosterone (DOC), all GR mutants were able to induce ß-galactosidase expression. Interestingly, GR variants displayed increased hormone responsiveness compared to GR *wt*, which likely reflects their increased *in vivo* half-times. However, upon addition of the Hsp90 inhibitor radicicol, the activities of GR mutants and *wt* significantly decreased, indicating that stabilizing mutations do not abolish Hsp90 dependence *in vivo*. GRm transactivation was less Hsp90-dependent compared to GR *wt* and

GR single point mutants (~ 35 % and ~ 10 % residual transcriptional activity upon radicicol treatment, respectively), which could explain the finding, that its respective LBD displays enhanced stability and solubility compared to GR *wt in vitro* (4.1.1.1,4.1.2.1,4.1.2.2). Of note, a similar pattern in ß-galactosidase expression was observed when the ligand DEX was used instead (not shown), although hormone responsiveness was significantly higher than in measurements with DOC. The reason for this finding could not be resolved but it could be due to the fact, that the GR-LBD mutants were evolved for solubility and stability in the presence of DEX (Seitz et al., 2010).

4.2.1.2 Mutant GR-LBD forms complexes with Hsp90 *in vitro*

Despite the relevance of the Hsp90 system for GR activity in the cell, the underlying mechanism of their interaction remained elusive. Having confirmed that GRm and other GR mutants are *bona fide* clients of Hsp90 (4.2.1.1), reconstitution experiments with GR-LBDm were performed. It turned out that the apo-GR-LBDm could not be handled in reconstitution studies, consistent with its high instability *in vitro* (Figure 20, Figure 21). Since hormone binding to SHRs does not directly seem to stimulate Hsp90 release (Smith, 1993), it was decided to work with the ligand-bound form of GR-LBDm to define the principles of the interaction of a client with Hsp90.

In a first attempt, classical immunoprecipitation experiments were performed (Pratt and Toft, 1997). Purified His_6-Halo-GR-LBDm was incubated with rabbit reticulocyte lysate (RLL, a rich source of molecular chaperones) at 30 °C under ATP conditions and then captured by covalent bead coupling (3.9.3). After several washing steps, GR-LBDm was eluted and samples were analyzed by Western blotting using antibodies specific for Hsp90, Hsp70, Hop, Hsp40, p23 and GR (Figure 26A). It turned out, that GR co-immunoprecipitated with Hsp90 and p23. Hsp70 was detected in the control as well, indicating mainly unspecific binding to GR. No signals for Hsp40 and Hop were detected. However, these results strongly suggest that GR-LBDm forms complexes with Hsp90 and/or p23 consistent with the notion that those complexes represent late assemblies in the GR maturation cycle (Pratt and Toft, 1997).

Next, the question was addressed whether GR-LBDm interacts also with Hsp90 in the absence of the ‘complete’ chaperone system present in RLL. Thus, His_6-Halo-GR-LBDm was covalently labeled at its N-terminal Halo moiety with a rhodamine dye (TMR) using *HaloTag-technology* (Promega) and analyzed by AUC coupled to fluorescent detection for binding to yeast Hsp90 under ATP conditions (Figure 26B).

Fluorescently labeled GR sedimented with an s-value of 3.8 S. Upon addition of Hsp90, a shift of ~ 2 S-values was observed, demonstrating complex formation of the GR fusion with the chaperone. The N-terminal Halo-tag did not bind unspecific to yeast Hsp90 as determined in AUC experiments using fluorescently labeled yeast Hsp90 and the Halo-tag protein (not shown).

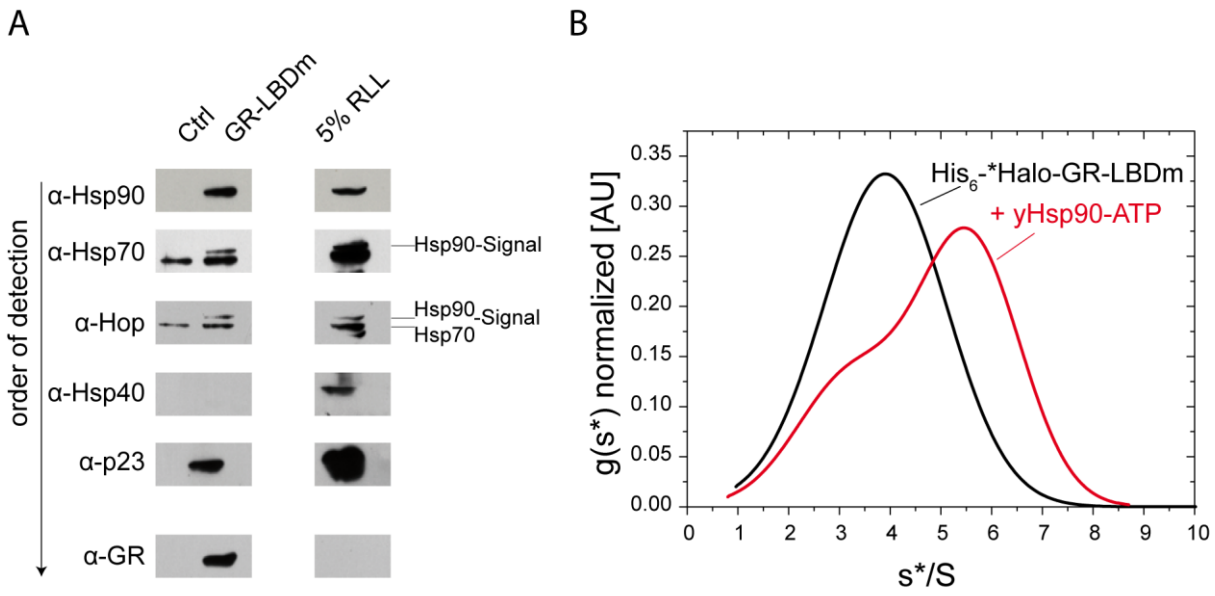

Figure 26 GR-LBDm binds Hsp90 *in vitro*. A) Pull-Down experiment. 20 µg His_6-Halo-tag (Ctrl) or 20 µg His_6-Halo-GR-LBDm (GR-LBDm) was incubated with 45 µl rabbit reticulocyte lysate (RLL) (Promega) for 2 h at 30 °C. 5 mM ATP was added to the reaction mix. Then, 10 µl HaloLink Magnetic beads (Promega) were added to capture His_6-Halo-GR-LBDm and the control protein, respectively. Beads were washed with 20 mM Tris, 50 mM KCl, 5 mM $MgCl_2$, 0.01 % NP-40, 20 mM Na_2MoO_4, 2 mM DTT, pH 7.5, and eluted in the same buffer supplemented with TEV protease. Eluates were subjected to SDS-PAGE (3.6.3) and subsequent Western blot analysis (3.6.4). Proteins were detected in a sequential manner by specific antibodies. Dilutions of primary antibodies: α-Hsp90 total: 1:300; α-Hsc70: 1:10,000; α-Hop: 1:5,000; α-Hdj1: 1:1,600; α-p23: 1:5,000; α-GR: 1:100. Secondary antibodies (α-mouse and α-rabbit-POD) were used at a dilution of 1:30,000. B) AUC sedimentation velocity experiments. 300 nM His_6-Halo-GR-LBDm was assayed for binding to 3 µM yeast Hsp90. Sedimentation profiles for His_6-Halo-GR-LBDm alone and with Hsp90 are depicted in black and red, respectively. Normalized g (s*) values were plotted against s*/S-values. Measurements were performed at 20 °C in 20 mM Hepes, 20 mM KCl, 5 mM $MgCl_2$, 5 mM DTT, pH 7.5 supplemented with 20 mM Na_2MoO_4 and 2 mM ATP.

4.2.1.3 GR-LBDm-Hsp90 complex formation is nucleotide-dependent

So far, it could be demonstrated that GR-LBDm binds Hsp90 *in vitro* using either RLL as chaperone source or purified protein (4.2.1.2). Next, the question was addressed which nucleotide parameters affect complex formation. In contrast to previous measurements (4.2.1.2), molybdate was omitted as it is known to stabilize receptor-Hsp90 complexes (Pratt and Toft, 1997) and thus might bias the interaction of Hsp90 with GR. In addition, hormone was added to the measurement buffer to ensure complete saturation of GR throughout the experiment. Also, work was continued with the individual GR-LBDm to rule out any influence of the Halo-tag on binding efficiency.

GR-LBDm was labeled at cysteine residues with a fluorescent Atto-488 dye (3.6.2) and again, AUC coupled to fluorescence detection was used to monitor the association of Hsp90 with GR (Figure 27). Fluorescently labeled GR-LBDm alone (*GR-LBDm) sedimented with an s-value of 2.7 S, consistent with its monomeric state in solution (4.1.2.2). Upon addition of yeast Hsp90, the s-value increased to 5.6 S, demonstrating complex formation between *GR-LBDm and Hsp90 (Figure 27A). This interaction was observed both in the absence of nucleotides and in the presence of ADP. However, binding of GR was strongly enhanced in the presence of ATP and moderately increased with the slowly hydrolyzing ATP analog ATPγS (Figure 27A). Consistent with a gain in compaction of the Hsp90 dimer upon ATP or ATPγS binding (Li et al., 2013), the s-value of the complex increased to 5.9-6.1 S. The addition of the nonhydrolysable ATP analogue 5'–adenylyl-ß,γ-imido-diphosphate (AMP-PNP), which induces a fully closed Hsp90 conformation (Ali et al., 2006) was less efficient in promoting complex formation. The specificity of the interaction was further demonstrated by the addition of the Hsp90 inhibitor radicicol, which binds to the nucleotide binding site of Hsp90 (Schulte et al., 1998), as a significant fraction of *GR-LBDm was released from Hsp90-ATP upon its addition (Figure 27B).

This scenario is conserved between yeast and man, as complex formation of GR with human Hsp90ß was also nucleotide-dependent (Figure 27C). Without nucleotides present, only a fraction of the GR was found in a complex with human Hsp90ß. Nucleotide addition promoted the interaction between *GR-LBDm and Hsp90 with ATP being most efficient for complex formation. The s-value of the complex was not altered by ATP or its analogues (6.6-6.7 S throughout), which is consistent with observations that human Hsp90 populates closed states to a lesser extent than its yeast counterpart (Krukenberg et al., 2011).

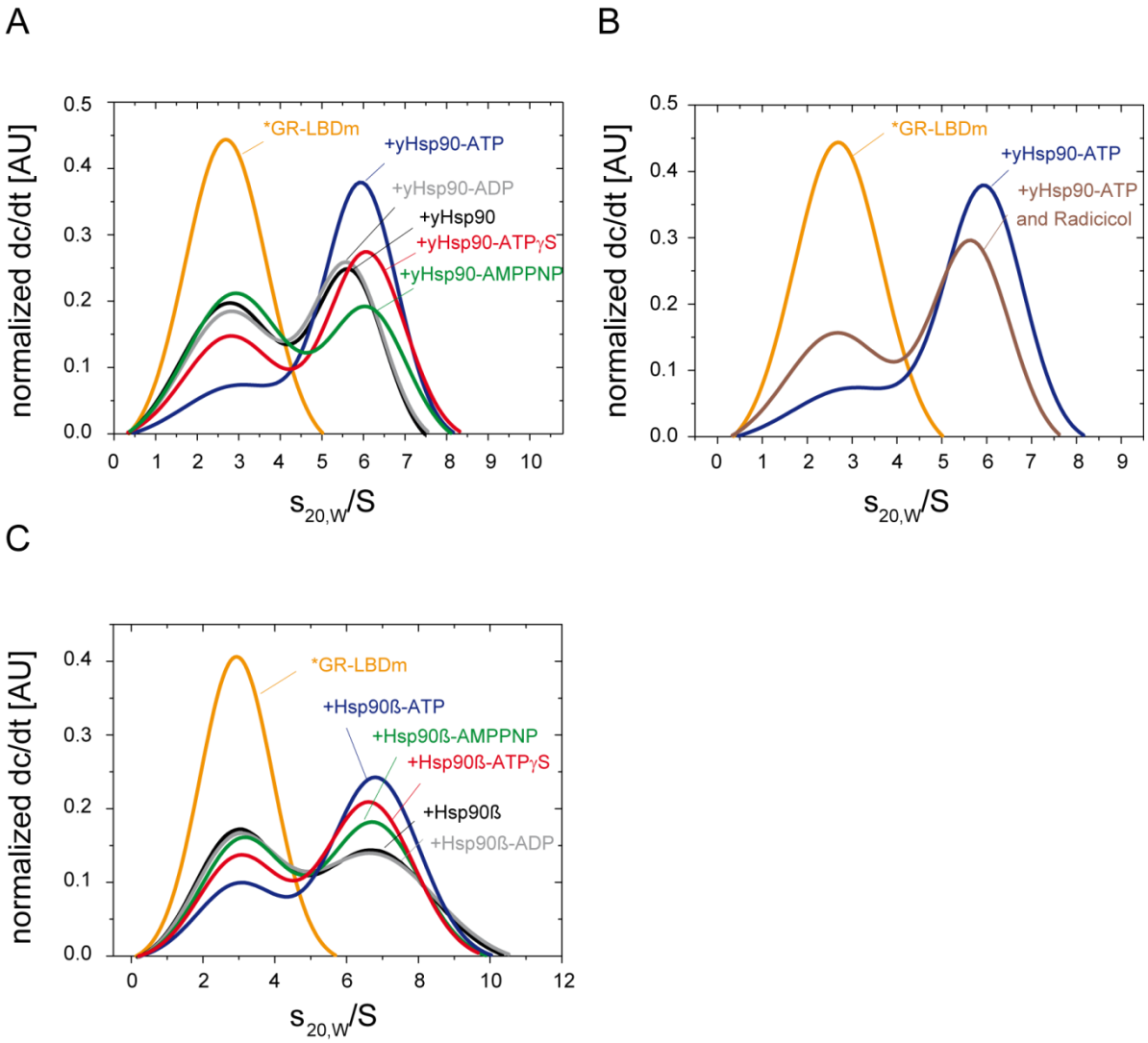

Figure 27 GR-LBDm binds preferentially to a partially closed Hsp90 conformation. AUC sedimentation velocity experiments with 400 nM fluorescently labeled GR-LBDm (*GR-LBDm) and 3 µM Hsp90. A) Complex formation with yeast Hsp90 in the presence and absence of various nucleotides as indicated. B) Yeast Hsp90-*GR-LBDm complexes can be disrupted with the Hsp90 inhibitor radicicol. Radicicol (in DMSO) was used at a concentration of 100 µM. Untreated samples were supplemented with DMSO. C) Complex formation with human Hsp90ß in the presence and absence of various nucleotides as indicated. Measurements were performed at 20 °C in 20 mM Hepes, 20 mM KCl, 5 mM $MgCl_2$, 5 mM DTT, pH 7.5 supplemented with 50 µM DEX and 2 mM of the respective nucleotides. Normalized dc/dt values were plotted against $s_{20,W}$/S-values.

Taken together, these results suggest that the GR-LBDm binds preferentially to an intermediate conformation of the Hsp90 dimer which forms during the ATP-dependent transition from the open to the closed state. To further test the notion that binding to a partially closed state of Hsp90 is preferred over binding to open Hsp90, AUC titration experiments were carried out in which different amounts of yeast Hsp90 were incubated with the *GR-LBDm in the absence and presence of various nucleotides (Figure 28). The affinity of the *GR-LBDm for different conformations of Hsp90 was calculated from the bound GR-LBDm fraction. GR-LBDm binds yeast Hsp90 in the presence of ATP or ATPγS with a K_D of 0.8 µM and 1.5 µM, respectively, whereas open yeast Hsp90 bound more weakly to GR-LBDm (K_D = 2.9 µM for apo-Hsp90 and K_D = 2.5 µM for Hsp90-ADP). A completely closed conformation in the presence of AMP-PNP leads to a further reduction of affinity (K_D = 4.5 µM).

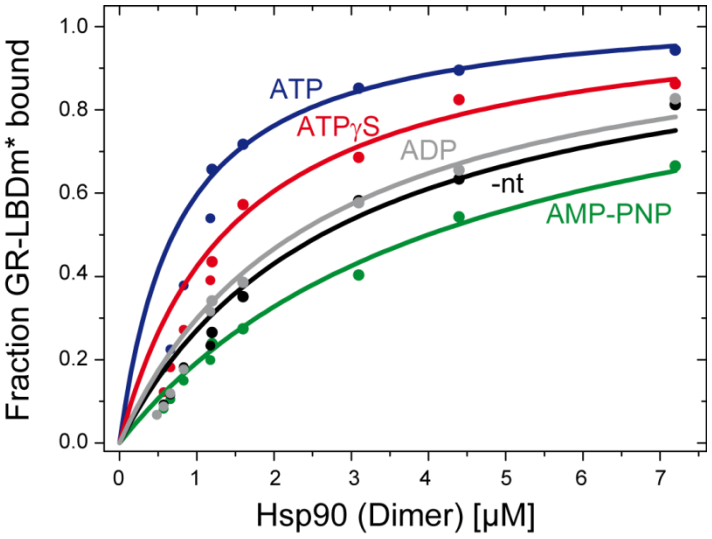

Figure 28 GR-LBDm binds Hsp90 with micromolar affinity. AUC sedimentation velocity experiments. 400 nm *GR-LBDm was titrated to increasing amounts of yeast Hsp90. Bound *GR-LBDm fraction was plotted versus Hsp90-dimer concentration. Data were fitted with a single-site binding model resulting in a K_D of 0.8 µM for Hsp90-ATP, 1.5 µM for Hsp90-ATPγS, 4.5 µM for Hsp90-AMP-PNP, 2.5 µM for Hsp90-ADP and 2.9 µM for apo-Hsp90 (Hsp90-dimer concentration). Analysis was performed in 20 mM Hepes, 20 mM KCl, 5 mM $MgCl_2$, 5 mM DTT, pH 7.5 supplemented with 50 µM DEX and 2 mM of the respective nucleotides. Analysis was performed in collaboration with Daniel Rutz (Technische Universität München).

Notably, the interaction of GR with Hsp90 was not biased by the mutations present in GR-LBDm. Although helix 12 of GR-LBDm might be partially shifted towards an antagonistic conformation (see 4.1.2.2) that could alter Hsp90-dependence (Ricketson et al., 2007), the binding affinity of GR-LBD-F602S (agonistic conformation) to fluorescently labeled yeast Hsp90-ATP was comparable (Figure 29A). As expected, GR-DBD-LBDm bound Hsp90 in a similar fashion (Figure 29B).

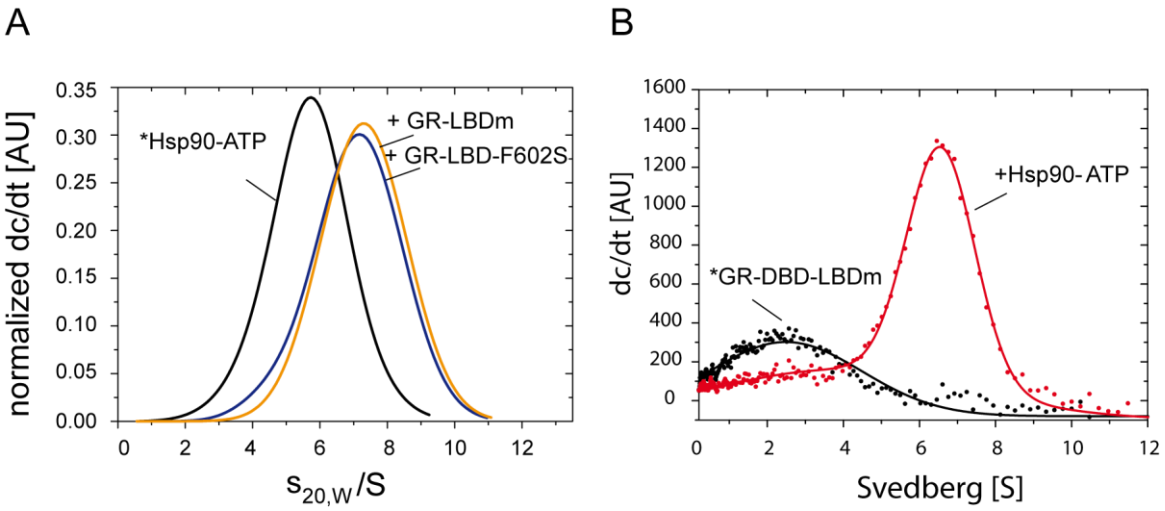

Figure 29 GR-LBD-F602S and GR-DBD-LBDm bind Hsp90 with comparable affinity. AUC sedimentation velocity experiments. A) 500 nM fluorescently labeled yeast Hsp90 was incubated with 6 µM GR-LBDm or GR-LBD-F602S. Experiment was performed by Andreas Kohlmeier (Technische Universität München). B) 400 nM fluorescently labeled GR-DBD-LBDm (*GR-DBD-LBDm) was incubated with 3 µM yeast Hsp90. Measurements were performed at 20 °C in 20 mM Hepes, 20 mM KCl, 5 mM $MgCl_2$, 5 mM DTT, pH 7.5 supplemented with 50 µM DEX and 2 mM ATP. Dc/dt values were plotted against S-values.

4.2.1.4 GR-LBDm binds Hsp90 in a 2:2 stoichiometry

It could be demonstrated that GR-LBDm binds Hsp90 with micromolar affinity in a nucleotide-dependent manner (4.2.1.3). It was generally believed that only one GR-molecule interacts consistently with Hsp90 during GR transactivation (Pratt and Toft, 1997). However, Hsp90 is a dimeric molecule and might provide two client binding sites. Thus, in the next step, the binding stoichiometry of the GR-LBDm-Hsp90 complex was investigated. *GR-LBDm-Hsp90 complexes were formed and the influence of excess unlabeled GR-LBDm was monitored by AUC sedimentation velocity experiments (Figure 30A). Unlabeled GR-LBDm only partially competed with *GR-LBDm for binding. Instead, the s-value further increased, suggesting a 2:2 complex stoichiometry (Hsp90 monomer: GR-LBDm). To confirm this interesting finding, SAXS experiments (3.8.1) were carried out (Figure 30B, C, D). Both, radius of gyration (R_g) and maximum dimension (D_{max}) values were high for Hsp90 in its nucleotide-free form (Figure 30B, Supplemental table 2) consistent with the observation that apo-Hsp90 adopts an open conformation (Krukenberg et al., 2011). Binding of nucleotides (ATP, ATPγS or AMP-PNP) shifts the equilibrium towards a closed conformation. As expected, the most compact state of Hsp90 was found in the presence of AMP-PNP (Figure 30B). Next, Hsp90-GR-LBDm complex formation was studied under ATP conditions using different Hsp90-GR ratios. It turned out that both the apparent molecular mass and the R_g of the Hsp90-GR-LBDm complex increased up to a 2:2 ratio (Figure 30C, Supplemental table 2). Above this ratio, both the apparent molecular mass and the R_g decreased due to the presence of unbound GR-LBDm. Comparison of SAXS data obtained for free Hsp90 and in the presence of increasing equivalents of GR-LBDm revealed, a stepwise increase of the apparent molecular mass by approximately 25 kDa (from 160 kDa to 185 to 208 kDa) which matches well the mass of GR-LBDm (29 kDa) (Figure 30C). This result suggests that the two subunits of Hsp90 exhibit two independent binding sites for the GR-LBDm. Interestingly, the R_g and the D_{max} of Hsp90 and the Hsp90-GR-LBDm complex in the presence of ATP are very similar (R_g: 58.3 Å, D_{max}: 200/220 Å) which indicates that the GR-LBDm binds to the central part of Hsp90. In the nucleotide-free complex, GR-LBDm binds weakly to Hsp90 (strong concentration-dependence of the molecular mass) and Hsp90 adopts an open conformation. Binding of ATPγS and AMP-PNP shifts the complex towards a more compact conformation (R_g: 54.9/51.3 Å, D_{max}: 220/220 Å, Figure 30D, Supplemental table 2).

Notably, Hsp90 may also accommodate two GR-DBD-LBDm molecules as judged from AUC sedimentation velocity experiments (not shown). However, this complex stoichiometry

could not be further confirmed by SAXS experiments since GR-DBD-LBDm tended to aggregate over time at the applied concentrations.

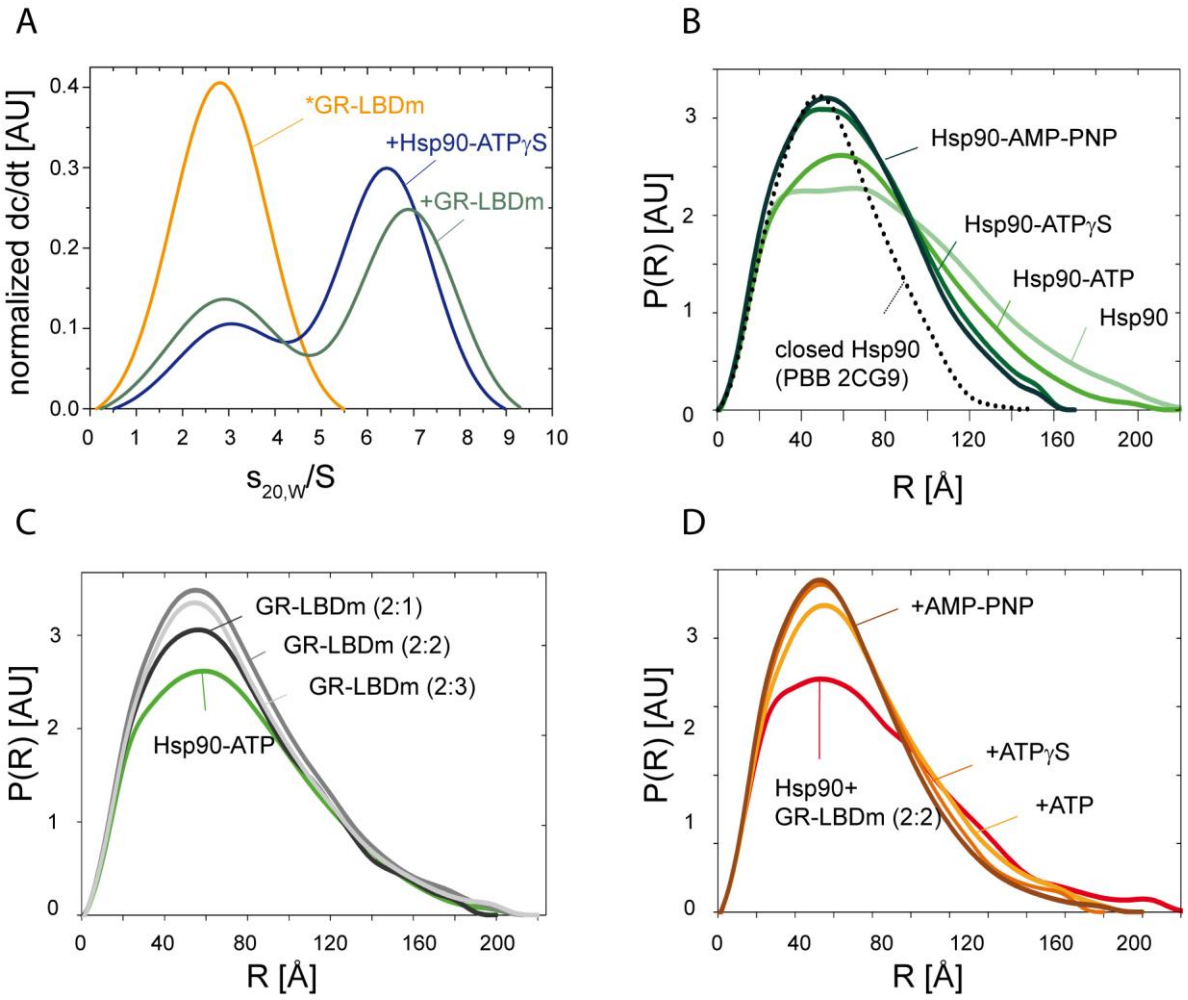

Figure 30 Determination of the Hsp90-GR complex stoichiometry. A) AUC sedimentation velocity experiment. 400 nM *GR-LBDm was incubated with 3 µM yeast Hsp90 to form a binary complex. Addition of 6 µM unlabeled GR-LBDm resulted in an additional shift in s-value. Analysis was performed at 20 °C in 20 mM Hepes, 20 mM KCl, 5 mM $MgCl_2$, 5 mM DTT, pH 7.5 supplemented with 50 µM DEX and 2 mM ATPγS. Normalized dc/dt values were plotted against $s_{20,W}$/S-values. B) SAXS analysis of free Hsp90 (3.3 mg/ml) in the presence of 4 mM nucleotide as indicated. Experimental radial density distributions and the back-calculated radial density distribution of the closed Hsp90 crystal structure (PDB: 2CG9) are shown. C) SAXS analysis of the Hsp90-GR-LBDm complex. Different Hsp90-GR-LBDm ratios (Hsp90 momomer: GR-LBDm) were investigated in the presence of 4 mM ATP. Concentrations were 9.0 (Hsp90-ATP), 3.9 (Hsp90-ATP + GR-LBDm, 2:1), 4.5 (2:2), and 5.1 mg/ml (2:3) respectively. A comparison of experimental radial distributions is shown. D) SAXS analysis of the Hsp90-GR-LBDm 2:2 complex under various nucleotide conditions as indicated. Measurements were performed at a concentration of 4.5 mg/ml. A comparison of experimental radial distributions is shown. For further experimental details see 3.8.1. SAXS analysis and figure preparation was performed by Tobias Madl (Technische Universität München).

4.2.1.5 Mapping of the GR-Hsp90 binding interface

There is limited knowledge on the Hsp90 site that accommodates GR. It seems that mainly the Hsp90-M domain is involved in GR binding with contributions from the Hsp90-N and -C domain (Bohen and Yamamoto, 1993; Cadepond et al., 1993; Fang et al., 2006; Hawle et al., 2006).

A divide and conquer approach using Hsp90 fragments was taken to determine the Hsp90-GR interaction site. In a first attempt, individual Hsp90-N (1-210), -M (259-527), -C (528-709) domains and Hsp90-NM (1-527), -MC domain constructs (275-709), respectively, were investigated for binding to GR using AUC sedimentation velocity experiments (Figure 31A-D). As a control, GR-binding was compared to full-length yeast Hsp90 in its apo- and ATP state (Figure 31B). In contrast to full-length Hsp90, all three individual Hsp90 domains did not interact with *GR-LBDm, as no additional shift in s-value was observed upon addition of the respective Hsp90 fragment (Figure 31B-C). Hsp90-NM and Hsp90-MC domain constructs behaved differently (Figure 31D). The disulfide-bridged Hsp90-NM dimer (Hsp90-NMox) as well as the reduced, monomeric Hsp90-NM fragment (Hsp90-NMred) interacted with GR in a nucleotide-dependent fashion. While no binding was observed in the absence of nucleotides, the addition of ATP shifted the s-value from 2.8 S to 3.5 S and 4.8 S, respectively. Further, *GR-LBDm seems to bind Hsp90-NMox with higher affinity than Hsp90-NMred (Figure 31D). The Hsp90-MC domain construct was also found to interact with *GR-LBDm as the s-value increased from 2.8 S to 4.7 S upon its addition (Figure 31D).

Taken together, these results suggest that the Hsp90-N, -M and -C domain act in concert to facilitate GR binding to Hsp90, with major contributions from Hsp90-M. It seems likely that conformational rearrangements upon ATP binding generate a GR-binding competent site at the N-M interface of Hsp90. The fact, that dimeric Hsp90-MC and dimeric Hsp90-NM-ATP, respectively, bound *GR-LBDm with moderate affinity further supports Hsp90's need for homo-dimerization to efficiently bind GR. The question whether Hsp90-C directly contributes to GR binding or whether Hsp90-C facilitates dimerization and proper orientation of the Hsp90-M domains, could not be answered here. GR failed to interact with an artificial Hsp90-M dimer construct (Hsp90-M^2) in AUC experiments, which may argue for a direct involvement of Hsp90-C. However, Hsp90-M^2 displayed an extended conformation in SAXS experiments and may thus not represent a proper substitute for the orientation of the M-domains in the Hsp90 dimer. It seems possible, that both Hsp90-M domains influence each other to promote the interaction with GR and that their close proximity in the Hsp90 dimer

increases client binding affinity. In this respect, it is also conceivable that the two M-domains in the closed Hsp90 dimer may further stabilize the interaction of GR with Hsp90-M by additional contacts.

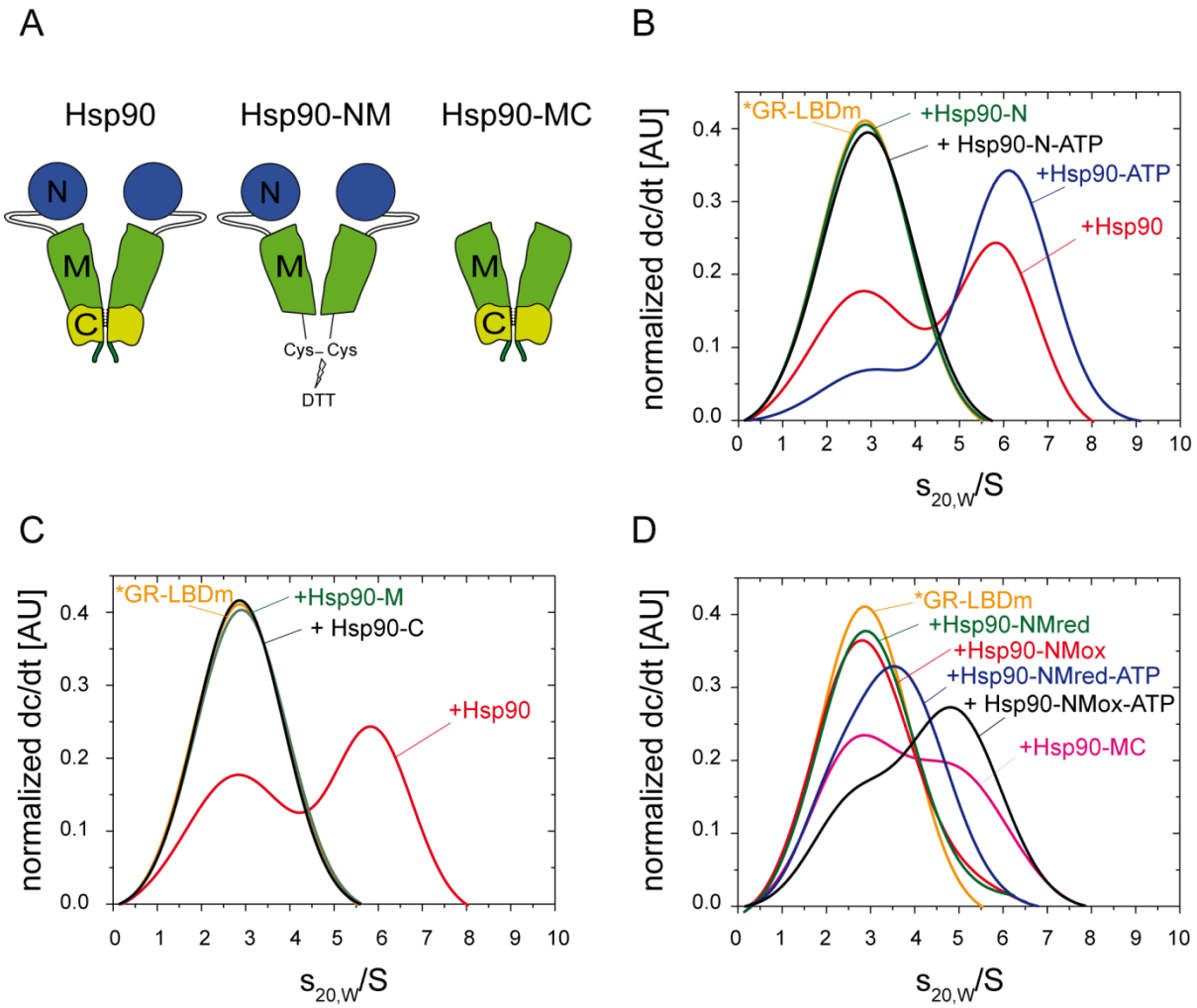

Figure 31 Analysis of various Hsp90 fragments for GR-LBDm binding. A) Hsp90 NM- and MC-domain constructs. To obtain monomeric Hsp90-NMred, dimeric Hsp90-NMox was reduced with 5-10 mM DTT overnight at 4 °C. B-D) AUC sedimentation velocity experiments. 400 nM *GR-LBDm was incubated with Hsp90 or different Hsp90 fragments (3 µM, the covalent dimer Hsp90-NMox was added at 1.5 µM) as indicated. (Hsp90-N) Hsp90-N domain, (Hsp90-M) Hsp90-M domain, (Hsp90-C) Hsp90-C domain, (Hsp90-NMred) reduced, monomeric Hsp90-NM domain construct, (Hsp90-NMox) dimeric Hsp90-NM domain construct, (Hsp90-MC) dimeric Hsp90-MC domain construct. Analysis was performed at 20 °C in 20 mM Hepes, 20 mM KCl, 5 mM $MgCl_2$, 5 mM DTT, pH 7.5 supplemented with 50 µM DEX. 2 mM ATP was added to samples as indicated. Complex formation with Hsp90-NMox was investigated in the absence of DTT. Normalized dc/dt values were plotted against $s_{20,W}$/S-values. Analysis was performed in collaboration with Daniel Rutz (Technische Universität München).

For residue-specific resolution of the interactions in the Hsp90-GR-LBDm complex, NMR spectroscopy was applied (3.8.2). Similar to previous AUC experiments, Hsp90 fragments were used. First, the interaction of GR with individual, isotopically enriched Hsp90-N (1-259) and -M domains (259-527) was investigated (Figure 32A, C).

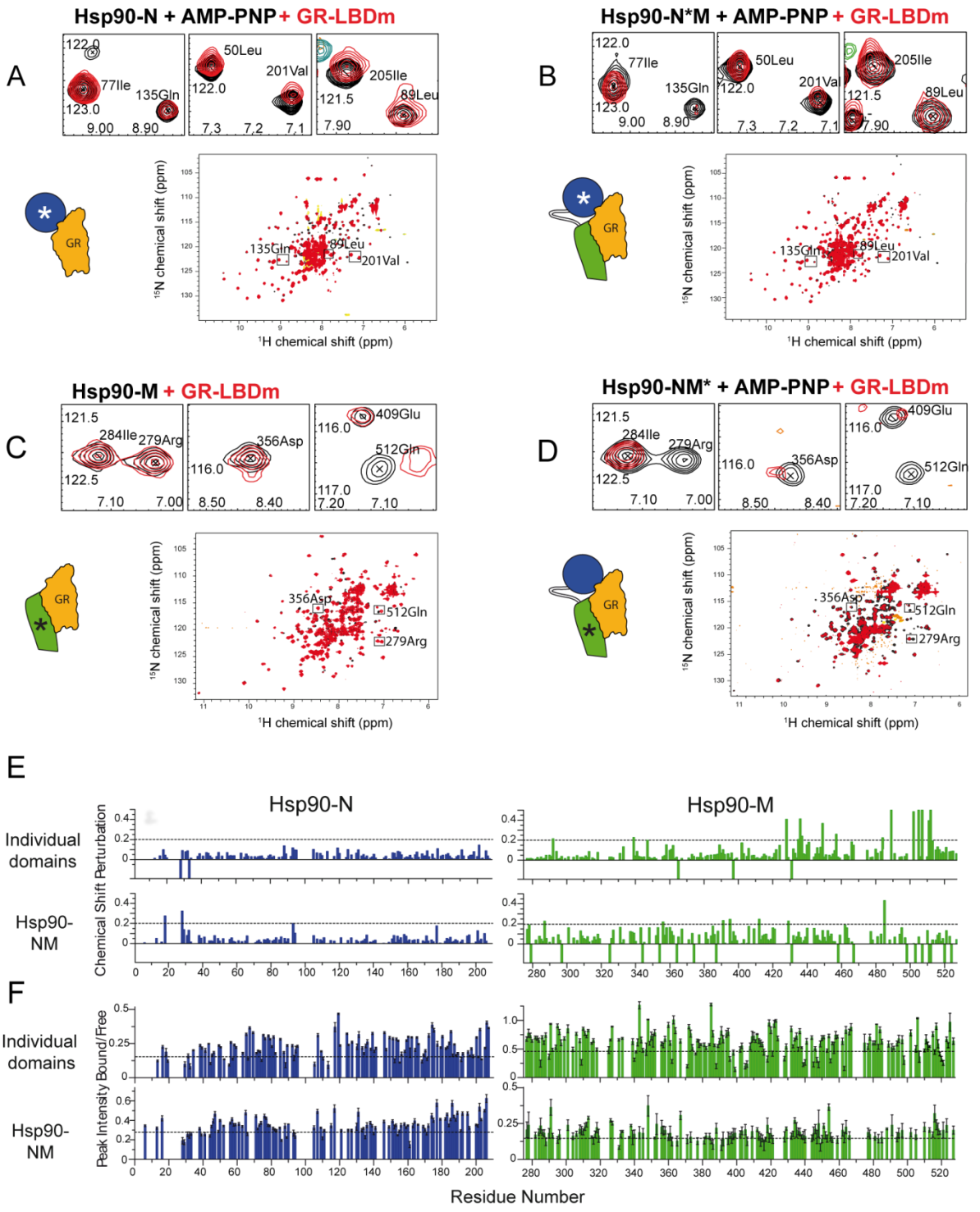

Figure 32 NMR analysis of the Hsp90-GR interaction. A, C) ^{1}H-^{15}N-HSQC spectra (lower panel) and zoomed views (upper panel) of 100-200 µM Hsp90-N and Hsp90-M domains free (black) and in presence of one molar equivalent of GR-LBDm (red). B, D) ^{1}H-^{15}N-HSQC spectra (lower panel) and zoomed views (upper panel) of 200 µM segmentally labeled Hsp90-NM, where either the -N domain (Hsp90-N*M) or the -M domain (Hsp90-NM*) is detected. Free and bound Hsp90-NM is depicted in black and red, respectively. 2mM AMP-PNP was added as indicated. E, F) Chemical shift pertubations and ratio of signal intensities in the presence and absence of GR-LBDm. Negative bars correspond to signals which disappeared or could not be traced upon GR-LBDm addition. CSPs above 0.2 ppm were considered as significant (dashed line). The intensity threshold was chosen to be 1 σ below the average peak intensity using a 5 % truncated mean (dashed line). The average level of intensity was not normalized and the overall reduction in intensity might in part also reflect protein precipitation during measurements. Experiments and data analysis were performed by Lee Freiburger (Technische Universität München).

Consistent with a previous report (Dehner et al., 2003), Hsp90-N alone experienced significant chemical shift pertubations (CSP) upon addition of AMP-PNP (not shown). In the presence of GR-LBDm, additional chemical shift changes occurred or reduced intensities of several NMR signals were recorded (Figure 32A, E, F, Supplemental table 1).

Next, ^{1}H-^{15}N-HSQC experiments with isotopically labeled Hsp90-M were performed. The overall spectral similarity of ^{1}H, ^{15}N correlation experiments in the presence and absence of GR-LBDm indicate that GR does not induce large conformational rearrangements in Hsp90-M (Figure 32C). However, several CSPs or severe line broadening upon binding of GR (Figure 32C, E, F, Supplemental table 1) were recorded. To investigate whether affected residues cluster in a specific region in the context of full-length Hsp90, NMR chemical shift data for both Hsp90-N and Hsp90-M were mapped onto the closed form of the Hsp90 crystal structure (Figure 33A). It turned out that most of the affected residues in Hsp90-N are located close to the ATP binding pocket. In Hsp90-M the majority of spectral changes occurred on one side of the Hsp90-M domain facing the interior of the closed Hsp90 dimer (Figure 33A), consistent with the SAXS results, which strongly suggest that GR binds to the central part of the molecule (4.2.1.4).

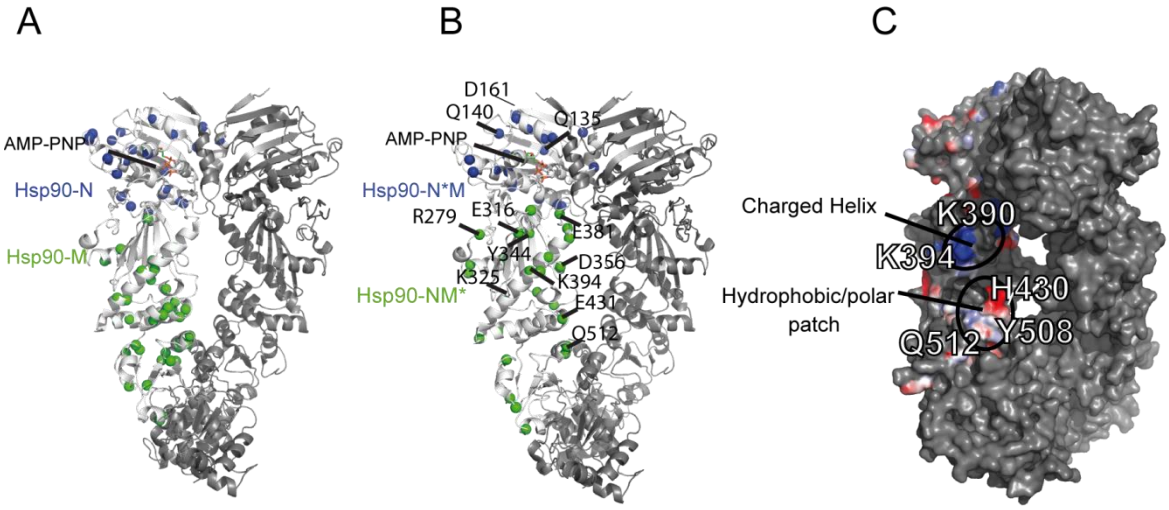

Figure 33 Affected Hsp90 residues in the -M and -N domain upon GR-LBDm binding. Significant spectral changes were mapped onto the Hsp90 crystal structure (PDB 2CG9). A) Spectral changes upon GR binding are highlighted as green and blue spheres for amides in the individual Hsp90-N and Hsp90-M domain, respectively. B) Significant spectral changes observed in titration experiments with Hsp90-NM. Color code as in (A). C) Hsp90-GR interaction surface. Negative (red), positve (blue) and neutral (white) surface potential was determined by the Pymol APBS tool (Baker et al., 2001). Analysis and figure preparation was performed by Lee Freiburger (Technische Universität München).

In a second approach, the interaction of GR with segmentally labeled Hsp90-NM domain constructs (1-527) was investigated, in which either the Hsp90-N or the Hsp90-M domain was uniformly ^{15}N, ^{13}C, ^{2}H (70 %)-labeled (Hsp90-N*M and Hsp90-NM*, respectively) (Figure 32B, D). As expected, the addition of AMP-PNP to the two-domain construct produced significant CSPs in Hsp90-N, while Hsp90-M was only marginally affected (not shown). Upon GR binding, several NMR signals experienced intensity changes or CSPs in Hsp90-NM (Figure 32B, D, E, F, Supplemental table 1). The number and magnitude of effects in Hsp90-N*M were less compared to Hsp90-NM*, indicating that the GR-LBDm interacts primarily with the Hsp90-M domain. Mapping of the affected residues onto the Hsp90 structure (Figure 33B) revealed that many of them cluster at the inside cleft of the closed Hsp90 dimer, similar to the observations with the individual domains (Figure 33A). However, spectral changes upon GR binding were stronger and more widespread than those seen for the individual domains (Figure 32A, B, C, D). Moreover, many additional affected residues were found close to the Hsp90-NM interface (Supplemental table 1), likely reflecting a more extended binding surface or allosteric effects upon ATP and GR binding. This is also consistent with previous AUC experiments, which demonstrated that ATP-bound Hsp90-NMred is preferred over the isolated Hsp90-N and -M domain for binding to GR. Analysis of the affected residues concerning electrostatic charge revealed that the interaction surface likely involves mainly hydrophobic and polar residues including R426-H430, I505-Y508, T511 and Q512 as well as a long positively charged α-helix in Hsp90-M (residues Q385-K394) (Figure 33C). Importantly, the binding surface could be extended to the MC-interface in titration experiments with the Hsp90-C domain (not shown; in collaboration with Lee Freiburger and Daniel Rutz, Technische Universität München). Thus, in agreement with the AUC data above, it seems that a defined set of residues in all three Hsp90 domains provide a binding interface for GR.

Little information is available on the conformation of Hsp90-bound GR. Therefore, ^{15}N-labeled GR-LBDm was produced and NMR spectra were recorded in the absence and presence of Hsp90-M and Hsp90-NM, respectively (Figure 34). ^{1}H-^{15}N-HSQC spectra of GR-LBDm are well dispersed, demonstrating that GR-LBDm is folded in solution. Upon addition of Hsp90-M, many NMR signals experienced CSPs or reduction in signal intensity. Consistent with the observations above, the effects were more pronounced with Hsp90-NM.

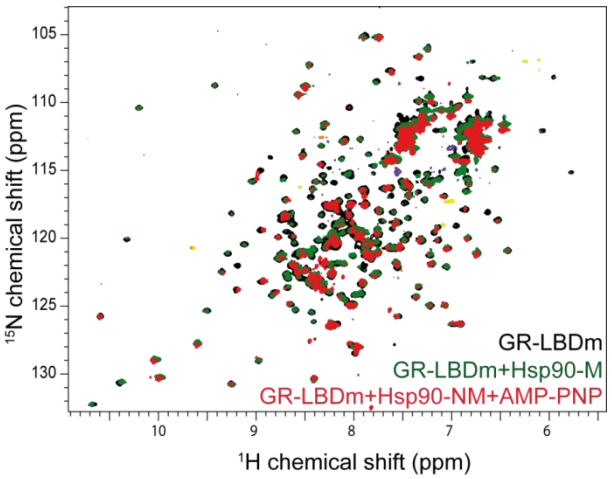

Figure 34 GR-LBDm binds Hsp90 in a folded conformation. ^{1}H-^{15}N-HSQC spectra of ^{15}N-GR-LBDm alone (black) and in the presence of Hsp90-M (green) or Hsp90-NM (red). 2 mM AMP-PNP was added as indicated. Analysis and figure preparation was performed by Lee Freiburger (Technische Universität München). ^{15}N-GR-LBDm was purified according to 3.6.1.1 by Daniel Rutz (Technische Universität München).

Taken together, these results demonstrate that GR-LBDm binds as a globular, folded protein to Hsp90 and that no dramatic conformational changes occur upon binding. Rather, it seems that a defined set of residues is involved in the Hsp90-GR interaction. However, at this point, the obtained NMR signals could not be assigned. Although a small amount of ^{15}N, ^{13}C, ^{2}H (80 %)-labeled GR-LBDm was successfully purified, unfortunately, all recorded NMR spectra were of too poor quality to address GR-residues that are critical for Hsp90 binding.

4.2.1.6 Structural model of the GR-Hsp90 complex

SAXS data were combined with high resolution crystal structures (‘closed’ yeast Hsp90, PDB 2CG9 and GR-LBD-F602S, PDB 1M2Z) and NMR chemical shift data for the Hsp90-GR interface (Supplemental table 1) to build a structural model of the Hsp90-GR-LBDm complex. The ratio between ‘open’ and ‘closed’ populations was estimated using the SAXS model for Hsp90 and the crystal structure of Hsp90 as end-point structures. Assuming that the scattering intensities of the end-point structures are known (form factors), SAXS data are a measure of the populations in the ‘open’ and ‘closed’ conformations (in the form of volume fractions of each component). The overall conformation of the Hsp90-GR-LBDm complex (2:2) in the presence of ATP is extended (Figure 35A, left) and similar to free Hsp90-ATP (Figure 30B, Figure 35B, C). GR-LBDm is located in the central part of Hsp90 in-between the Hsp90-NM arms and the Hsp90-C domains. The SAXS rigid body calculations are well converged in terms of the overall shape and orientation of the complex (Figure 35D). Since SAXS data provide low-resolution shape information, the rotation of the Hsp90-NM arm and of the GR-LBDm show the strongest variation. In the ‘open’ complex, the interaction surface is large and covers a region of 1500-2000 Å, with ~ 90 % being located within the Hsp90-M

domain. The addition of ATPγS or AMP-PNP induces large conformational changes, resulting in the accumulation of more compact populations. However, it seems that Hsp90-GR-LBDm complexes are not completely 'closed', which suggest a continuous equilibrium between open and closed states (Figure 35F, G). A structural model for the 'closed' state was generated by docking of the GR-LBDm onto the 'closed' Hsp90 crystal structure using NMR data (Supplemental table 1) as restraints (Figure 35A right). Docking calculations are well converged in terms of the overall shape and localization of the GR-LBDm (Figure 35E). As observed for the 'open' complex, the two GR-LBDm molecules bind Hsp90 in a symmetric fashion. Interestingly, consistent with the distribution of NMR chemical shifts (Figure 33), additional contacts with the Hsp90-N domain at the opposite Hsp90 subunit can be observed (Figure 35A right, E), which might further stabilize the complex.

Of note, the SAXS structures could be further improved in later experiments through the addition of NMR chemical shift data of the GR titration with Hsp90-C and electron microscopy data of the Hsp90-GR-LBDm complex (Collaboration with José Maria Valpuesta, Centro Nacional de Biotecnología, Madrid, Spain) in the calculations (not shown). Further the orientation of the GR-LBDm in the complex could be defined more precisely by NMR-paramagnetic relaxation enhancement (PRE) experiments with spin-labeled GR-LBDm (collaboration with Lee Freiburger and Daniel Rutz, Technische Universität München).

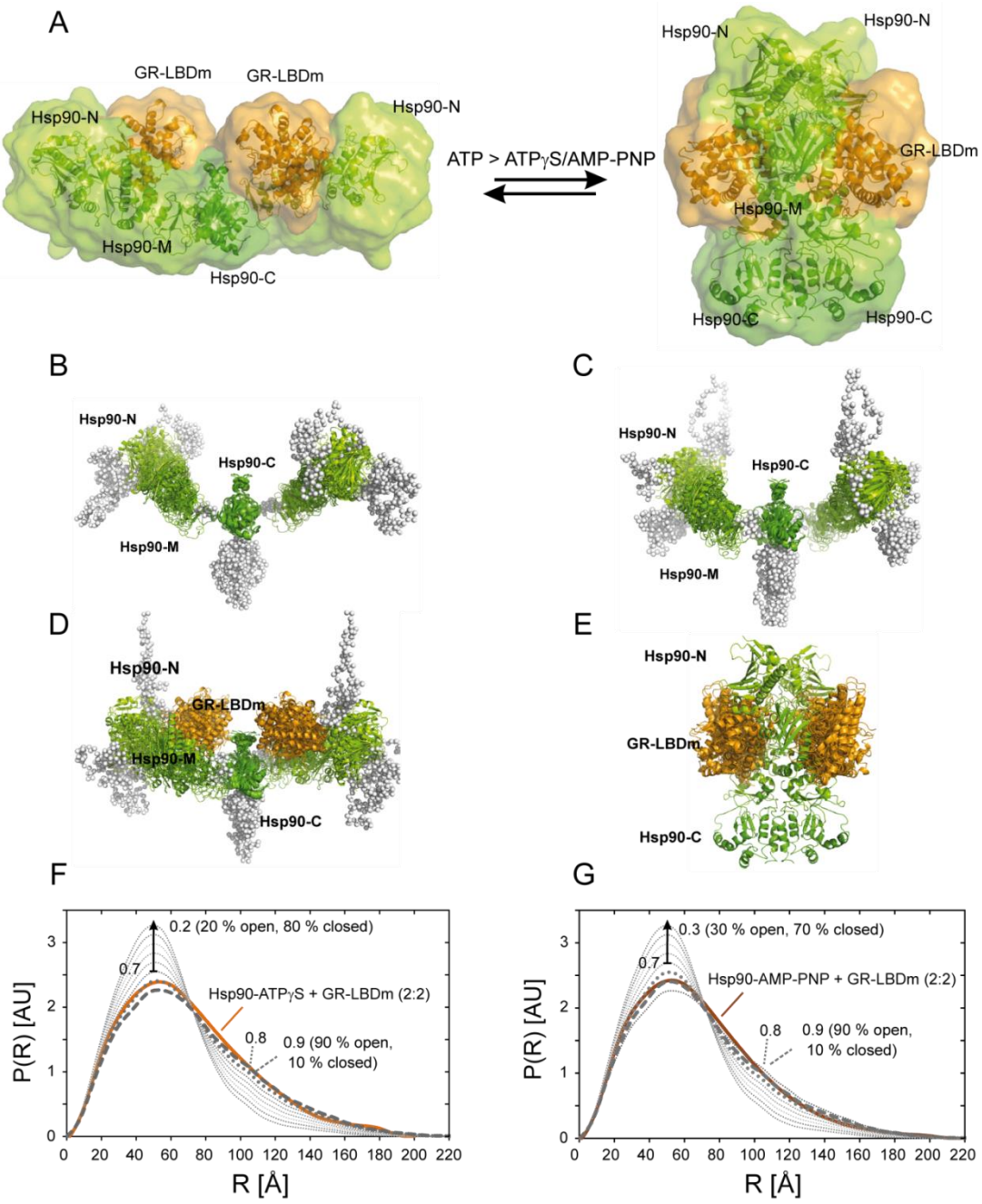

Figure 35 SAXS analysis of the Hsp90-GR-LBDm complex. A) SAXS model of the GR-Hsp90 complex. Surface and cartoon representation of Hsp90-GR-LBDm complexes in their open (left) and closed states (right). B) Rigid body models of free Hsp90 and ATP-bound Hsp90 (C). Cα dummy atoms of flexible residues were modeled by the program CORAL (Petoukhov et al., 2012) and are shown as white spheres. D) Cartoon representation of a bundle of 5 lowest energy structures from rigid body docking calculations of the Hsp90-ATP-GR-LBDm- and the closed Hsp90-GR-LBDm complex (E), respectively. Docking calculations were carried out using NMR data as restraints (Supplemental table 1). Hsp90 domains are shown in different greens, GR-LBDm is depicted in orange. F-G) Experimental radial density distributions of the Hsp90-GR-LBDm complex in the presence of nucleotides as indicated. SAXS data was compared to theoretical radial density distributions, which were calculated for a mixture of open and closed Hsp90-GR-LBDm complexes. For population analysis, the radial density distribution of Hsp90-ATP-GR-LBDm and of the closed Hsp90-GR-LBDm docking model (E), back-calculated with the program Crysol (Svergun et al., 1995), was taken as input. SAXS data analysis and figure preparation was performed by Tobias Madl (Technische Universität München).

4.2.1.7 Summary and conclusions

To characterize the interaction of Hsp90 with GR *in vitro*, a GR-LBD mutant comprising five stabilizing mutations was employed (GR-LBDm), as its respective full-length form still showed significant Hsp90 dependence *in vivo*. Reconstitution experiments demonstrated that hormone-bound GR-LBDm can stably bind Hsp90, consistent with earlier reports on the progesterone receptor (Smith, 1993). This interaction is sensitive to the Hsp90 conformation and thus relies on the nucleotide present.

NMR studies together with AUC and SAXS experiments revealed that two GR-LBDm molecules can simultaneously bind Hsp90 and that predominantly the Hsp90-M domain is involved in the Hsp90-GR interaction. The interaction surface involves distinct Hsp90-M residues that cluster in the internal cleft of the two Hsp90 monomers formed in the closed homo-dimer. Thereby, a combination of hydrophobic and polar residues as well as positively charged helix in the Hsp90-M domain likely modulates GR binding. Remarkably, several of the matched residues, including E507, T511D, G313, E431, E381 in the Hsp90-M domain were suggested to be important for GR function *in vivo* (Bohen and Yamamoto, 1993; Genest et al., 2013; Nathan and Lindquist, 1995). In addition some residues of the Hsp90-N and the Hsp90-C domain seem to contribute to the GR-interface. These findings indicate that all three domains act in concert to promote GR binding to Hsp90. This might be an allosteric driven process that is initially governed by ATP binding to the Hsp90-N domain. As a results Hsp90-N, -M and Hsp90-C form a surface area capable for efficient client binding.

Interestingly, previous interaction studies with other Hsp90 clients such as the kinase CDK4 and the transcription factor p53 suggested the Hsp90-M domain as important element as well (Hagn et al., 2011; Park et al., 2011; Vaughan et al., 2006). Although binding regions of CDK4, p53 and GR partly overlap, the binding interface of CDK4 and p53 is different from GR and involves mainly hydrophobic and charged residues located at the outside of the closed Hsp90 dimer. This suggests that Hsp90 might provide different binding areas for the specific needs of its various client proteins.

Further, it could be demonstrated that a defined set of GR residues mediate Hsp90 binding and that GR-LBDm does not unfold upon association with Hsp90, consistent with the fact that Hsp90 recognizes already folded conformations rather than nascent protein chains (Hagn et al., 2011; Jakob et al., 1995; Nathan et al., 1997).

All of the performed experiments were carried out with a mutant receptor ligand binding domain. The future will show whether the observed GR binding mode- and complex stoichiometry holds also true for a full-length receptor lacking any stabilizing mutations.

It would be also interesting to investigate the impact of Hsp90 on a ligand-free receptor or its respective ligand binding domain. Despite several attempts, so far, no conditions were found to reconstitute apo-GR-LBDm-Hsp90 complexes *in vitro*. Whether this finding is based on its high aggregation propensity during measurements or whether the Hsp70 chaperone machinery is required for its handover to Hsp90 remains elusive.

4.2.2 Functional consequences of the Hsp90-GR interaction

4.2.2.1 'Chaperoning' of GR by Hsp90

In the last chapter, it could be demonstrated that holo-GR-LBDm-Hsp90 complexes can be reconstituted with purified components *in vitro*. Next, the functional consequences were analyzed.

In vivo, GR requires Hsp90 for high-affinity ligand binding (Picard et al., 1990). Fluorescence polarization assays (Figure 36A) revealed no enhancement in hormone binding affinity when apo-GR-LBDm was pre-incubated with Hsp90 (IC_{50} = 114 nM and IC_{50} = 168 nM, respectively). Also, ligand binding and exchange kinetics were strikingly similar (not shown). Considering early reconstitution experiments in which isolated and stripped SHRs were re-activated by the subsequent addition of Hsp40, Hsp70, Hop, Hsp90 and p23 (Morishima et al., 2000), it seems likely that the purified receptor studied here compares to an receptor intermediate of the GR maturation pathway or its conformation even resembles an end-result. Unfortunately, pre-incubation of Hsp70 and/or Hsp40 with GR prior to measurements did neither change hormone binding affinity (not shown), indicating that re-modeling of the GR structure to early states of GR maturation (low-affinity conformation) is not possible under the applied conditions or that other factors are required.

In the cell, binding of hormone to GR results in its translocation into the nucleus where it binds specific genomic GREs. However, upon hormone withdrawal, Hsp90 (and p23) seem to play a role in active disassembly of GR-DNA complexes (Freeman and Yamamoto, 2002). In this respect, ligand release is not necessarily a prerequisite for GR release from GREs (Meijsing et al., 2007). Thus in the next step, the influence of Hsp90 on GRE-binding was assessed by fluorescence polarization experiments (Figure 36B). It turned out, that binding of GR-DBD-LBDm to its respective GRE elements was largely unaffected by Hsp90 (IC_{50} = 410 nM and IC_{50} = 347 nM, respectively). Thus, it seems likely that further factors such as p23 or components of the transcriptional machinery are required to explain the observations made *in vivo*.

Fang et al., (2006) provided some evidence that Hsp90 may influence binding of nuclear co-regulators to GR, consistent with the finding that Hsp90 seems to disrupt the formation of GR-mediated, transcriptional regulatory complexes *in vivo* (Freeman and Yamamoto, 2002). Therefore, it was speculated whether GR-LBDm co-activator or GR-LBDm co-repressor complexes can be formed in the presence of Hsp90. Fluorescence polarization assays with

DEX- and MIF-bound GR-LBDm were conducted and the influence of Hsp90 on binding to fluorescently labeled Tif2-peptide (co-activator) and NcoR-peptide (co-repressor) was investigated. As the affinity of GR-LBDm for the Tif2-peptide is rather low (4.1.2.2), GR-LBD-F602S was assayed as well in a control experiment. The experiments showed that neither Tif2-GR-LBDm- nor Tif2-GR-LBD-F602S complexes could be disturbed by Hsp90-ATP (not shown). Interestingly, slight competition was observed when Hsp90-ATP was titrated to NcoR-GR-LBDm or NcoR-GR-LBD-F602S complexes (not shown). However, although the obtained results were interesting, one can only speculate about their physiological relevance. So far, Hsp90-GR-LBDm complexes were reconstituted in the presence of an agonist (DEX) and little information is available about GR-chaperone assemblies with antagonist (MIF) present.

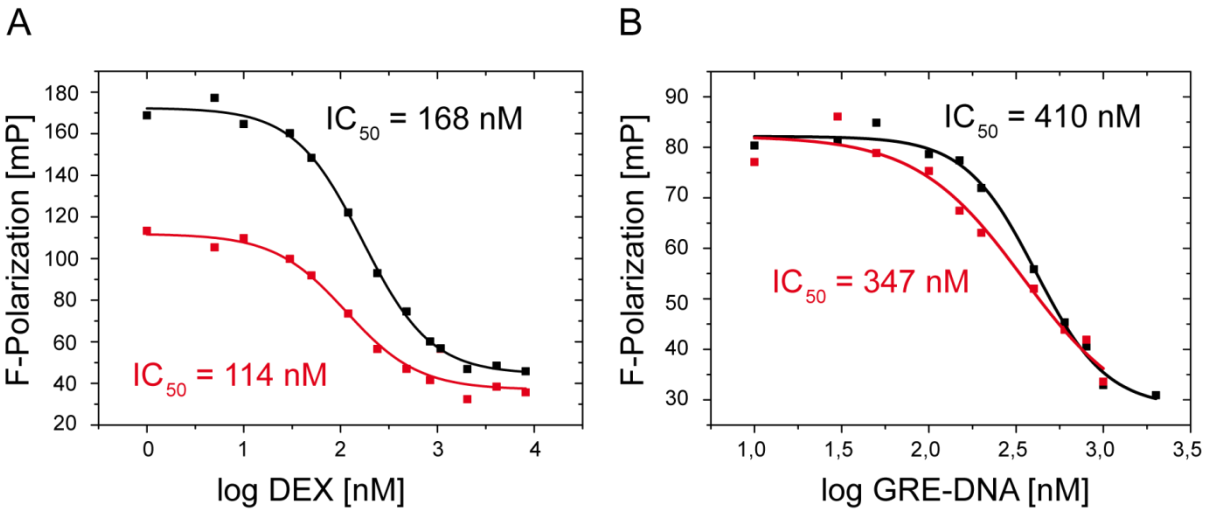

Figure 36 Influence of Hsp90 on receptor functionality. A) Hormone binding affinity of GR-LBDm in the presence (black) and absence (red) of Hsp90. 300 nM apo-GR-LBDm alone or pre-incubated with 9 µM yeast Hsp90 and 4 mM ATP was titrated to a mixture of 50 nM F-DEX and increasing amounts of unlabeled DEX. Samples were incubated until equilibrium was reached and fluorescence polarization was measured at 25 °C in 25 mM Tris, 100 mM NaCl, 0.5 % CHAPS, 10 % Glycerol, 2 mM DTT, pH 7.9. B) 400 nM GR-DBD-LBDm alone or pre-incubated with 3 µM yeast Hsp90 and 2 mM ATP was titrated to a mixture of 10 nM FAM-labeled GRE-DNA and increasing amounts of unlabeled GRE-DNA. Binding of GR-DBD-LBDm to GRE-DNA (black trace) was shown already in Figure 24B. Fluorescence polarization was measured at 25 °C in 25 mM Tris, 100 mM NaCl, 10 % Glycerol, 2 mM DTT, 50 µM DEX, pH 7.9. A-B) Excitation and emission wavelengths were set to 485 and 520 nm, respectively. The IC_{50}-values are indicated in figures and were obtained by a dose-response fit of the data.

4.2.2.2 Modulation of the Hsp90 cycle by GR

GR binding to Hsp90 is strongly nucleotide-dependent (4.2.1.3). Thus, it was speculated whether GR influences the ATPase cycle of Hsp90. Yeast Hsp90 was incubated with increasing amounts of GR-LBDm and the ATPase activity was monitored using a regenerative assay (3.9.2). Hsp90 alone showed an ATPase activity of ~ 0.5 min^{-1} at 30 °C. GR-LBDm addition reduced the ATPase activity of Hsp90 by a factor of 8 in a concentration-dependent manner (Figure 37A). From these data, an apparent K_i of 7.1 µM was calculated. The ATPase rate of a dimeric Hsp90-NM construct decreased as well upon GR-LBDm addition, consistent with the involvement of the Hsp90-N and Hsp90-M domain in GR-binding (Figure 37B) (4.2.1.5). Of note, also GR-DBD-LBDm decreased the Hsp90-ATPase (not shown). However, GR-DBD-LBDm was not analyzed as detailed as GR-LBDm since it tended to aggregate at elevated temperatures. Further, the reduction in ATPase activity was also evident when Hsp90 was incubated with GR-LBD-F602S, indicating that additional mutations present in GR-LBDm do not affect observations made here (not shown).

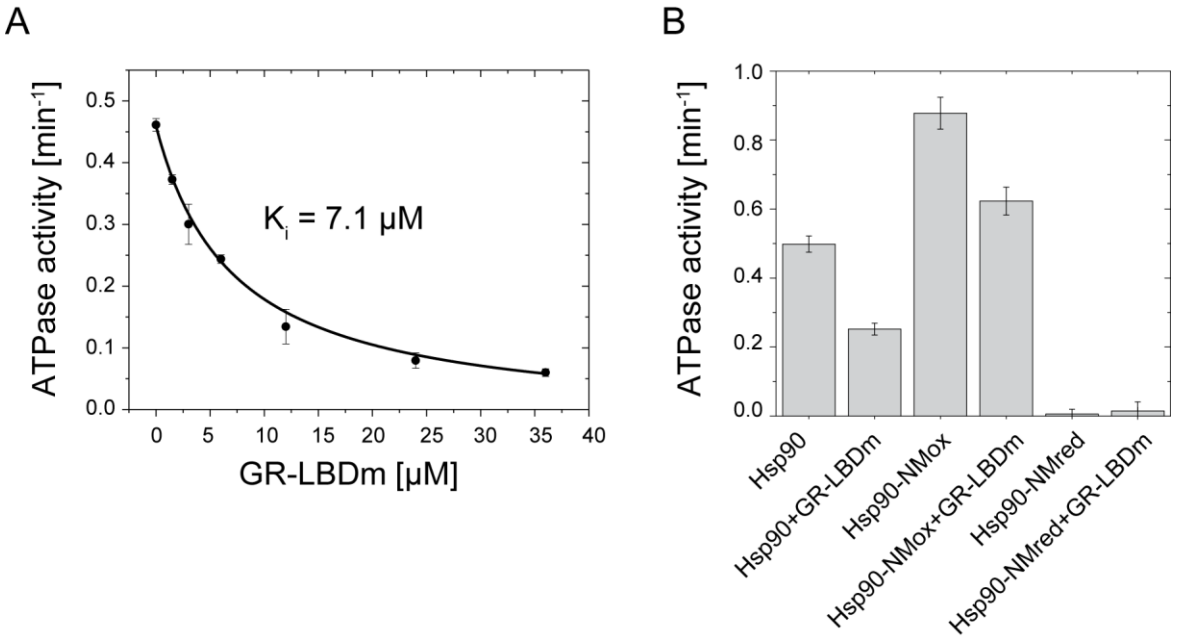

Figure 37 GR-LBDm compromises the ATPase activity of Hsp90 and Hsp90 domain constructs A) GR-LBDm decreases the Hsp90-ATPase activity in a concentration-dependent manner. Yeast Hsp90 was incubated with increasing amounts of GR-LBDm and the mean values of three independent experiments were plotted against the GR-LBDm concentration. Data were fit with a single-site binding-model resulting in a K_i of 7.1 µM. B) ATPase activities of monomeric and dimeric Hsp90-NM domain constructs (Hsp90-NMred and Hsp90-NMox, respectively) in the presence and absence of 6 µM GR-LBDm. Shown are mean values and standard deviations from three independent experiments. A-B) The ATPase activity was assayed as described in 3.9.2 at 30 °C using 3 µM Hsp90 and 3 µM Hsp90-NMox/Hsp90-NMred, respectively. Measurements with Hsp90-NMox were performed in ATPase buffer lacking DTT. Analysis was performed in collaboration with Daniel Rutz (Technische Universität München).

The results above suggest that the rate-limiting conformational rearrangements of Hsp90 associated with the ATPase cycle are affected upon complex formation with GR-LBDm. To directly monitor the conformational changes of Hsp90 in the presence of GR, a FRET system was applied (Hessling et al., 2009). Yeast Hsp90 was fluorescent labeled with donor- and acceptor dye (3.6.2) and mixed in a 1:1 ratio to form a Hsp90-FRET complex. Upon addition of ATPγS, the closing reaction of the labeled Hsp90 dimer can be monitored by an increase in FRET efficiency (Hessling et al., 2009). It turned out that the closing rate was significantly slower when the FRET pair was pre-incubated with GR-LBDm (Figure 38A). Closing rates strongly depended on the GR-LBDm concentration (Figure 38B). Fitting of the data resulted in a K_i of 1.9 µM which is in excellent agreement with the observed binding affinity of GR to Hsp90 under ATPγS conditions measured by AUC. Then, the half-time of the FRET complex in the presence and absence of GR-LBDm was investigated by chase experiments (Figure 38C). As expected, the addition of unmodified Hsp90 to the FRET complex resulted in a slow decrease in acceptor fluorescence, as heterodimers between labeled Hsp90 and unmodified subunits form. Upon equilibration, the FRET signal was lost. However, in the presence of GR-LBDm, chase kinetics were markedly different. GR-LBDm almost completely inhibited the dissociation of the FRET complex which likely reflects the formation of a stabilized partially closed state of the Hsp90 dimer upon GR binding.

The reopening reaction of the Hsp90 dimer upon addition of excess ADP was not as strongly affected by GR-LBDm, consistent with the notion that GR-LBDm has a lower affinity for an (open) Hsp90 post-hydrolysis state (Figure 38C). Taken together, the results suggest that the GR-LBDm favors a partially closed conformation of Hsp90 and that its binding decelerates cycle progression.

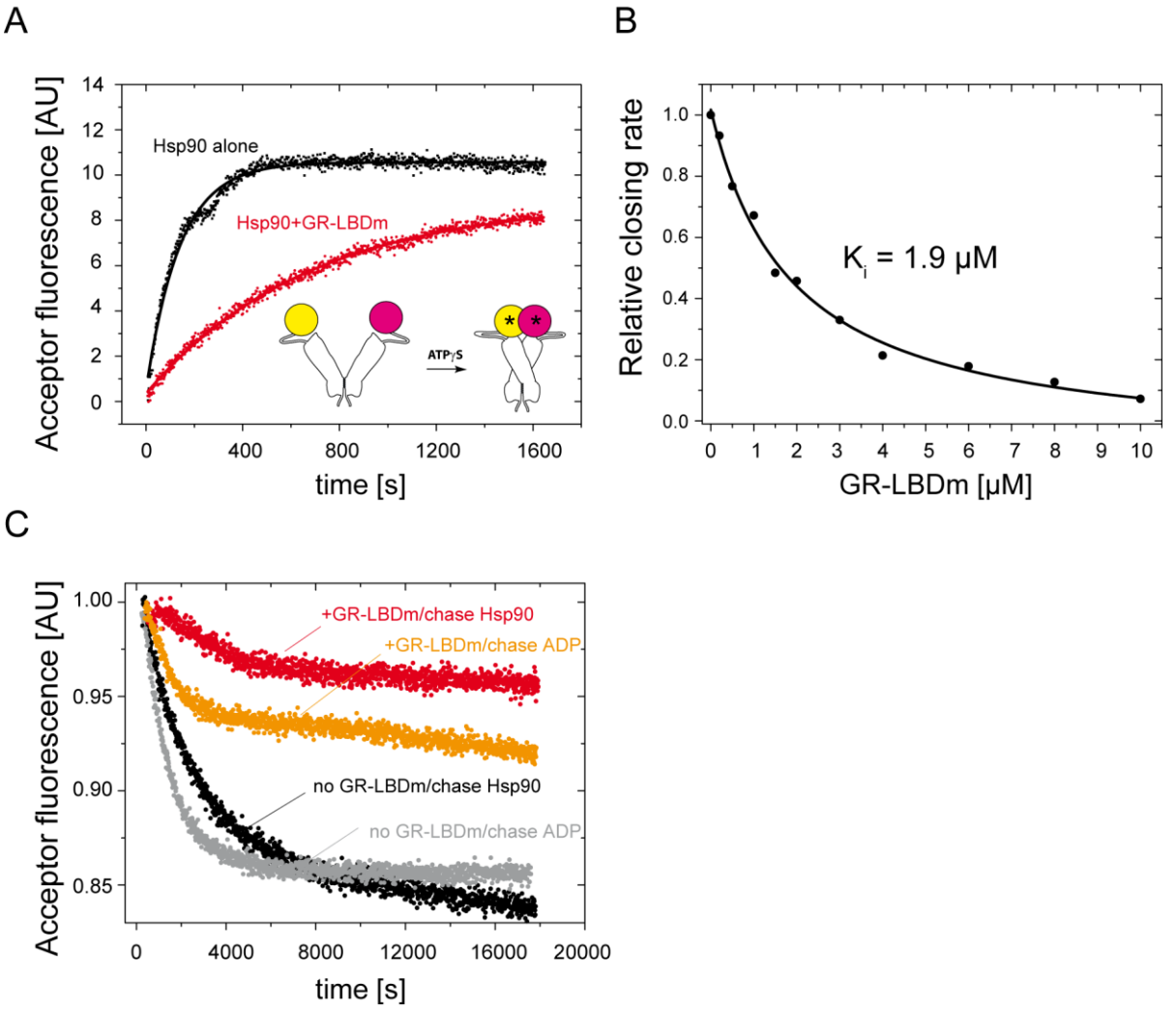

Figure 38 GR-LBDm modulates the conformational cycle of Hsp90. A) Nucleotide-induced closing reaction of Hsp90 in the presence of GR-LBDm monitored by FRET experiments. 200 nM donor- and 200 nM acceptor-labeled Hsp90 was incubated in the presence or absence of 4 µM GR-LBDm (red and black curve, respectively) and the change in acceptor fluorescence upon addition of 2 mM ATPγS was monitored over time. The inset indicates conformational changes within the Hsp90 dimer. B) GR-LBDm decreases the nucleotide-induced closing reaction of the Hsp90 dimer in a concentration-dependent manner. The relative closing reaction was plotted against the GR-LBDm concentration. From a single-site binding fit a K_i of 1.9 µM was calculated. C) GR-LBDm stabilizes a partially closed Hsp90 conformation. Chase kinetics upon addition of 4 µM Hsp90 or 50 mM ADP after pre-incubation of the Hsp90 fret pair with 10 µM GR-LBDm. FRET experiments were carried out as described in 3.7.2.2.

4.2.2.1 Summary and conclusions

In the previous chapter, the functional consequences of the Hsp90-GR interplay were analyzed. *In vivo* studies clearly showed that Hsp90 modulates hormone binding to GR (Picard et al., 1990). In particular, it was suggested that Hsp90 modulates the steroid binding cleft to allow high-affinity ligand binding (Morishima et al., 2000). Surprisingly, experiments with purified components showed no influence of Hsp90 on hormone binding. Even in the absence of Hsp90, ligand was freely accessible to GR-LBDm. Perhaps, in the absence of hormone, stabilizing mutations in GR-LBDm shift the equilibrium towards a more folded conformation compared to GR *wt* which allows hormone binding also in the absence of Hsp90. However, the purified receptor conformation might also compare to intermediate or final GR conformations which form during GR cycling and thus possess already high hormone binding affinity.

It was also proposed, that Hsp90 plays a role in active disassembly of GR-chromatin complexes (Freeman and Yamamoto, 2002). However, so far, using GR-DBD-LBDm and DNA fragments containing GRE response elements, no influence on DNA binding was observed in the presence of Hsp90. Most likely, this issue cannot be adequately addressed with DNA fragments as they do not sufficiently substitute for the far more complex chromatin structures, or additional factors are required (such as p23 or PPIases). Further in this respect, the influence of Hsp90 on co-regulator binding was studied, since they are part of the GR-mediated transcriptional machinery in the nucleus. Within this study, unfortunately, no influence on co-activator binding was observed either. Although Hsp90 may compete in part with the co-repressor NcoR for binding to GR-LBDm that had an antagonist bound, additional experiments are required to draw final conclusions, especially because co-regulator derived peptides were used.

Hsp90 can adopt a number of different conformations during its functional cycle (Graf et al., 2009; Hessling et al., 2009). Strikingly, GR influences the conformational equilibrium of these states. GR-LBDm binds preferentially to a partially closed Hsp90 conformation and stabilizes this state, which in turn leads to an inhibition of the Hsp90 cycle resulting in a decrease of the ATPase activity. Notably, McLaughlin et al., (2002) reported a strong stimulatory effect of GR on the Hsp90-ATPase. However, the refolded protein used in this study was likely not functional as it displayed only very weak hormone binding activity (K_D = 46 µM), consistent with similar results presented in 4.1.1.3. In addition, the presence of

the detergent Zwittergent 3-12 was required to maintain the refolded GR-LBD in solution, which possibly affected the conformational dynamics of Hsp90.

For other interacting model clients, such as the ribosomal protein L2 or a fragment of staphylococcal nuclease (Δ131Δ), an increase in ATPase activity was observed (Genest et al., 2013; Street et al., 2011). At the moment, one can only speculate about the contrary results. Differences may reflect diverse binding modes or distinct demands of the client itself.

Unfortunately, apo-GR-LBDm aggregated during ATPase or FRET measurements and its influence on the Hsp90 cycle – if binding to Hsp90 is possible at all without the Hsp70 system – remains further elusive. It would be of interest whether ligand-free GR follows a different pattern compared to holo-GR as one could derive more mechanistic details of the Hsp90-GR interplay in the absence of ligand.

Taken together, until now, the *in vitro* experiments reveal surprisingly little information about the effect of Hsp90 binding to GR. However, GR modulates the conformational cycle of Hsp90 in a specific way. Thus, apart from establishing high-affinity hormone binding activity during GR maturation, Hsp90 very likely fulfils also other functions in complex with GR, which will be further discussed in the context of co-chaperones in 4.3.

4.3 Synergistic and antagonistic regulation of GR-Hsp90 complex formation by co-chaperones and GR release from chaperone assemblies

Parts of this work will be published soon (including figures, text and related methods):

'Modulation of the Hsp90 chaperone cycle by a stringent client protein'
Oliver Robin Lorenz, Lee Freiburger, Daniel Andreas Rutz, Maike Krause, Bettina Karolina Zierer, Sara Alvira, Jorge Cuéllar, José María Valpuesta, Tobias Madl, Michael Sattler & Johannes Buchner, Mol.Cell 2014, *Accepted*

4.3.1 Effects of Hsp90 co-chaperones on the Hsp90-GR interaction

Hsp90 co-chaperones provide an additional level of regulation as they shape the conformational transition and modulate ATP turnover of Hsp90 (Li et al., 2012). For GR, several co-chaperones such as Hop, p23 and PPIases (e.g. FKBP51, FKBP52, Cyp40 or PP5) have been isolated from cells together with Hsp90. These co-chaperones contribute to various aspects of GR signaling including maturation, transport and transcriptional activity (Grad and Picard, 2007).

Here, the influence of co-chaperones on the Hsp90-GR interplay was investigated by AUC experiments. For simplicity, the main focus was set on yeast proteins as *S. cerevisiae* comprises a comparable complex Hsp90 machinery and co-chaperones are well conserved (Chang and Lindquist, 1994; Johnson and Brown, 2009).

Hop/Sti1 connects the Hsp70 system with the Hsp90 system during GR maturation (Chen and Smith, 1998). In the Hsp90 cycle, it blocks the conformational rearrangements leading to the closed state (Hessling et al., 2009; Lee et al., 2012; Richter et al., 2003), which in turn results in the inhibition of the Hsp90-ATPase. Sti1 was fluorescent labeled (*Sti) and probed for interaction with Hsp90 in the simultaneous presence of GR-LBDm under ATPγS conditions. Whereas *Sti1 formed a binary complex with Hsp90 (7.5 S), no indication for a ternary Hsp90-GR-LBDm-Sti1 complex was observed, when GR-LBDm was added in excess (7.6 S) (Figure 39, Panel 1-3). Further, in a vice versa experiment with *GR-LBDm, Sti1 triggered the release of a major GR fraction that was pre-bound to Hsp90 (Figure 39, Panel 12-14). This competing Hsp90 binding behavior of Sti1 and GR-LBDm could be explained by two possible scenarios (or a combination of both): On the one hand, Sti1 could negatively affect GR binding by keeping Hsp90 in a fully open conformation, which would be consistent with the fact that GR prefers a partially closed conformation. On the other hand, Sti1 and GR-LBDm binding sites could partly overlap, which seems possible as the proposed binding site for the Sti1-TPR2A-TPR2B domains in complex with Hsp90 is in close proximity to that of the GR-LBDm (Schmid et al., 2012). However, Sti1 contains several TPR domains and their localization in the Hsp90 complex is unknown. Thus, further experiments are required to solve this issue.

No.	* protein	added components	AUC trace (signal vs. s-value)	s-value of complex (unbound *protein)	Fraction bound (*protein)
1	Sti1			4.0	0
2	Sti1	Hsp90		7.5	0.86
3	Sti1	90, GR-LBDm$^{\#1}$		7.6	0.83
4	Sti1	90, Cpr6		7.9	0.45
5	Sti1	90, Cpr6, GR-LBDm		8.4	0.28
6	Cpr6			3.2	0
7	Cpr6	90	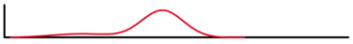	7.0	0.66
8	Cpr6	90, GR-LBDm	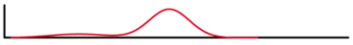	7.2	0.65
9	Cpr6	90, Sti1	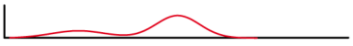	7.6	0.47
10	Cpr6	90, Sti1$^{\#1}$, GR-LBDm	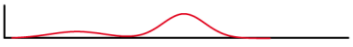	7.9	0.48
11	Cpr6	90, GR-LBDm, p23	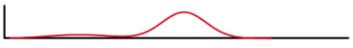	7.9	0.61
12	GR-LBDm			2.7	0
13	GR-LBDm	90	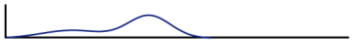	6.2	0.49
14	GR-LBDm	90, Sti1$^{\#1}$		8.4	0.11
15	GR-LBDm	90, Sti1,Cpr6	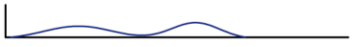	8.4	0.28
16	GR-LBDm	90, Cpr6	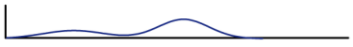	7.8	0.42
17	GR-LBDm	90, Cpr6, p23	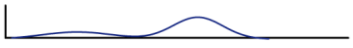	8.4	0.45
18	GR-LBDm	90, p23	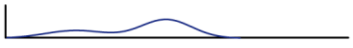	7.0	0.45

Figure 39 Hsp90 co-chaperones modulate the Hsp90-GR-LBDm interaction. Shown are AUC sedimentation velocity experiments. Fluorescently labeled proteins (*protein), added components, AUC traces, s-values and bound fractions of labeled proteins are indicated. Fluorescently labeled proteins were added at a concentration of 400 nM. For complex formation and competition experiments, 2 mM ATPγS and 3 µM or 9 µM ($^{\#1}$) of unmodified components were added. Experiments were performed as described in 3.6.6. Analysis was performed in collaboration with Daniel Rutz (Technische Universität München).

It was previously shown that in the absence of clients, the PPIase Cpr6, Sti1 and Hsp90 form an asymmetric intermediate complex, which allows further progression of the Hsp90 cycle (Li et al., 2011). Hence, it was speculated whether binding of Cpr6 would promote GR binding to a Sti1-Hsp90 complex. AUC experiments under ATPγS conditions revealed that GR-LBDm addition to a preformed *Sti1-Hsp90-Cpr6 complex resulted in the release of Sti1. Moreover, the s-value further increased (7.9 S to 8.4 S), indicative for the formation of a complex comprising GR-LBDm, Sti1, Hsp90 and Cpr6 (Figure 39, Panel 3-5). Notably, the quaternary complex was also observed when fluorescently labeled Cpr6 (*Cpr6) or *GR-LBDm was used instead (Figure 39, Panel 10, 13-16).

The results above show that binding of GR to a Sti1-Hsp90-Cpr6 complex is preferred over binding to a binary Sti1-Hsp90 complex. Given the fact that already folded GR-LBDm in its holo-form was fed to the system, the asymmetric ternary complex may provide a loading

platform for GR that was initially pre-folded by the Hsp70 system in early steps of GR maturation. Further evidence for the importance of this complex for cycle progression was found in ATPase measurements. It turned out, that Cpr6 could almost completely compensate the loss in ATPase activity induced by GR-binding and slightly increased ATPase turnover even in the simultaneous presence of Sti1 and GR-LBDm (Figure 40).

Aha1, a potent activator of the Hsp90-ATPase (Panaretou et al., 2002; Retzlaff et al., 2010) could not bind together with GR-LBDm to Hsp90. Even mixed Aha1-Hsp90-Cpr6 assemblies which were suggested to be important for client binding and cycle progression (Li et al., 2013) did not interact with GR-LBDm (not shown). These results were unexpected as there is literature evidence that Aha1 enhances the efficiency of GR activation *in vivo* (Harst et al., 2005). However, the Hsp90-binding regions for GR-LBDm described in 4.2.1.5 match closely with the reported binding site for the N-terminal domain of Aha1 (Panaretou et al., 2002; Retzlaff et al., 2010) consistent with the above-mentioned observation. Considering this, it remains elusive how Aha1-mediated GR activation functions *in vivo*.

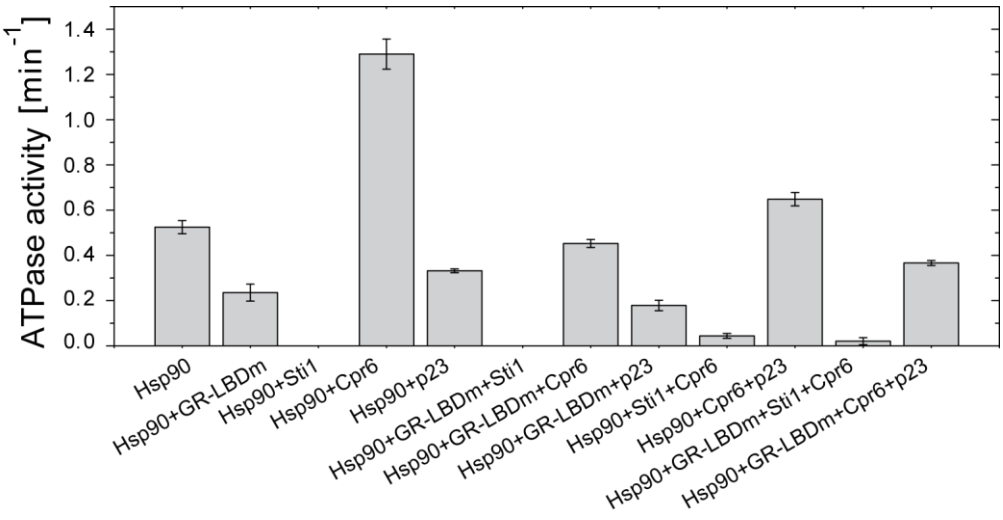

Figure 40 The ATPase activity of Hsp90 in the simultaneous presence of GR-LBDm and co-chaperones. Shown are averages and standard deviations of three independent experiments for each combination. The ATPase activity was assayed as described in 3.9.2 at 30 °C using 3 µM Hsp90. GR-LBDm, Sti1, Cpr6 were added at a concentration of 6 µM. The final concentration of p23 was 9 µM. Analysis was performed in collaboration with Daniel Rutz (Technische Universität München).

p23 enters the Hsp90 cycle in later steps and promotes the release of Sti1 in a concerted action with Cpr6 (Li et al., 2011). AUC experiments revealed, as expected, an increase in s-values when p23 was added to binary *GR-LBDm-Hsp90 complexes and ternary *GR-LBDm-Hsp90-Cpr6 complexes (7 S and 8.4 S) (Figure 39, Panel 17-18).

ATPase measurements showed that p23 inhibits the Hsp90-ATPase by ~ 40 %, consistent with earlier reports (Richter et al., 2004; Siligardi et al., 2004). Moreover, the ATPase rate decreased by 66 % in the simultaneous presence of GR-LBDm, and further addition of Cpr6 partly restored ATP turnover (Figure 40). These results suggest that the formation of late Hsp90-hetero-complexes described above, prolong the interaction of Hsp90 with GR as ATP hydrolysis is slowed down. This is also consistent with the notion that p23 extends the Hsp90-GR interaction *in vivo* (Morishima et al., 2003).

Initial AUC experiments revealed that GR binding stoichiometry might depend on Hsp90 associated co-chaperones (not shown). To further investigate this finding, work was focused on the Hsp90-GR-LBDm-p23 complex and its composition was analyzed by SAXS measurements. p23 binds Hsp90-ATPγS in a 2:2 stoichiometry and shifts the Hsp90 conformation towards a closed state (not shown), which is consistent with the published crystal structure of the binary complex (Ali et al., 2006). However, for the Hsp90-GR-LBDm-p23 complex, a 2:1:1 stoichiometry was established (Figure 41A). Above that stoichiometry, no further increase in the molecular mass corresponding to an additional binding of p23 or GR-LBDm could be observed. To provide molecular details of the complex, the structures of the ternary complexes were modeled using the crystal structures of the Hsp90-p23 complex (Ali et al., 2006) and the GR-LBD-F602S (Bledsoe et al., 2002), as well as NMR data of the Hsp90-GR-LBDm binding interface (Supplemental table 1) and SAXS data as input (Figure 41B,C,D). Docking calculations suggest that the position of the GR-LBDm is identical to the ‘closed’ Hsp90-GR-LBDm complex (Figure 35E, Figure 41D). Moreover, the model reveals that simultaneous binding of GR-LBD and p23 to one Hsp90 monomer seems disfavored. In the presence of p23, only one of the two individual GR binding sites located in the Hsp90 dimer seems accessible for GR (Figure 41B). p23 binds to the opposite side of the Hsp90-N-N interface and thus likely prevents additional GR binding to the other Hsp90 protomer. Whether these observations result from competition with GR or from allosteric effects could not be resolved in this study. Also, the functional relevance of the modulation of GR binding stoichiometry by p23 has to be elucidated. However, as similar observations were made with Cpr6 in initial AUC experiments mentioned above, the change in client binding stoichiometry by Hsp90 co-chaperones could reflect their general importance for client recruitment and/or further processing.

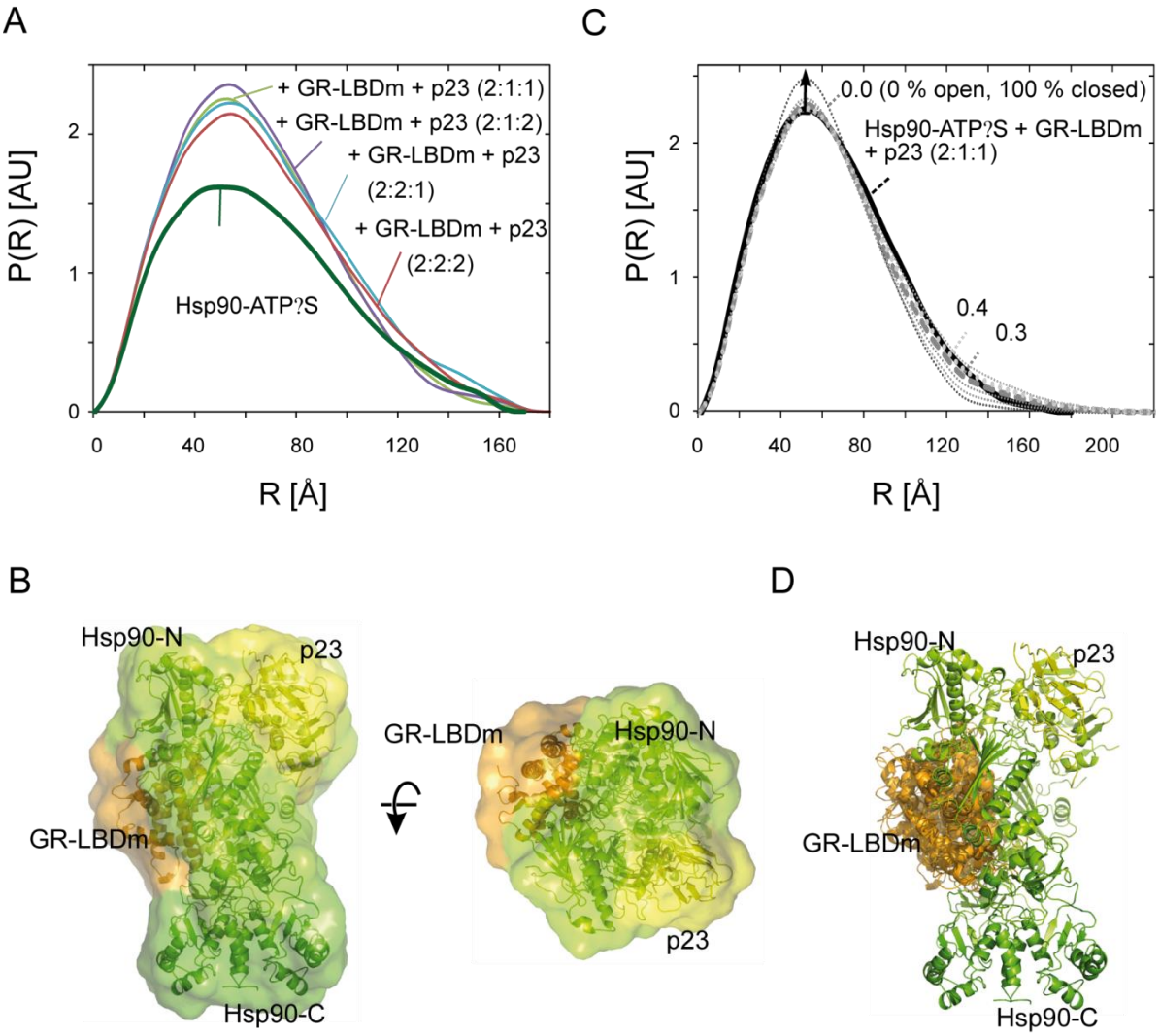

Figure 41 SAXS analysis of the Hsp90-GR-LBDm-p23 complex. A) Comparison of the experimental radial density distributions of Hsp90-ATPγS at increasing stoichiometric ratios of GR-LBDm and p23. Concentrations were 4.4 (Hsp90-ATPγS+ GR-LBDm + p23, 2:1:1), 4.8 (2:1:2), 4.9 (2:2:1), and 5.4 mg/ml (2:2:2). B) Model of the Hsp90-GR-LBDm-p23 complex in different orientations. Hsp90 domains are shown in different greens, GR-LBDm in orange, and p23 in yellow. C) Comparison of the experimental with theoretical radial density distributions calculated for a mixture of open and closed complexes. D) Cartoon representation of the bundle of 5 lowest energy structures from the rigid body modeling calculations of closed Hsp90-GR-LBDm-p23. In these calculations GR-LBDm was docked to the closed form of Hsp90-p23 (PDB 2CG9) using the NMR chemical shift perturbation data (Supplemental table 1) as restraints. For population analysis, the radial density distributions of Hsp90-GR-LBDm-p23 and of the closed Hsp90-GR-LBDm-p23 docking model (D), back-calculated using the program Crysol (Svergun et al., 1995) were taken as input. See Figure 35 for comparison with the model of the Hsp90-GR-LBDm complex. Of note, the orientation and the binding interface of the GR-LBDm in the ternary complex could be defined more precisely in later experiments by including NMR binding data of GR-LBDm with Hsp90-C and NMR-PRE experiments as well as electron microscopy data in SAXS calculations (see also 4.2.1.6). SAXS data analysis and figure preparation was performed by Tobias Madl (Technische Universität München).

4.3.2 GR release from Hsp90 hetero-complexes is achieved by ATP hydrolysis

For a long time it was believed that hormone binding triggers the dissociation of the receptor from Hsp90 prior to its translocation into the nucleus. However, this scenario seems now outdated. Recent studies argue against the notion that ligand binding induces Hsp90 release from GR (Vandevyver et al., 2012). Moreover, earlier studies on the progesterone receptor revealed that neither hormone binding nor conformational rearrangements of the GR-LBD seem to directly affect Hsp90 dissociation (Smith, 1993). Since ATP-hydrolysis may stimulate client release from Hsp90 (Smith, 1993), it was speculated whether Hsp90-GR complexes can be disrupted by ADP.

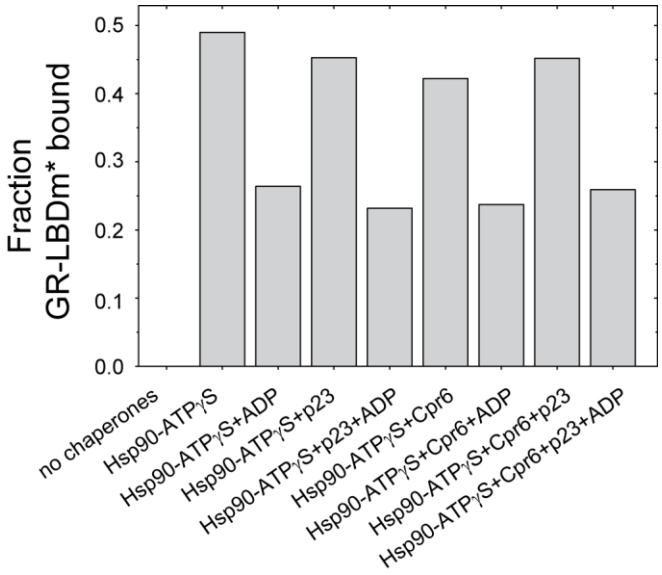

Figure 42 Addition of excess ADP disrupts Hsp90 hetero-complexes. Complexes between *GR-LBDm and Hsp90 or between *GR-LBDm, Hsp90, Cpr6 and/or p23 were formed under ATPγS conditions as described in 4.3.1 and chased with 10 mM ADP. The fractions of complexed *GR-LBDm were calculated from AUC sedimentation velocity experiments and plotted for each combination. Analysis was performed in collaboration with Daniel Rutz (Technische Universität München).

AUC experiments that were performed under ATPγS conditions showed, as expected, an increase in s-values when *GR-LBDm was incubated with Hsp90 or various combinations of Hsp90, Cpr6 and p23 (compare Figure 39). Whereas ~ 50 % of GR-LBDm was bound to Hsp90 or Hsp90 co-chaperone assemblies, the addition of excess ADP significantly decreased the affinity for GR-LBDm and resulted in the release of Hsp90-bound *GR-LBDm (Figure 42). This observation is also in agreement with the FRET experiments described in 4.2.2.2, in which the re-opening of the Hsp90 dimer by ADP was influenced by GR-binding. Interestingly, the release in the presence of ADP was not affected by the nature of GR-Hsp90 complexes studied, suggesting that mainly the restoration of the open conformation after ATP hydrolysis is important for the dissociation of GR.

In this respect, it would be interesting to compare release kinetics for the different hetero-complexes. For instance, it seems likely, that p23 prolongs the half-time of GR-Hsp90 complexes simply by slowing down ATP-hydrolysis. However, it has to be investigated whether this hypothesis holds true and accounts for the function of p23 *in vivo* (Freeman et al., 2000; Morishima et al., 2003).

4.3.3 Integration of GR into the Hsp90 cycle

The observations made in 4.3 highlight the importance of Hsp90 co-chaperones in the Hsp90-GR interplay. Both, synergistic and antagonistic effects were discovered, which helped to establish a comprehensive picture of the Hsp90 cycle in the presence of a stringent client (Figure 43).

Hop/Sti1 plays a key role in mediating client transfer from the Hsp70 system to the Hsp90 cycle (Chen and Smith, 1998). It was found that Sti1 negatively influences the binding of holo-GR to Hsp90 presumably by keeping Hsp90 in an open conformation. At first glance, this finding seems counterproductive. However, once the client is transferred to Hsp90, the Hsp90 cycle will arrest as long as Sti1 remains bound to Hsp90 as it blocks the conformational transitions to the closed state. Thus, the exit of Sti1 is a prerequisite for the progression of the cycle and subsequent binding of p23, which binds exclusively to closed Hsp90. In contrast to previous proposals (Harst et al., 2005; Li et al., 2013), the Hsp90-ATPase activator Aha1 is probably not involved in GR cycling as it competed with GR-LBDm for Hsp90 binding. However, the PPIase Cpr6 could relieve the inhibitory behavior of Sti1 and promoted cycle progression of Hsp90-bound GR. In this respect, the formation of a ternary Hsp90-Sti1-Cpr6 complex seems an important intermediate of the Hsp90 cycle. Concerning GR maturation, the asymmetric complex may also reflect the client loading conformation for apo-GR that was initially pre-folded by the Hsp70 system. Apart from that, hetero-complexes with Hsp90, p23 and/or Cpr6 could be formed, which likely represent the end-result of the GR maturation pathway. These complexes formed with holo-GR were stable and provide further evidence that liganded GR does not as dissociate from Hsp90 upon hormone binding, consistent with the idea that those chaperone assemblies regulate receptor trafficking and transcriptional activity (Freeman and Yamamoto, 2002; Vandevyver et al., 2012). Notably, binding of the co-chaperones Cpr6 and p23 modulate GR binding stoichiometry. Only one of the two individual GR binding sites located in each of the Hsp90 protomers remains accessible once the co-chaperones enter the cycle. However, the functional relevance remains elusive. The release of GR from Hsp90 is very likely regulated by ATP hydrolysis. In this respect, p23 seems an important component of the cycle, as it arrests Hsp90 in a closed state and thus prolongs the dwell-time of GR-Hsp90 complexes.

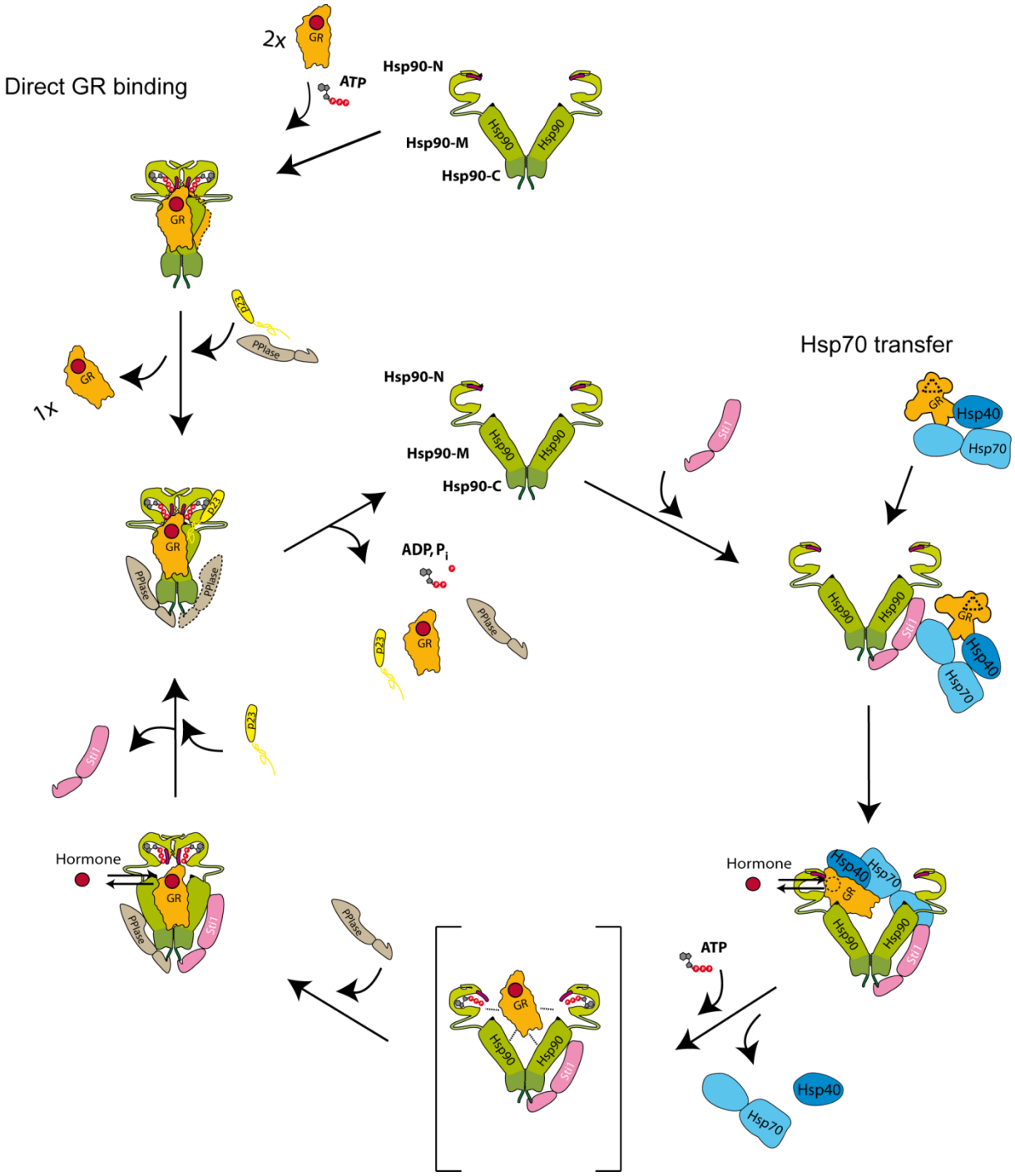

Figure 43 Integration of GR into the Hsp90 co-chaperone cycle. The model shows two scenarios for feeding GR into the Hsp90 machine. In the case of apo-GR, the client assembles with the Hsp70 system to form an early complex, which is subsequently connected to the Hsp90 cycle through the adaptor protein Sti1. In complex with Hsp90, GR binds hormone with high affinity. Upon nucleotide binding, Hsp70 and Hsp40 are released, which results in a highly transient complex between Hsp90, Sti1 and GR (shown in brackets). In this state, the cycle is arrested since Sti1blocks the conformational transition leading to a closed state. The entry of a PPIase (e.g. Cpr6) accelerates the cycle and stabilizes the Hsp90-GR interaction. p23 facilitates the exit of Sti1 in concert with the PPIase. The end-result is a closed holo-GR-Hsp90-p23-PPIase complex. In addition, p23 promotes further closure of the Hsp90 dimer and reduces its ATPase activity resulting in a prolonged interaction of Hsp90 with its client.
In the second scenario, holo-GR is bound directly by Hsp90. It is not known whether the GR conformation bound directly or delivered by the Hsp70 system differs. However, in the absence of co-chaperones, Hsp90 can accommodate two GR molecules. Subsequent binding of p23 and/or Cpr6 changes GR binding stoichiometry. ATP hydrolysis drives GR release from Hsp90 and its associated co-chaperones.

Within this study, the influence of GR on the Hsp90 cycle was mainly studied with yeast components. Preliminary binding experiments with GR, human Hsp90 and its co-chaperones suggest a similar scenario in men as late chaperone complexes with GR, Hsp90, p23 and a PPIase (e.g. FKBP51, FKBP52 and Cyp40) could be formed. However, besides binding analysis, the conformational rearrangements in human Hsp90 are difficult to follow in the context of a client. Human Hsp90 displays only a very weak ATPase (0.04 min^{-1}). The inhibition of the Hsp90-ATPase by GR could only be demonstrated in the presence of Aha1, which was later shown to compete with GR for binding to Hsp90. Thus, more sophisticated methods (e.g. a human Hsp90-FRET system, cross-linking approaches) are required to study the impact of GR on the human Hsp90 machine. This would be of great interest, since more pronounced co-chaperones effects have to be expected to drive the rather slow cycle of human Hsp90.

5 Summary

In the cell, the glucocorticoid receptor (GR), in particular its ligand binding domain (GR-LBD), assembles with the Hsp70-Hsp90 multi-chaperone machinery to become active as a transcription factor. At the beginning of this project, little molecular and mechanistic details were known on how the receptor interacts with Hsp90, as most of the work that established its complex maturation pathway was conducted with receptors that were isolated with antibodies from eukaryotic cell sources.

To elucidate the complex relationship of Hsp90 with its most stringent client, the first aim of this project was to acquire a source of functional GR protein that would in turn allow experiments with purified components *in vitro*. Efforts to produce ligand-free, soluble and functional GR-LBD *wt* from *E. coli* or insect cells failed. However, this problem could be circumvented by a GR-LBD mutant (GR-LBDm) that expresses at moderate levels in bacteria and which can be purified in milligram quantities in the presence of hormone. Its characterization revealed excellent biochemical properties in terms of folding, stability and hormone binding. Moreover, a larger construct comprising also the DNA-binding domain of GR (GR-DBD-LBDm) was successfully purified in its functional form.

In the following the Hsp90-GR interplay was extensively studied using a variety of biochemical and structural approaches. Whereas stable complexes with holo-GR-LBDm could be formed, reconstitution experiments with apo-GR-LBDm failed presumably due to its high intrinsic instability. However, complex formation between holo-GR-LBDm and Hsp90 was specific and depended on nucleotides. It turned out, that holo-GR-LBDm binds mainly to the Hsp90-M domain in the inside cleft of the closed Hsp90 dimer with contributions from the Hsp90-N and -C domain. Analysis of the conformational cycle of Hsp90 showed that a partially closed Hsp90 state is preferred for interaction with GR. This results in a deceleration of the Hsp90 cycle and concomitantly in a decrease of the Hsp90-ATPase. Hsp90 co-chaperones serve as important elements within the Hsp90 cycle as they modulate GR binding, both in a synergistic and antagonistic manner. So far, one can only speculate about the structural impacts on holo-GR upon Hsp90 binding. However, this dissertation provides fundamental new insights in the Hsp90 client relationship and may encourage others to further participate in this interesting field of research.

6 Abbreviations

Å	Angström
A	Ampere
AMP-PNP	5'–Adenylyl-ß,γ-imido-diphosphate
AR	Androgen receptor
ATPγS	Adenosine-5'-(γ-thio)-triphosphate
AUC	Analytical ultracentrifugation
CD	Circular dichroism
CSP	Chemical shift pertubations
CV	Column volume
DEX	Dexamethasone
D_{max}	Maximum dimension
DNA	Deoxyribonucleic acid
E. coli	*Escherichia coli*
EM	Electron microscopy
ER	Estrogen receptor
et al.	And others
F-DEX	Dexamethasone Fluorescein
FPLC	Fast protein liquid chromatography
FRET	Fluorescence resonance energy transfer
g	Gram
GC	Glucocorticoids
GR	Glucocorticoid receptor
GR-DBD	DNA binding domain of the glucocorticoid receptor
GR-DBD-LBDm	GR-DBD-LBD-F602S/A605V/V702A/E705G/M752T
GRE	Glucocorticoid transcriptional response element
GR-LBD	Ligand binding domain of the glucocorticoid receptor
GR-LBDm	GR-LBD-F602S/A605V/V702A/E705G/M752T
GR-NTD	N-terminal domain of the glucocorticoid receptor
h	Hour
HPLC	High-performance liquid chromatography
Hsp	Heat shock protein
Hsp90-C	C-terminal domain of Hsp90
Hsp90-M	Middle domain of Hsp90
Hsp90-N	N-terminal domain of Hsp90
IC_{50}	half maximal inhibitory concentration
IP	Immunoprecipitation
K_D	Dissociation constant
kDa	Kilodalton
K_i	Inhibition constant
l	Liter

M	Molar
MIF	Mifepristone
min	Minute
ml	Milliliter
MR	Mineralocorticoid receptor
MS	Mass spectrometry
MW	Molecular mass
nm	Nanometer
nM	Nanomolar
NMR	Nuclear magnetic resonance
OD_{600}	Optical density at 600 nm
p.a.	*pro analysi*
PCR	Polymerase chain reaction
POD	Peroxidase
PR	Progesterone receptor
P(R)	Inter-atomic distance distribution function
R_g	Radius of gyration
RLL	Rabbit reticulocyte lysate
rpm	Revolutions per minute
RT	Room temperature
s	Second
S. cerevisae	*Saccharomyces cerevisiae*
SAXS	Small angle x-ray scattering
SDS-PAGE	Sodium dodecyl sulfate polyacrylamide gel electrophoresis
SHR	Steroid hormone receptor
TPR	Tetratricopeptide repeat domain
µl	Microliter
µM	Micromolar
UV	Ultraviolet
V	Volt
v/v	Volume per volume
w/v	Weight per volume
wt	Wild type
x g	multiple of the acceleration of gravity

7 Literature

Acevedo, M.L., and Kraus, W.L. (2004). Transcriptional activation by nuclear receptors. Essays Biochem *40*, 73-88.

Schmid, A.B., (2009). The adaptor protein Sti1/Hop connects the Hsp70 and Hsp90 chaperone cycle. Verlag Dr. Hut, Biochemie, Dissertation Technische Universität München

Akner, G., Mossberg, K., Sundqvist, K.G., Gustafsson, J.A., and Wikstrom, A.C. (1992). Evidence for reversible, non-microtubule and non-microfilament-dependent nuclear translocation of hsp90 after heat shock in human fibroblasts. Eur J Cell Biol *58*, 356-364.

Alarcon, S.V., Mollapour, M., Lee, M.J., Tsutsumi, S., Lee, S., Kim, Y.S., Prince, T., Apolo, A.B., Giaccone, G., Xu, W., *et al.* (2012). Tumor-intrinsic and tumor-extrinsic factors impacting hsp90- targeted therapy. Curr Mol Med *12*, 1125-1141.

Ali, M.M., Roe, S.M., Vaughan, C.K., Meyer, P., Panaretou, B., Piper, P.W., Prodromou, C., and Pearl, L.H. (2006). Crystal structure of an Hsp90-nucleotide-p23/Sba1 closed chaperone complex. Nature *440*, 1013-1017.

Alnemri, E.S., and Litwack, G. (1993). The steroid binding domain influences intracellular solubility of the baculovirus overexpressed glucocorticoid and mineralocorticoid receptors. Biochemistry *32*, 5387-5393.

Anfinsen, C.B., Haber, E., Sela, M., and White, F.H., Jr. (1961). The kinetics of formation of native ribonuclease during oxidation of the reduced polypeptide chain. Proc Natl Acad Sci U S A *47*, 1309-1314.

Baker, N.A., Sept, D., Joseph, S., Holst, M.J., and McCammon, J.A. (2001). Electrostatics of nanosystems: Application to microtubules and the ribosome. Proc Natl Acad Sci U S A *98*, 10037-10041.

Balch, W.E., Morimoto, R.I., Dillin, A., and Kelly, J.W. (2008). Adapting proteostasis for disease intervention. Science *319*, 916-919.

Ballinger, C.A., Connell, P., Wu, Y., Hu, Z., Thompson, L.J., Yin, L.Y., and Patterson, C. (1999). Identification of CHIP, a novel tetratricopeptide repeat-containing protein that interacts with heat shock proteins and negatively regulates chaperone functions. Mol Cell Biol *19*, 4535-4545.

Barent, R.L., Nair, S.C., Carr, D.C., Ruan, Y., Rimerman, R.A., Fulton, J., Zhang, Y., and Smith, D.F. (1998). Analysis of FKBP51/FKBP52 chimeras and mutants for Hsp90 binding and association with progesterone receptor complexes. Mol Endocrinol *12*, 342-354.

Bergerat, A., de Massy, B., Gadelle, D., Varoutas, P.C., Nicolas, A., and Forterre, P. (1997). An atypical topoisomerase II from Archaea with implications for meiotic recombination. Nature *386*, 414-417.

Bichet, P., Mollat, P., Capdevila, C., and Sarubbi, E. (2000). Endogenous glutathione-binding proteins of insect cell lines: characterization and removal from glutathione S-transferase (GST) fusion proteins. Protein Expr Purif *19*, 197-201.

Blanchet, C.E., and Svergun, D.I. (2013). Small-angle X-ray scattering on biological macromolecules and nanocomposites in solution. Annu Rev Phys Chem *64*, 37-54.

Bledsoe, R.K., Montana, V.G., Stanley, T.B., Delves, C.J., Apolito, C.J., McKee, D.D., Consler, T.G., Parks, D.J., Stewart, E.L., Willson, T.M., *et al.* (2002). Crystal structure of the glucocorticoid receptor ligand binding domain reveals a novel mode of receptor dimerization and coactivator recognition. Cell *110*, 93-105.

Bohen, S.P., and Yamamoto, K.R. (1993). Isolation of Hsp90 mutants by screening for decreased steroid receptor function. Proc Natl Acad Sci U S A *90*, 11424-11428.

Borkovich, K.A., Farrelly, F.W., Finkelstein, D.B., Taulien, J., and Lindquist, S. (1989). hsp82 is an essential protein that is required in higher concentrations for growth of cells at higher temperatures. Mol Cell Biol *9*, 3919-3930.

Brinker, A., Scheufler, C., Von Der Mulbe, F., Fleckenstein, B., Herrmann, C., Jung, G., Moarefi, I., and Hartl, F.U. (2002). Ligand discrimination by TPR domains. Relevance and selectivity of EEVD-recognition in Hsp70 x Hop x Hsp90 complexes. J Biol Chem *277*, 19265-19275.

Buchner, J., and Walter, S. (2008). Analysis of Chaperone Function in Vitro. In Protein Folding Handbook (Wiley-VCH Verlag GmbH), pp. 162-196.

Burke, L.J., and Baniahmad, A. (2000). Co-repressors 2000. FASEB J *14*, 1876-1888.

Cadepond, F., Binart, N., Chambraud, B., Jibard, N., Schweizer-Groyer, G., Segard-Maurel, I., and Baulieu, E.E. (1993). Interaction of glucocorticosteroid receptor and wild-type or mutated 90-kDa heat shock protein coexpressed in baculovirus-infected Sf9 cells. Proc Natl Acad Sci U S A *90*, 10434-10438.

Cantor C. R., and Schimmel P. R., Biophysical Chemistry (Freeman & Co, San Francisco, 1980), pp. 374-451.

Chang, H.C., and Lindquist, S. (1994). Conservation of Hsp90 macromolecular complexes in Saccharomyces cerevisiae. J Biol Chem *269*, 24983-24988.

Chen, B., Zhong, D., and Monteiro, A. (2006). Comparative genomics and evolution of the HSP90 family of genes across all kingdoms of organisms. BMC Genomics *7*, 156.

Chen, S., and Smith, D.F. (1998). Hop as an adaptor in the heat shock protein 70 (Hsp70) and hsp90 chaperone machinery. J Biol Chem *273*, 35194-35200.

Clark, P.L. (2004). Protein folding in the cell: reshaping the folding funnel. Trends Biochem Sci *29*, 527-534.

Cliff, M.J., Harris, R., Barford, D., Ladbury, J.E., and Williams, M.A. (2006). Conformational diversity in the TPR domain-mediated interaction of protein phosphatase 5 with Hsp90. Structure *14*, 415-426.

Cluning, C., Ward, B.K., Rea, S.L., Arulpragasam, A., Fuller, P.J., and Ratajczak, T. (2013). The helix 1-3 loop in the glucocorticoid receptor LBD is a regulatory element for FKBP cochaperones. Mol Endocrinol *27*, 1020-1035.

Csermely, P., Schnaider, T., Soti, C., Prohaszka, Z., and Nardai, G. (1998). The 90-kDa molecular chaperone family: structure, function, and clinical applications. A comprehensive review. Pharmacol Ther *79*, 129-168.

Dahlman-Wright, K., Wright, A., Gustafsson, J.A., and Carlstedt-Duke, J. (1991). Interaction of the glucocorticoid receptor DNA-binding domain with DNA as a dimer is mediated by a short segment of five amino acids. J Biol Chem *266*, 3107-3112.

Dehner, A., Furrer, J., Richter, K., Schuster, I., Buchner, J., and Kessler, H. (2003). NMR chemical shift perturbation study of the N-terminal domain of Hsp90 upon binding of ADP, AMP-PNP, geldanamycin, and radicicol. Chembiochem *4*, 870-877.

Delaglio, F., Grzesiek, S., Vuister, G.W., Zhu, G., Pfeifer, J., and Bax, A. (1995). NMRPipe: a multidimensional spectral processing system based on UNIX pipes. J Biomol NMR *6*, 277-293.

DeZwaan, D.C., and Freeman, B.C. (2010). HSP90 manages the ends. Trends Biochem Sci *35*, 384-391.

Dill, K.A., and MacCallum, J.L. (2012). The protein-folding problem, 50 years on. Science *338*, 1042-1046.

Dittmar, K.D., Demady, D.R., Stancato, L.F., Krishna, P., and Pratt, W.B. (1997). Folding of the glucocorticoid receptor by the heat shock protein (hsp) 90-based chaperone machinery. The role of p23 is to stabilize receptor.hsp90 heterocomplexes formed by hsp90.p60.hsp70. J Biol Chem *272*, 21213-21220.

Dollins, D.E., Warren, J.J., Immormino, R.M., and Gewirth, D.T. (2007). Structures of GRP94-nucleotide complexes reveal mechanistic differences between the hsp90 chaperones. Mol Cell *28*, 41-56.

Dutta, R., and Inouye, M. (2000). GHKL, an emergent ATPase/kinase superfamily. Trends Biochem Sci *25*, 24-28.

Echeverria, P.C., Mazaira, G., Erlejman, A., Gomez-Sanchez, C., Piwien Pilipuk, G., and Galigniana, M.D. (2009). Nuclear import of the glucocorticoid receptor-hsp90 complex through the nuclear pore complex is mediated by its interaction with Nup62 and importin beta. Mol Cell Biol *29*, 4788-4797.

Echeverria, P.C., and Picard, D. (2010). Molecular chaperones, essential partners of steroid hormone receptors for activity and mobility. Biochim Biophys Acta *1803*, 641-649.

Ellis, R.J. (2007). Protein misassembly: macromolecular crowding and molecular chaperones. Adv Exp Med Biol *594*, 1-13.

Escriva, H., Bertrand, S., and Laudet, V. (2004). The evolution of the nuclear receptor superfamily. Essays Biochem *40*, 11-26.

Fairbanks, G., Steck, T.L., and Wallach, D.F. (1971). Electrophoretic analysis of the major polypeptides of the human erythrocyte membrane. Biochemistry *10*, 2606-2617.

Fang, L., Ricketson, D., Getubig, L., and Darimont, B. (2006). Unliganded and hormone-bound glucocorticoid receptors interact with distinct hydrophobic sites in the Hsp90 C-terminal domain. Proc Natl Acad Sci U S A *103*, 18487-18492.

Felts, S.J., Owen, B.A., Nguyen, P., Trepel, J., Donner, D.B., and Toft, D.O. (2000). The hsp90-related protein TRAP1 is a mitochondrial protein with distinct functional properties. J Biol Chem *275*, 3305-3312.

Fersht, A. (1999). Structure and mechanism in protein science : a guide to enzyme catalysis and protein folding (New York: Freeman), pp 575-576

Fink, A.L. (2005). Natively unfolded proteins. CurrOpin in Struc Biol *15*, 35-41.

Freedman, N.D., and Yamamoto, K.R. (2004). Importin 7 and importin alpha/importin beta are nuclear import receptors for the glucocorticoid receptor. Mol Biol Cell *15*, 2276-2286.

Freeman, B.C., Felts, S.J., Toft, D.O., and Yamamoto, K.R. (2000). The p23 molecular chaperones act at a late step in intracellular receptor action to differentially affect ligand efficacies. Genes Dev *14*, 422-434.

Freeman, B.C., Toft, D.O., and Morimoto, R.I. (1996). Molecular chaperone machines: chaperone activities of the cyclophilin Cyp-40 and the steroid aporeceptor-associated protein p23. Science *274*, 1718-1720.

Freeman, B.C., and Yamamoto, K.R. (2002). Disassembly of transcriptional regulatory complexes by molecular chaperones. Science *296*, 2232-2235.

Frydman, J. (2001). Folding of newly translated proteins in vivo: the role of molecular chaperones. Annu Rev Biochem *70*, 603-647.

Fuhrmann, U., Parczyk, K., Klotzbucher, M., Klocker, H., and Cato, A.C. (1998). Recent developments in molecular action of antihormones. J Mol Med (Berl) *76*, 512-524.

Gaiser, A.M., Kretzschmar, A., and Richter, K. (2010). Cdc37-Hsp90 complexes are responsive to nucleotide-induced conformational changes and binding of further cofactors. J Biol Chem *285*, 40921-40932.

Galigniana, M.D., Echeverria, P.C., Erlejman, A.G., and Piwien-Pilipuk, G. (2010). Role of molecular chaperones and TPR-domain proteins in the cytoplasmic transport of steroid receptors and their passage through the nuclear pore. Nucleus *1*, 299-308.

Galigniana, M.D., Harrell, J.M., Housley, P.R., Patterson, C., Fisher, S.K., and Pratt, W.B. (2004). Retrograde transport of the glucocorticoid receptor in neurites requires dynamic assembly of complexes with the protein chaperone hsp90 and is linked to the CHIP component of the machinery for proteasomal degradation. Brain Res Mol Brain Res *123*, 27-36.

Galigniana, M.D., Harrell, J.M., Murphy, P.J., Chinkers, M., Radanyi, C., Renoir, J.M., Zhang, M., and Pratt, W.B. (2002). Binding of hsp90-associated immunophilins to cytoplasmic dynein: direct binding and in vivo evidence that the peptidylprolyl isomerase domain is a dynein interaction domain. Biochemistry *41*, 13602-13610.

Galigniana, M.D., Radanyi, C., Renoir, J.M., Housley, P.R., and Pratt, W.B. (2001). Evidence that the peptidylprolyl isomerase domain of the hsp90-binding immunophilin FKBP52 is involved in both dynein interaction and glucocorticoid receptor movement to the nucleus. J Biol Chem *276*, 14884-14889.

Genest, O., Reidy, M., Street, T.O., Hoskins, J.R., Camberg, J.L., Agard, D.A., Masison, D.C., and Wickner, S. (2013). Uncovering a region of heat shock protein 90 important for client binding in E. coli and chaperone function in yeast. Mol Cell *49*, 464-473.

Grad, I., and Picard, D. (2007). The glucocorticoid responses are shaped by molecular chaperones. Mol Cell Endocrinol *275*, 2-12.

Graf, C., Stankiewicz, M., Kramer, G., and Mayer, M.P. (2009). Spatially and kinetically resolved changes in the conformational dynamics of the Hsp90 chaperone machine. EMBO J *28*, 602-613.

Grenert, J.P., Sullivan, W.P., Fadden, P., Haystead, T.A., Clark, J., Mimnaugh, E., Krutzsch, H., Ochel, H.J., Schulte, T.W., Sausville, E., *et al.* (1997). The amino-terminal domain of heat shock protein 90 (hsp90) that binds geldanamycin is an ATP/ADP switch domain that regulates hsp90 conformation. J Biol Chem *272*, 23843-23850.

Hagn, F., Lagleder, S., Retzlaff, M., Rohrberg, J., Demmer, O., Richter, K., Buchner, J., and Kessler, H. (2011). Structural analysis of the interaction between Hsp90 and the tumor suppressor protein p53. Nat Struct Mol Biol *18*, 1086-1093.

Hainzl, O., Lapina, M.C., Buchner, J., and Richter, K. (2009). The charged linker region is an important regulator of Hsp90 function. J Biol Chem *284*, 22559-22567.

Harris, S.F., Shiau, A.K., and Agard, D.A. (2004). The crystal structure of the carboxy-terminal dimerization domain of htpG, the Escherichia coli Hsp90, reveals a potential substrate binding site. Structure *12*, 1087-1097.

Harrison, S.C., and Durbin, R. (1985). Is there a single pathway for the folding of a polypeptide chain? Proc Natl Acad Sci U S A *82*, 4028-4030.

Harst, A., Lin, H., and Obermann, W.M. (2005). Aha1 competes with Hop, p50 and p23 for binding to the molecular chaperone Hsp90 and contributes to kinase and hormone receptor activation. Biochem J *387*, 789-796.

Haslbeck, M., Franzmann, T., Weinfurtner, D., and Buchner, J. (2005). Some like it hot: the structure and function of small heat-shock proteins. Nat Struct Mol Biol *12*, 842-846.

Hawle, P., Siepmann, M., Harst, A., Siderius, M., Reusch, H.P., and Obermann, W.M. (2006). The middle domain of Hsp90 acts as a discriminator between different types of client proteins. Mol Cell Biol *26*, 8385-8395.

Heery, D.M., Kalkhoven, E., Hoare, S., and Parker, M.G. (1997). A signature motif in transcriptional co-activators mediates binding to nuclear receptors. Nature *387*, 733-736.

Heitzer, M.D., Wolf, I.M., Sanchez, E.R., Witchel, S.F., and DeFranco, D.B. (2007). Glucocorticoid receptor physiology. Rev Endocr Metab Disord *8*, 321-330.

Helms, V. (2008). Fluorescence Resonance Energy Transfer. Principles of Computational Cell Biology. Weinheim: Wiley-VCH. p. 202.

Hernandez, M.P., Chadli, A., and Toft, D.O. (2002). HSP40 binding is the first step in the HSP90 chaperoning pathway for the progesterone receptor. J Biol Chem *277*, 11873-11881.

Hessling, M., Richter, K., and Buchner, J. (2009). Dissection of the ATP-induced conformational cycle of the molecular chaperone Hsp90. Nat Struct Mol Biol *16*, 287-293.

Hodgson, M.C., Shen, H.C., Hollenberg, A.N., and Balk, S.P. (2008). Structural basis for nuclear receptor corepressor recruitment by antagonist-liganded androgen receptor. Mol Cancer Ther *7*, 3187-3194.

Hohfeld, J., Minami, Y., and Hartl, F.U. (1995). Hip, a novel cochaperone involved in the eukaryotic Hsc70/Hsp40 reaction cycle. Cell *83*, 589-598.

Hollenberg, S.M., Weinberger, C., Ong, E.S., Cerelli, G., Oro, A., Lebo, R., Thompson, E.B., Rosenfeld, M.G., and Evans, R.M. (1985). Primary structure and expression of a functional human glucocorticoid receptor cDNA. Nature *318*, 635-641.

Horlein, A.J., Naar, A.M., Heinzel, T., Torchia, J., Gloss, B., Kurokawa, R., Ryan, A., Kamei, Y., Soderstrom, M., Glass, C.K., *et al.* (1995). Ligand-independent repression by the thyroid hormone receptor mediated by a nuclear receptor co-repressor. Nature *377*, 397-404.

Horwich, A.L., and Fenton, W.A. (2009). Chaperonin-mediated protein folding: using a central cavity to kinetically assist polypeptide chain folding. Q Rev Biophys *42*, 83-116.

Howard, K.J., Holley, S.J., Yamamoto, K.R., and Distelhorst, C.W. (1990). Mapping the HSP90 binding region of the glucocorticoid receptor. J Biol Chem *265*, 11928-11935.

Hudson, W.H., Youn, C., and Ortlund, E.A. (2013). The structural basis of direct glucocorticoid-mediated transrepression. Nat Struct Mol Biol *20*, 53-58.

Hyodo, M., Okamoto, K., Shibata, K., Suematsu, N., and Isohashi, F. (2001). Novel and simple two-step purification of a full-length rat glucocorticoid-receptor expressed in a baculovirus system. J Chromatogr B Biomed Sci Appl *765*, 89-97.

Jackson, S. (2013). Hsp90: Structure and Function. In Molecular Chaperones, S. Jackson, ed. (Springer Berlin Heidelberg), pp. 155-240.

Jakob, U., Lilie, H., Meyer, I., and Buchner, J. (1995). Transient interaction of Hsp90 with early unfolding intermediates of citrate synthase. Implications for heat shock in vivo. J Biol Chem *270*, 7288-7294.

John, S., Sabo, P.J., Thurman, R.E., Sung, M.H., Biddie, S.C., Johnson, T.A., Hager, G.L., and Stamatoyannopoulos, J.A. (2011). Chromatin accessibility pre-determines glucocorticoid receptor binding patterns. Nat Genet *43*, 264-268.

Johnson, J., and Brown, C. (2009). Plasticity of the Hsp90 chaperone machine in divergent eukaryotic organisms. Cell Stress Chaperon *14*, 83-94.

Johnson, J.L., and Toft, D.O. (1994). A novel chaperone complex for steroid receptors involving heat shock proteins, immunophilins, and p23. J Biol Chem *269*, 24989-24993.

Johnson, J.L., and Toft, D.O. (1995). Binding of P23 and Hsp90 during Assembly with the Progesterone-Receptor. Mol Endocrinol *9*, 670-678.

Kadota, Y., Amigues, B., Ducassou, L., Madaoui, H., Ochsenbein, F., Guerois, R., and Shirasu, K. (2008). Structural and functional analysis of SGT1-HSP90 core complex required for innate immunity in plants. EMBO Rep *9*, 1209-1215.

Kadota, Y., Shirasu, K., and Guerois, R. (2010). NLR sensors meet at the SGT1-HSP90 crossroad. Trends Biochem Sci *35*, 199-207.

Kampinga, H.H., and Craig, E.A. (2010). The HSP70 chaperone machinery: J proteins as drivers of functional specificity. Nat Rev Mol Cell Biol *11*, 579-592.

Karplus, M., and Weaver, D.L. (1994). Protein folding dynamics: the diffusion-collision model and experimental data. Protein Sci *3*, 650-668.

Kelly, S.M., Jess, T.J., and Price, N.C. (2005). How to study proteins by circular dichroism. Biochim Biophys Acta *1751*, 119-139.

Khan, S.H., Awasthi, S., Guo, C., Goswami, D., Ling, J., Griffin, P.R., Simons, S.S., Jr., and Kumar, R. (2012). Binding of the N-terminal region of coactivator TIF2 to the intrinsically disordered AF1 domain of the glucocorticoid receptor is accompanied by conformational reorganizations. J Biol Chem *287*, 44546-44560.

Kim, P.S., and Baldwin, R.L. (1990). Intermediates in the folding reactions of small proteins. Annu Rev Biochem *59*, 631-660.

Kimura, Y., Rutherford, S.L., Miyata, Y., Yahara, I., Freeman, B.C., Yue, L., Morimoto, R.I., and Lindquist, S. (1997). Cdc37 is a molecular chaperone with specific functions in signal transduction. Genes Dev *11*, 1775-1785.

Kino, T., and Chrousos, G.P. (2004). Glucocorticoid and mineralocorticoid receptors and associated diseases. Essays Biochem *40*, 137-155.

Kino, T., Vottero, A., Charmandari, E., and Chrousos, G.P. (2002). Familial/sporadic glucocorticoid resistance syndrome and hypertension. Ann N Y Acad Sci *970*, 101-111.

Kroe, R.R., Baker, M.A., Brown, M.P., Farrow, N.A., Gautschi, E., Hopkins, J.L., LaFrance, R.R., Kronkaitis, A., Freeman, D., Thomson, D., *et al.* (2007). Agonist versus antagonist induce distinct thermodynamic modes of co-factor binding to the glucocorticoid receptor. Biophys Chem *128*, 156-164.

Krukenberg, K.A., Forster, F., Rice, L.M., Sali, A., and Agard, D.A. (2008). Multiple conformations of E. coli Hsp90 in solution: insights into the conformational dynamics of Hsp90. Structure *16*, 755-765.

Krukenberg, K.A., Street, T.O., Lavery, L.A., and Agard, D.A. (2011). Conformational dynamics of the molecular chaperone Hsp90. Q Rev Biophys *44*, 229-255.

Kullmann, M., Schneikert, J., Moll, J., Heck, S., Zeiner, M., Gehring, U., and Cato, A.C. (1998). RAP46 is a negative regulator of glucocorticoid receptor action and hormone-induced apoptosis. J Biol Chem *273*, 14620-14625.

Kumar, R., Johnson, B.H., and Thompson, E.B. (2004). Overview of the structural basis for transcription regulation by nuclear hormone receptors. Essays Biochem *40*, 27-39.

Kumar, R., and Thompson, E.B. (2012). Folding of the glucocorticoid receptor N-terminal transactivation function: dynamics and regulation. Mol Cell Endocrinol *348*, 450-456.

Kuwajima, K. (1989). The molten globule state as a clue for understanding the folding and cooperativity of globular-protein structure. Proteins *6*, 87-103.

Laemmli, U.K. (1970). Cleavage of structural proteins during the assembly of the head of bacteriophage T4. Nature *227*, 680-685.

Laue, T.M., Shah, B.D., Ridgeway, T.M., and Pelletier, S.L (1992). Computer-aided interpretation of analytical sedimentation data for proteins. Analytical Ultracentrifugation in Biochemistry and Polymer. Science *pp. 90-125*.

Lavery, L.A., Partridge, J.R., Ramelot, T.A., Elnatan, D., Kennedy, M.A., and Agard, D.A. (2014). Structural Asymmetry in the Closed State of Mitochondrial Hsp90 (TRAP1) Supports a Two-Step ATP Hydrolysis Mechanism. Mol Cell *53*, 330-343.

Lea, W.A., and Simeonov, A. (2011). Fluorescence polarization assays in small molecule screening. Expert Opin Drug Discov *6*, 17-32.

Lee, C.-T., Graf, C., Mayer, F.J., Richter, S.M., and Mayer, M.P. (2012). Dynamics of the regulation of Hsp90 by the co-chaperone Sti1. EMBO J *31*, 1518-1528.

Lee, G.J., Roseman, A.M., Saibil, H.R., and Vierling, E. (1997). A small heat shock protein stably binds heat-denatured model substrates and can maintain a substrate in a folding-competent state. EMBO J *16*, 659-671.

Lemon, B., and Tjian, R. (2000). Orchestrated response: a symphony of transcription factors for gene control. Genes Dev *14*, 2551-2569.

Levinthal, C. (1968). Are there pathways for protein folding? Journal De Chimie Physique Et De Physico-Chimie Biologique *65*, 44-45.

Li, J., Richter, K., and Buchner, J. (2011). Mixed Hsp90-cochaperone complexes are important for the progression of the reaction cycle. Nat Struct Mol Biol *18*, 61-66.

Li, J., Richter, K., Reinstein, J., and Buchner, J. (2013). Integration of the accelerator Aha1 in the Hsp90 co-chaperone cycle. Nat Struct Mol Biol *20*, 326-331.

Li, J., Soroka, J., and Buchner, J. (2012). The Hsp90 chaperone machinery: conformational dynamics and regulation by co-chaperones. Biochim Biophys Acta *1823*, 624-635.

Louvion, J.F., Warth, R., and Picard, D. (1996). Two eukaryote-specific regions of Hsp82 are dispensable for its viability and signal transduction functions in yeast. Proc Natl Acad Sci U S A *93*, 13937-13942.

Luders, J., Demand, J., and Hohfeld, J. (2000). The ubiquitin-related BAG-1 provides a link between the molecular chaperones Hsc70/Hsp70 and the proteasome. J Biol Chem *275*, 4613-4617.

Luisi, B.F., Xu, W.X., Otwinowski, Z., Freedman, L.P., Yamamoto, K.R., and Sigler, P.B. (1991). Crystallographic analysis of the interaction of the glucocorticoid receptor with DNA. Nature *352*, 497-505.

MacLean, M., and Picard, D. (2003). Cdc37 goes beyond Hsp90 and kinases. Cell Stress Chaperon *8*, 114-119.

Madl, T. (2013). Integration von NMR und SAXS/SANS in der Strukturbiologie. BIOspektrum *19*, 386-389.

Mayr, C., Richter, K., Lilie, H., and Buchner, J. (2000). Cpr6 and Cpr7, two closely related Hsp90-associated immunophilins from Saccharomyces cerevisiae, differ in their functional properties. J Biol Chem *275*, 34140-34146.

McClellan, A.J., Tam, S., Kaganovich, D., and Frydman, J. (2005). Protein quality control: chaperones culling corrupt conformations. Nat Cell Biol *7*, 736-741.

McDonough, H., and Patterson, C. (2003). CHIP: a link between the chaperone and proteasome systems. Cell Stress Chaperon *8*, 303-308.

McKay, L.I., and Cidlowski, J.A. (1999). Molecular control of immune/inflammatory responses: interactions between nuclear factor-kappa B and steroid receptor-signaling pathways. Endocr Rev *20*, 435-459.

McLaughlin, S.H., and Jackson, S.E. (2002). Folding and stability of the ligand-binding domain of the glucocorticoid receptor. Protein Sci *11*, 1926-1936.

McLaughlin, S.H., Smith, H.W., and Jackson, S.E. (2002). Stimulation of the weak ATPase activity of human hsp90 by a client protein. J Mol Biol *315*, 787-798.

Meijsing, S.H., Elbi, C., Luecke, H.F., Hager, G.L., and Yamamoto, K.R. (2007). The ligand binding domain controls glucocorticoid receptor dynamics independent of ligand release. Mol Cell Biol *27*, 2442-2451.

Meyer, P., Prodromou, C., Hu, B., Vaughan, C., Roe, S.M., Panaretou, B., Piper, P.W., and Pearl, L.H. (2003). Structural and functional analysis of the middle segment of hsp90: implications for ATP hydrolysis and client protein and cochaperone interactions. Mol Cell *11*, 647-658.

Meyer, P., Prodromou, C., Liao, C., Hu, B., Roe, S.M., Vaughan, C.K., Vlasic, I., Panaretou, B., Piper, P.W., and Pearl, L.H. (2004). Structural basis for recruitment of the ATPase activator Aha1 to the Hsp90 chaperone machinery. EMBO J *23*, 1402-1410.

Mickler, M., Hessling, M., Ratzke, C., Buchner, J., and Hugel, T. (2009). The large conformational changes of Hsp90 are only weakly coupled to ATP hydrolysis. Nat Struct Mol Biol *16*, 281-286.

Minami, Y., Kimura, Y., Kawasaki, H., Suzuki, K., and Yahara, I. (1994). The carboxy-terminal region of mammalian HSP90 is required for its dimerization and function in vivo. Mol Cell Biol *14*, 1459-1464.

Moehren, U., Eckey, M., and Baniahmad, A. (2004). Gene repression by nuclear hormone receptors. Essays Biochem *40*, 89-104.

Mollapour, M., and Neckers, L. (2012). Post-translational modifications of Hsp90 and their contributions to chaperone regulation. Biochim Biophys Acta *1823*, 648-655.

Morishima, Y., Kanelakis, K.C., Murphy, P.J., Lowe, E.R., Jenkins, G.J., Osawa, Y., Sunahara, R.K., and Pratt, W.B. (2003). The hsp90 cochaperone p23 is the limiting component of the multiprotein hsp90/hsp70-based chaperone system in vivo where it acts to stabilize the client protein: hsp90 complex. J Biol Chem *278*, 48754-48763.

Morishima, Y., Murphy, P.J., Li, D.P., Sanchez, E.R., and Pratt, W.B. (2000). Stepwise assembly of a glucocorticoid receptor.hsp90 heterocomplex resolves two sequential ATP-dependent events involving first hsp70 and then hsp90 in opening of the steroid binding pocket. J Biol Chem *275*, 18054-18060.

Motojima-Miyazaki, Y., Yoshida, M., and Motojima, F. (2010). Ribosomal protein L2 associates with E. coli HtpG and activates its ATPase activity. Biochem Biophys Res Commun *400*, 241-245.

Mumberg, D., Muller, R., and Funk, M. (1995). Yeast vectors for the controlled expression of heterologous proteins in different genetic backgrounds. Gene *156*, 119-122.

Nagy, L., Kao, H.Y., Love, J.D., Li, C., Banayo, E., Gooch, J.T., Krishna, V., Chatterjee, K., Evans, R.M., and Schwabe, J.W. (1999). Mechanism of corepressor binding and release from nuclear hormone receptors. Genes Dev *13*, 3209-3216.

Nathan, D.F., and Lindquist, S. (1995). Mutational analysis of Hsp90 function: interactions with a steroid receptor and a protein kinase. Mol Cell Biol *15*, 3917-3925.

Nathan, D.F., Vos, M.H., and Lindquist, S. (1997). In vivo functions of the Saccharomyces cerevisiae Hsp90 chaperone. Proc Natl Acad Sci U S A *94*, 12949-12956.

Nicolaides, N.C., Galata, Z., Kino, T., Chrousos, G.P., and Charmandari, E. (2010). The human glucocorticoid receptor: molecular basis of biologic function. Steroids *75*, 1-12.

Ohana, R.F., Encell, L.P., Zhao, K., Simpson, D., Slater, M.R., Urh, M., and Wood, K.V. (2009). HaloTag7: a genetically engineered tag that enhances bacterial expression of soluble proteins and improves protein purification. Protein Expr Purif *68*, 110-120.

Owen, B.A., Sullivan, W.P., Felts, S.J., and Toft, D.O. (2002). Regulation of heat shock protein 90 ATPase activity by sequences in the carboxyl terminus. J Biol Chem *277*, 7086-7091.

Panaretou, B., Prodromou, C., Roe, S.M., O'Brien, R., Ladbury, J.E., Piper, P.W., and Pearl, L.H. (1998). ATP binding and hydrolysis are essential to the function of the Hsp90 molecular chaperone in vivo. EMBO *17*, 4829-4836.

Panaretou, B., Siligardi, G., Meyer, P., Maloney, A., Sullivan, J.K., Singh, S., Millson, S.H., Clarke, P.A., Naaby-Hansen, S., Stein, R., *et al.* (2002). Activation of the ATPase activity of hsp90 by the stress-regulated cochaperone aha1. Mol Cell *10*, 1307-1318.

Park, S.J., Borin, B.N., Martinez-Yamout, M.A., and Dyson, H.J. (2011). The client protein p53 adopts a molten globule-like state in the presence of Hsp90. Nat Struct Mol Biol *18*, 537-541.

Petoukhov, M.V., Franke, D., Shkumatov, A.V., Tria, G., Kikhney, A.G., Gajda, M., Gorba, C., Mertens, H.D.T., Konarev, P.V., and Svergun, D.I. (2012). New developments in the ATSAS program package for small-angle scattering data analysis. . J Appl Crystallogr *45*, 342-350.

Philo, J.S. (2006). Improved methods for fitting sedimentation coefficient distributions derived by time-derivative techniques. Anal Biochem *354*, 238-246.

Picard, D. (2002). Heat-shock protein 90, a chaperone for folding and regulation. Cell Mol Life Sci *59*, 1640-1648.

Picard, D., Khursheed, B., Garabedian, M.J., Fortin, M.G., Lindquist, S., and Yamamoto, K.R. (1990). Reduced levels of hsp90 compromise steroid receptor action in vivo. Nature *348*, 166-168.

Picard, D., and Yamamoto, K.R. (1987). Two signals mediate hormone-dependent nuclear localization of the glucocorticoid receptor. EMBO J *6*, 3333-3340.

Pirkl, F., and Buchner, J. (2001). Functional analysis of the Hsp90-associated human peptidyl prolyl cis/trans isomerases FKBP51, FKBP52 and Cyp40. J Mol Biol *308*, 795-806.

Pratt, W.B., and Dittmar, K.D. (1998). Studies with Purified Chaperones Advance the Understanding of the Mechanism of Glucocorticoid Receptor-hsp90 Heterocomplex Assembly. Trends Endocrinol Metab *9*, 244-252.

Pratt, W.B., Galigniana, M.D., Morishima, Y., and Murphy, P.J. (2004). Role of molecular chaperones in steroid receptor action. Essays Biochem *40*, 41-58.

Pratt, W.B., Morishima, Y., and Osawa, Y. (2008). The Hsp90 chaperone machinery regulates signaling by modulating ligand binding clefts. J Biol Chem *283*, 22885-22889.

Pratt, W.B., and Toft, D.O. (1997). Steroid receptor interactions with heat shock protein and immunophilin chaperones. Endocr Rev *18*, 306-360.

Prodromou, C., Roe, S.M., O'Brien, R., Ladbury, J.E., Piper, P.W., and Pearl, L.H. (1997). Identification and structural characterization of the ATP/ADP-binding site in the Hsp90 molecular chaperone. Cell *90*, 65-75.

Prodromou, C., Siligardi, G., O'Brien, R., Woolfson, D.N., Regan, L., Panaretou, B., Ladbury, J.E., Piper, P.W., and Pearl, L.H. (1999). Regulation of Hsp90 ATPase activity by tetratricopeptide repeat (TPR)-domain co-chaperones. EMBO J *18*, 754-762.

Ratajczak, T., Hlaing, J., Brockway, M.J., and Hahnel, R. (1990). Isolation of untransformed bovine estrogen receptor without molybdate stabilization. J Steroid Biochem *35*, 543-553.

Ratajczak, T., Ward, B.K., Cluning, C., and Allan, R.K. (2009). Cyclophilin 40: an Hsp90-cochaperone associated with apo-steroid receptors. Int J Biochem Cell Biol *41*, 1652-1655.

Ratajczak, T., Ward, B.K., and Minchin, R.F. (2003). Immunophilin chaperones in steroid receptor signalling. Curr Top Med Chem *3*, 1348-1357.

Retzlaff, M., Hagn, F., Mitschke, L., Hessling, M., Gugel, F., Kessler, H., Richter, K., and Buchner, J. (2010). Asymmetric activation of the hsp90 dimer by its cochaperone aha1. Mol Cell *37*, 344-354.

Reynolds, P.D., Ruan, Y., Smith, D.F., and Scammell, J.G. (1999). Glucocorticoid resistance in the squirrel monkey is associated with overexpression of the immunophilin FKBP51. J Clin Endocrinol Metab *84*, 663-669.

Rhen, T., and Cidlowski, J.A. (2005). Antiinflammatory action of glucocorticoids--new mechanisms for old drugs. N Engl J Med *353*, 1711-1723.

Richter, K., Haslbeck, M., and Buchner, J. (2010). The heat shock response: life on the verge of death. Mol Cell *40*, 253-266.

Richter, K., Meinlschmidt, B., and Buchner, J. (2008a). Hsp90: From Dispensable Heat Shock Protein to Global Player. In Protein Folding Handbook (Wiley-VCH Verlag GmbH), pp. 768-829.

Richter, K., Soroka, J., Skalniak, L., Leskovar, A., Hessling, M., Reinstein, J., and Buchner, J. (2008b). Conserved conformational changes in the ATPase cycle of human Hsp90. J Biol Chem *283*, 17757-17765.

Richter, K., Moser, S., Hagn, F., Friedrich, R., Hainzl, O., Heller, M., Schlee, S., Kessler, H., Reinstein, J., and Buchner, J. (2006). Intrinsic inhibition of the Hsp90 ATPase activity. J Biol Chem *281*, 11301-11311.

Richter, K., Muschler, P., Hainzl, O., Reinstein, J., and Buchner, J. (2003). Sti1 is a non-competitive inhibitor of the Hsp90 ATPase. Binding prevents the N-terminal dimerization reaction during the atpase cycle. J Biol Chem *278*, 10328-10333.

Richter, K., Walter, S., and Buchner, J. (2004). The Co-chaperone Sba1 connects the ATPase reaction of Hsp90 to the progression of the chaperone cycle. J Mol Biol *342*, 1403-1413.

Ricketson, D., Hostick, U., Fang, L., Yamamoto, K.R., and Darimont, B.D. (2007). A conformational switch in the ligand-binding domain regulates the dependence of the glucocorticoid receptor on Hsp90. J Mol Biol *368*, 729-741.

Riggs, D.L., Roberts, P.J., Chirillo, S.C., Cheung-Flynn, J., Prapapanich, V., Ratajczak, T., Gaber, R., Picard, D., and Smith, D.F. (2003). The Hsp90-binding peptidylprolyl isomerase FKBP52 potentiates glucocorticoid signaling in vivo. EMBO J *22*, 1158-1167.

Roe, S.M., Ali, M.M., Meyer, P., Vaughan, C.K., Panaretou, B., Piper, P.W., Prodromou, C., and Pearl, L.H. (2004). The Mechanism of Hsp90 regulation by the protein kinase-specific cochaperone p50(cdc37). Cell *116*, 87-98.

Röhl, A., Rohrberg, J., and Buchner, J. (2013). The chaperone Hsp90: changing partners for demanding clients. Trends Biochem Sci *38*, 253-262.

Rüdiger, S., Freund, S.M., Veprintsev, D.B., and Fersht, A.R. (2002). CRINEPT-TROSY NMR reveals p53 core domain bound in an unfolded form to the chaperone Hsp90. Proc Natl Acad Sci U S A *99*, 11085-11090.

Salek, R.M., Williams, M.A., Prodromou, C., Pearl, L.H., and Ladbury, J.E. (2002). Backbone resonance assignments of the 25kD N-terminal ATPase domain from the Hsp90 chaperone. J Biomol NMR *23*, 327-328.

Sambrook, J., Fritsch, E.F., and Maniatis, T. (1989). Molecular cloning: a laboratory manual (Cold Spring Harbor Laboratory).

Scheufler, C., Brinker, A., Bourenkov, G., Pegoraro, S., Moroder, L., Bartunik, H., Hartl, F.U., and Moarefi, I. (2000). Structure of TPR domain-peptide complexes: critical elements in the assembly of the Hsp70-Hsp90 multichaperone machine. Cell *101*, 199-210.

Schmid, A.B., Lagleder, S., Grawert, M.A., Rohl, A., Hagn, F., Wandinger, S.K., Cox, M.B., Demmer, O., Richter, K., Groll, M., *et al.* (2012). The architecture of functional modules in the Hsp90 co-chaperone Sti1/Hop. EMBO J *31*, 1506-1517.

Schoch, G.A., D'Arcy, B., Stihle, M., Burger, D., Bar, D., Benz, J., Thoma, R., and Ruf, A. (2010). Molecular switch in the glucocorticoid receptor: active and passive antagonist conformations. J Mol Biol *395*, 568-577.

Schuck, P. (2000). Size-distribution analysis of macromolecules by sedimentation velocity ultracentrifugation and lamm equation modeling. Biophys J *78*, 1606-1619.

Schulte, T.W., Akinaga, S., Soga, S., Sullivan, W., Stensgard, B., Toft, D., and Neckers, L.M. (1998). Antibiotic radicicol binds to the N-terminal domain of Hsp90 and shares important biologic activities with geldanamycin. Cell Stress Chaperones *3*, 100-108.

Seitz, T., Thoma, R., Schoch, G.A., Stihle, M., Benz, J., D'Arcy, B., Wiget, A., Ruf, A., Hennig, M., and Sterner, R. (2010). Enhancing the stability and solubility of the glucocorticoid receptor ligand-binding domain by high-throughput library screening. J Mol Biol *403*, 562-577.

Shiau, A.K., Harris, S.F., Southworth, D.R., and Agard, D.A. (2006). Structural Analysis of E. coli hsp90 reveals dramatic nucleotide-dependent conformational rearrangements. Cell *127*, 329-340.

Siligardi, G., Hu, B., Panaretou, B., Piper, P.W., Pearl, L.H., and Prodromou, C. (2004). Co-chaperone regulation of conformational switching in the Hsp90 ATPase cycle. J Biol Chem *279*, 51989-51998.

Silverstein, A.M., Galigniana, M.D., Chen, M.S., Owens-Grillo, J.K., Chinkers, M., and Pratt, W.B. (1997). Protein phosphatase 5 is a major component of glucocorticoid receptor.hsp90 complexes with properties of an FK506-binding immunophilin. J Biol Chem *272*, 16224-16230.

Silverstein, A.M., Grammatikakis, N., Cochran, B.H., Chinkers, M., and Pratt, W.B. (1998). p50(cdc37) binds directly to the catalytic domain of Raf as well as to a site on hsp90 that is topologically adjacent to the tetratricopeptide repeat binding site. J Biol Chem *273*, 20090-20095.

Simmons, C.A., Bledsoe, R.K., Guex, N., and Pearce, K.H. (2008). Expression, purification, and characterization of multiple, multifunctional human glucocorticoid receptor proteins. Protein Expr Purif *62*, 29-35.

Sivashanmugam, A., Murray, V., Cui, C., Zhang, Y., Wang, J., and Li, Q. (2009). Practical protocols for production of very high yields of recombinant proteins using Escherichia coli. Protein Sci *18*, 936-948.

Smith, D.F. (1993). Dynamics of heat shock protein 90-progesterone receptor binding and the disactivation loop model for steroid receptor complexes. Mol endocrinol *7*, 1418-1429.

Smith, D.F., Faber, L.E., and Toft, D.O. (1990). Purification of unactivated progesterone receptor and identification of novel receptor-associated proteins. J Biol Chem *265*, 3996-4003.

Smith, D.F., and Toft, D.O. (2008). Minireview: the intersection of steroid receptors with molecular chaperones: observations and questions. Mol endocrinol *22*, 2229-2240.

Soroka, J., Wandinger, S.K., Mausbacher, N., Schreiber, T., Richter, K., Daub, H., and Buchner, J. (2012). Conformational switching of the molecular chaperone Hsp90 via regulated phosphorylation. Mol Cell *45*, 517-528.

Southworth, D.R., and Agard, D.A. (2008). Species-dependent ensembles of conserved conformational states define the Hsp90 chaperone ATPase cycle. Mol Cell *32*, 631-640.

Spitz, I.M. (2010). Mifepristone: where do we come from and where are we going? Clinical development over a quarter of a century. Contraception *82*, 442-452.

Srinivasan, G., Post, J.F., and Thompson, E.B. (1997). Optimal ligand binding by the recombinant human glucocorticoid receptor and assembly of the receptor complex with heat shock protein 90 correlate with high intracellular ATP levels in Spodoptera frugiperda cells. J Steroid Biochem Mol Biol *60*, 1-9.

Srinivasan, G., and Thompson, E.B. (1990). Overexpression of full-length human glucocorticoid receptor in Spodoptera frugiperda cells using the baculovirus expression vector system. Mol Endocrinol *4*, 209-216.

Street, T.O., Lavery, L.A., and Agard, D.A. (2011). Substrate binding drives large-scale conformational changes in the Hsp90 molecular chaperone. Mol Cell *42*, 96-105.

Studier, F.W. (2005). Protein production by auto-induction in high density shaking cultures. Protein Expr Purif *41*, 207-234.

Surjit, M., Ganti, K.P., Mukherji, A., Ye, T., Hua, G., Metzger, D., Li, M., and Chambon, P. (2011). Widespread negative response elements mediate direct repression by agonist-liganded glucocorticoid receptor. Cell *145*, 224-241.

Svergun, D. (1992). Determination of the regularization parameter in indirect-transform methods using perceptual criteria. J Appl Crystallogr *25*, 495-503.

Svergun, D., Barberato, C., and Koch, M.H.J. (1995). CRYSOL-a Program to Evaluate X-ray Solution Scattering of Biological Macromolecules from Atomic Coordinates. J Appl Crystallogr *28*, 768-773.

Taipale, M., Jarosz, D.F., and Lindquist, S. (2010). HSP90 at the hub of protein homeostasis: emerging mechanistic insights. Nat Rev Mol Cell Biol *11*, 515-528.

Taipale, M., Krykbaeva, I., Koeva, M., Kayatekin, C., Westover, K.D., Karras, G.I., and Lindquist, S. (2012). Quantitative analysis of HSP90-client interactions reveals principles of substrate recognition. Cell *150*, 987-1001.

Tao, T., Lan, J., Lukacs, G.L., Hache, R.J., and Kaplan, F. (2006). Importin 13 regulates nuclear import of the glucocorticoid receptor in airway epithelial cells. Am J Respir Cell Mol Biol *35*, 668-680.

Terpe, K. (2003). Overview of tag protein fusions: from molecular and biochemical fundamentals to commercial systems. Appl Microbiol Biotechnol *60*, 523-533.

Tsutsumi, S., Mollapour, M., Prodromou, C., Lee, C.-T., Panaretou, B., Yoshida, S., Mayer, M.P., and Neckers, L.M. (2012). Charged linker sequence modulates eukaryotic heat shock protein 90 (Hsp90) chaperone activity. Proc Natl Acad Sci U S A *109*, 2937-2942

Tsutsumi, S., and Neckers, L. (2007). Extracellular heat shock protein 90: a role for a molecular chaperone in cell motility and cancer metastasis. Cancer Sci *98*, 1536-1539.

Vandevyver, S., Dejager, L., and Libert, C. (2012). On the trail of the glucocorticoid receptor: into the nucleus and back. Traffic *13*, 364-374.

Vaughan, C.K., Gohlke, U., Sobott, F., Good, V.M., Ali, M.M., Prodromou, C., Robinson, C.V., Saibil, H.R., and Pearl, L.H. (2006). Structure of an Hsp90-Cdc37-Cdk4 complex. Mol Cell *23*, 697-707.

Vaughan, C.K., Mollapour, M., Smith, J.R., Truman, A., Hu, B., Good, V.M., Panaretou, B., Neckers, L., Clarke, P.A., Workman, P., *et al.* (2008). Hsp90-dependent activation of protein kinases is regulated by chaperone-targeted dephosphorylation of Cdc37. Mol Cell *31*, 886-895.

Vranken, W.F., Boucher, W., Stevens, T.J., Fogh, R.H., Pajon, A., Llinas, M., Ulrich, E.L., Markley, J.L., Ionides, J., and Laue, E.D. (2005). The CCPN data model for NMR spectroscopy: development of a software pipeline. Proteins *59*, 687-696.

Wagner, C., and Kiefhaber, T. (1999). Intermediates can accelerate protein folding. Proc Natl Acad Sci U S A *96*, 6716-6721.

Wandinger, S.K., Richter, K., and Buchner, J. (2008). The Hsp90 chaperone machinery. J Biol Chem *283*, 18473-18477.

Wang, X., Venable, J., LaPointe, P., Hutt, D.M., Koulov, A.V., Coppinger, J., Gurkan, C., Kellner, W., Matteson, J., Plutner, H., *et al.* (2006). Hsp90 cochaperone Aha1 downregulation rescues misfolding of CFTR in cystic fibrosis. Cell *127*, 803-815.

Weikl, T., Abelmann, K., and Buchner, J. (1999). An unstructured C-terminal region of the Hsp90 co-chaperone p23 is important for its chaperone function. J Mol Biol *293*, 685-691.

Weikl, T., Muschler, P., Richter, K., Veit, T., Reinstein, J., and Buchner, J. (2000). C-terminal regions of Hsp90 are important for trapping the nucleotide during the ATPase cycle. J Mol Biol *303*, 583-592.

Wetlaufer, D.B. (1973). Nucleation, rapid folding, and globular intrachain regions in proteins. Proc Natl Acad Sci U S A *70*, 697-701.

Wurtz, J.M., Bourguet, W., Renaud, J.P., Vivat, V., Chambon, P., Moras, D., and Gronemeyer, H. (1996). A canonical structure for the ligand-binding domain of nuclear receptors. Nat Struct Biol *3*, 87-94.

Xu, Z., Horwich, A.L., and Sigler, P.B. (1997). The crystal structure of the asymmetric GroEL-GroES-(ADP)7 chaperonin complex. Nature *388*, 741-750.

Yasukawa, T., Kanei-Ishii, C., Maekawa, T., Fujimoto, J., Yamamoto, T., and Ishii, S. (1995). Increase of solubility of foreign proteins in Escherichia coli by coproduction of the bacterial thioredoxin. J Biol Chem *270*, 25328-25331.

Young, J.C., Obermann, W.M., and Hartl, F.U. (1998). Specific binding of tetratricopeptide repeat proteins to the C-terminal 12-kDa domain of hsp90. J Biol Chem *273*, 18007-18010.

8 Supplement

Supplemental table 1 List of residues which shifted or lost intensity in the presence of GR.

	Hsp90-N				Hsp90-M			
	Polar Residues		Nonpolar Residues		Polar residues		Nonpolar residues	
	Chemical Shift Perturbation	Intensity Change	Chemical Shift Perturbation	Intensity Change	Chemical Shift Perturbation	Intensity Change	Chemical Shift Perturbation	Intensity Change
Individual domain		T13, E28, R32, E33, K44, D52, Q55, E57, E88, D113, T171, K191	I205	I29, I66, V74, L93, M105, A110, A152, S155, G168, V201	E353, H430, E431, R436, K449, D489, T502, D503, E507, T511, Q512	N290, N340, S371, K399, N405, E406, K416, Y418, Y445, T455, E507, T520	F332, V365, V397, G428, A437, L457, A490, I505	F309, L362, I396, G428, A440, V498, L521
Hsp90-NM domain construct	E28	E28, R32, S39, K44, S49, K86, Q135*, S140*, D161*, T171	L18, L93	I29, L31, A41, I66, L89, L93, G94, A110, G154	E287, D356	R279*, E288, S295, E316,* K325*, Y344*, E381*, E385, N386, K394, K416, E431, K449, S456, H467, T511, Q512	V391	L331, F364, L374, V391

* Indicates regions affected only in the Hsp90-NM domain constructs. Residues in the Hsp90-NM domain construct which are affected in the presence of GR and are greater than 5 residues from a residue which is affected in the individual domain. Analysis was performed by Lee Freiburger (Technische Universität München).

Supplemental table 2 SAXS data and analysis.

Sample	R_g [Å]	D_{max} [Å]	Molecular mass [kDa]*
Hsp90	64.2 ± 0.2	240	159
Hsp90-ATP	58.3 ± 0.1	220	160
Hsp90-ATPγS	53.5 ± 0.2	170	158
Hsp90-AMP-PNP	50.7 ± 0.2	170	165
Hsp90-ATP-GR-LBDm (2:1)	57.2 ± 0.1	200	185
Hsp90-ATP-GR-LBDm (2:2)	58.3 ± 0.1	200	208
Hsp90-ATP-GR-LBDm (2:3)	57.7 ± 0.1	200	195
Hsp90-GR-LBDm (2:2)	59.5 ± 0.4	250	189
Hsp90-ATPγS-GR-LBDm (2:2)	54.9 ± 0.3	220	225
Hsp90-AMP-PNP-GR-LBDm (2:2)	51.3 ± 0.2	220	221
Hsp90-ATPγS-p23 (2:1)	49.3 ± 0.2	150	200
Hsp90-ATPγS-p23 (2:2)	48.6 ± 0.1	150	210
Hsp90-ATPγS-p23 (2:3)	47.5 ± 0.1	150	210
Hsp90-ATPγS-GR-LBDm-p23 (2:1:1)	49.8 ± 0.2	180	210
Hsp90-ATPγS-GR-LBDm-p23 (2:2:1)	52.7 ± 0.2	180	214
Hsp90-ATPγS-GR-LBDm-p23 (2:1:2)	49.5 ± 0.2	180	214
Hsp90-ATPγS-GR-LBDm-p23 (2:2:2)	52.7 ± 0.2	180	208

*The molecular mass was determined from the scattering intensity at zero angle (I(0)) using BSA as reference. Analysis was performed by Tobias Madl (Technische Universität München).

9 Publications

'Modulation of the Hsp90 chaperone cycle by a stringent client protein'
Oliver Robin Lorenz, Lee Freiburger, Daniel Andreas Rutz, Maike Krause, Bettina Karolina Zierer, Sara Alvira, Jorge Cuéllar, José María Valpuesta, Tobias Madl, Michael Sattler & Johannes Buchner, Mol.Cell 2014, *Accepted*

10 Danksagung

An erster Stelle möchte ich mich bei meinem Doktorvater Johannes Buchner für das spannende Thema und sein Engagement bedanken, das wesentlich zum Gelingen dieser Arbeit beigetragen hat. Ich danke meinen Kollaborationspartnern Michael Sattler, Lee Freiburger und Tobias Madl für die strukturelle Aufklärung des Hsp90-GR Komplexes. Großen Dank geht an Daniel Rutz und Maike Krause für die Unterstützung dieses Projekts. Ich danke Anja Liebscher für die Hilfe im Labor, sowie Bettina Richter und Helmut Krause für massenspektrometrische Analysen. Frau Hilber und Frau Rubinstein danke ich für die Hilfe mit vielen bürokratischen Dingen. Besonderen Dank geht an alle Doktoranden und ehemaligen Kollegen für die tolle Arbeitsatmosphäre und die vielen unvergesslichen privaten Aktivitäten in München.

Ich danke meinen Eltern, Daniela und Charlotte für ihre moralische Unterstützung und ihre Geduld.

11 Eidesstattliche Erklärung

Hiermit erkläre ich an Eides statt, dass ich die vorliegende Arbeit selbständig verfasst und keine anderen als die angegebenen Quellen und Hilfsmittel verwendet habe. Die aus fremden Quellen übernommenen Gedanken sind als solche kenntlich gemacht. Die vorliegende Arbeit wurde noch keiner anderen Prüfungsbehörde vorgelegt. Teile dieser Arbeit werden in einem wissenschaftlichen Journal veröffentlicht.

Garching, den 27.02.2014 _____

Oliver Robin Lorenz